

EFFECT OF VIBRATION ON FREEZE-THAW RESISTANCE OF CONCRETE

by

AHMAD A. GHADBAN

B.S., American University of Sharjah, 2009

M.S., American University of Sharjah, 2012

AN ABSTRACT OF A DISSERTATION

submitted in partial fulfillment of the requirements for the degree

DOCTOR OF PHILOSOPHY

Department of Civil Engineering
College of Engineering

KANSAS STATE UNIVERSITY
Manhattan, Kansas

2016

Abstract

Pre-stressed concrete is used for manufacturing railroad ties. Air entrainment is used in concrete railroad ties to provide durability in freeze-thaw conditions commonly present in track. Vibration practices in pre-stressed concrete railroad tie plants could contribute to excessive air loss during manufacture and thus poor freeze-thaw resistance. Rheological properties of fresh concrete significantly influence the determination of how much air is lost during vibration. This research attempted to increase understanding of the effect of vibration on air bubble distribution and freeze-thaw resistance of concrete given certain compositions and rheological properties of concrete. The objective was achieved by examining the effect of different admixtures combinations, vibration parameters, and rheological properties on the air void system and freeze-thaw resistance of concrete. This research also proposed a method to measure rheological properties of concrete when vibrated and for concrete mixtures too stiff to measure using conventional rheology measurements. Results showed that delaying the initiation of vibration can cause significant air loss but does not necessarily decrease freeze-thaw performance of concrete. Results also showed that a majority of air loss occurs in the first 30 seconds of vibration. The types of admixtures used in the concrete mixture can significantly affect the air system and freeze-thaw durability of concrete; this effect was shown to be more pronounced in mixtures with low yield stress and plastic viscosity. While the peak vibration acceleration had a mild effect, the frequency and peak velocity of vibration did not seem to have a noticeable effect on the air system and freeze-thaw performance of concrete. Results also showed that rheological properties of stiff mixtures can be estimated by running the rheology test during vibration.

EFFECT OF VIBRATION ON FREEZE-THAW RESISTANCE OF CONCRETE

by

AHMAD A. GHADBAN

B.S., American University of Sharjah, 2009

M.S., American University of Sharjah, 2012

A DISSERTATION

submitted in partial fulfillment of the requirements for the degree

DOCTOR OF PHILOSOPHY

Department of Civil Engineering
College of Engineering

KANSAS STATE UNIVERSITY
Manhattan, Kansas

2016

Approved by:

Major Professor
Kyle A. Riding

Copyright

AHMAD A. GHADBAN

2016

Abstract

Pre-stressed concrete is used for manufacturing railroad ties. Air entrainment is used in concrete railroad ties to provide durability in freeze-thaw conditions commonly present in track. Vibration practices in pre-stressed concrete railroad tie plants could contribute to excessive air loss during manufacture and thus poor freeze-thaw resistance. Rheological properties of fresh concrete significantly influence the determination of how much air is lost during vibration. This research attempted to increase understanding of the effect of vibration on air bubble distribution and freeze-thaw resistance of concrete given certain compositions and rheological properties of concrete. The objective was achieved by examining the effect of different admixtures combinations, vibration parameters, and rheological properties on the air void system and freeze-thaw resistance of concrete. This research also proposed a method to measure rheological properties of concrete when vibrated and for concrete mixtures too stiff to measure using conventional rheology measurements. Results showed that delaying the initiation of vibration can cause significant air loss but does not necessarily decrease freeze-thaw performance of concrete. Results also showed that a majority of air loss occurs in the first 30 seconds of vibration. The types of admixtures used in the concrete mixture can significantly affect the air system and freeze-thaw durability of concrete; this effect was shown to be more pronounced in mixtures with low yield stress and plastic viscosity. While the peak vibration acceleration had a mild effect, the frequency and peak velocity of vibration did not seem to have a noticeable effect on the air system and freeze-thaw performance of concrete. Results also showed that rheological properties of stiff mixtures can be estimated by running the rheology test during vibration.

Table of Contents

List of Figures	ix
List of Tables	xvii
Acknowledgements	xviii
Dedication	xix
Chapter 1 - Introduction.....	1
1.1. Background.....	1
1.2. Scope of Research.....	2
1.3. Organization of Dissertation	3
Chapter 2 - Literature Review.....	4
2.1. Freeze-Thaw	4
2.1.1. Freeze-Thaw Mechanisms	6
2.1.1.1. Hydraulic Pressure Theory	6
2.1.1.2. Osmotic Pressure Theory	8
2.1.1.3. Litvan's Theory.....	8
2.1.2. Freeze-Thaw Testing.....	9
2.1.3. Air Entrainment	10
2.1.4. Measurement of Air Parameters	13
2.2. Concrete Vibration.....	15
2.3. Rheology	23
2.3.1. Introduction to the Mathematics of Rheology	24
2.3.1.1. The Constitutive Relation	27
2.3.1.2. Rheological Classification of Materials.....	28
2.3.2. Rheology and Vibration of Fresh Concrete	35
2.3.3. Rheology under Vibration.....	41
2.3.4. Methods for Measuring the Flow of Concrete	44
2.3.4.1. One-Parameter Rheometric Tests	44
2.3.4.2. Two-Parameter Rheometric Tests.....	47
2.4. Bubble Rising	49
Chapter 3 - Materials	53

3.1. Material Characterization	53
3.2. Mixture Proportions.....	55
3.2.1. Stability of Air Void System.....	55
3.2.2. Freeze-Thaw Durability of Externally Vibrated Concrete.....	57
3.2.3. Freeze-Thaw Durability of Internally Vibrated Concrete.....	59
3.2.4. Rheology under Vibration.....	59
Chapter 4 - Methodology	61
4.1. Equipment and Common Tests Description	61
4.1.1. Concrete Mixing	61
4.1.2. Rheology	62
4.1.3. Vibration	64
4.1.4. Freeze-Thaw Testing.....	70
4.1.5. Hardened Air Void Analysis.....	72
4.2. Specific Methods	80
4.2.1. Stability of Air Void System.....	80
4.2.2. Freeze-Thaw Durability of Externally Vibrated Concrete.....	80
4.2.3. Freeze-Thaw Durability of Internally Vibrated Concrete.....	81
4.2.4. Rheology under Vibration.....	83
Chapter 5 - Results and Discussions.....	91
5.1. Stability of Air Void System	91
5.2. Freeze-Thaw Durability of Externally Vibrated Concrete	102
5.2.1. Effect of Vibration Duration.....	102
5.2.2. Effect of Vibration Acceleration.....	107
5.2.3. Effect of Vibration Frequency	114
5.2.4. Effect of Vibration Velocity	119
5.2.5. Effect of Air Content before Vibration.....	123
5.2.6. Effect of Rheological Properties	127
5.2.7. Air Entrainment Requirements to Achieve Freeze-Thaw Durability	129
5.3. Freeze-Thaw Durability of Internally Vibrated Concrete.....	136
5.4. Rheology under Vibration	139
Chapter 6 - Conclusions and Recommendations	163

6.1. Summary	163
6.2. Conclusions.....	164
6.3. Recommendations.....	166
References.....	168

List of Figures

Figure 1.1 Pre-stressed concrete railroad ties	1
Figure 1.2 Factors contributing to freeze-thaw performance.....	2
Figure 2.1 Bad versus good air void distribution.....	7
Figure 2.2 Air entrainment mechanism	11
Figure 2.3 Immersion vibrator	19
Figure 2.4 Immersion vibrator mechanism.....	20
Figure 2.5 Table vibrator	20
Figure 2.6 Simple shear of a two-dimensional body	25
Figure 2.7 Rheological classification of bodies.....	29
Figure 2.8 Mechanical model of a viscous fluid.....	30
Figure 2.9 Mechanical model of an elastic solid	31
Figure 2.10 Mechanical model of a visco-elastic fluid.....	32
Figure 2.11 Mechanical model of an elastico-viscous solid.....	33
Figure 2.12 Mechanical model of a Bingham plastic	34
Figure 2.13 Bingham plastic versus Newtonian fluid.....	36
Figure 2.14 Behavior of two different Bingham plastics under vibration	50
Figure 2.15 Bubble rise mechanism.....	51
Figure 3.1 Particle size distribution of coarse aggregate	54
Figure 3.2 Particle size distribution of fine aggregate	55
Figure 4.1 Concrete after mixing.....	62
Figure 4.2 Rheometer concrete container	63
Figure 4.3 ICAR rheometer a) electronic equipment with vane and b) in concrete sample.....	64
Figure 4.4 Large vibrating table.....	65
Figure 4.5 Immersion vibrator	66
Figure 4.6 Control unit for the large vibrating table.....	66
Figure 4.7 Vibrating motor attached to the bottom of the table top	67
Figure 4.8 Vibrating motor weights inside the motor for the small vibrating table	67
Figure 4.9 Concrete block at the bottom of the large vibrating table	68
Figure 4.10 Freeze-thaw molds at the top of the large vibrating table	68

Figure 4.11 ASTM C231 concrete air content container bolted to the top of the large vibrating table.....	69
Figure 4.12 The large vibrating table with two freeze-thaw specimen molds and ASTM C231 specimen container bolted to the table top.....	69
Figure 4.13 The small vibrating table during vibration	70
Figure 4.14 Freeze-thaw machine.....	71
Figure 4.15 Electric saw	73
Figure 4.16 Saw-cut sample.....	75
Figure 4.17 Polishing machine	76
Figure 4.18 A concrete sample fixed to the plastic cylinder.....	77
Figure 4.19 Polishing machine during operation.....	77
Figure 4.20 Polishing discs (left to right: 80-grit, 1200-grit, 2200-grit)	78
Figure 4.21 Polished sample.....	78
Figure 4.22 Scanned image with orange powder.....	79
Figure 4.23 Black and white image	79
Figure 4.24 Immersion vibrator placement.....	81
Figure 4.25 Long beam after hardening.....	82
Figure 4.26 Saw-cutting long beams	82
Figure 4.27 Rheological behavior of granular materials	84
Figure 4.28 The rheometer bucket bolted to the top of the small vibrating table.....	85
Figure 4.29 The rheometer bolted to a wooden frame.....	86
Figure 4.30 Measuring vibration parameters on the vibrating table using an accelerameter	87
Figure 4.31 Measuring vibration parameters inside concrete using an accelerometer	88
Figure 4.32 Point of intersection between the initial tangent to the "under vibration" curve and the "without vibration" line.....	89
Figure 5.1 Rheological properties of HRWR + LRWR + synthetic AEA mixtures that experienced 3 g of vibration	91
Figure 5.2 Air loss versus time for HRWR + LRWR + synthetic AEA mixtures that experienced 3 g of vibration.....	92
Figure 5.3 Rheological properties of HRWR + wood rosin AEA mixtures that experienced 3 g of vibration	93

Figure 5.4 Air loss versus time for HRWR + wood rosin AEA mixtures that experienced 3 g of vibration	94
Figure 5.5 Rheological properties of HRWR + synthetic AEA mixtures that experienced 3 g of vibration	95
Figure 5.6 Air loss versus time for HRWR + synthetic AEA mixtures that experienced 3 g of vibration	95
Figure 5.7 Rheological properties of HRWR + tall oil AEA mixtures that experienced 3 g of vibration	96
Figure 5.8 Air loss versus time for HRWR + tall oil AEA mixtures that experienced 3 g of vibration	96
Figure 5.9 Rheological properties of selected mixtures that experienced 3 g of vibration	97
Figure 5.10 Air loss versus time for selected mixtures that experienced 3 g of vibration.....	98
Figure 5.11 Rheological properties of selected mixtures that experienced 10 g of vibration	99
Figure 5.12 Air loss versus time for selected mixtures that experienced 10 g of vibration.....	99
Figure 5.13 Rheological properties of tall oil AEA + HRWR mixtures (10 g versus 3 g vibrations)	100
Figure 5.14 Air loss versus time for tall oil AEA + HRWR mixtures (10 g versus 3 g vibrations)	100
Figure 5.15 Durability factor versus fresh air content before vibration (effect of admixtures on the air system)	101
Figure 5.16 Durability factor versus fresh air content after vibration (effect of admixtures on the air system).....	102
Figure 5.17 Effect of vibration duration on the durability factor with vibration acceleration of 8g at 75 Hz	104
Figure 5.18 Effect of vibration duration on final spacing factor with vibration acceleration of 8g at 75 Hz.....	104
Figure 5.19 Effect of vibration duration on decrease in air content with vibration acceleration of 8 g at 75 Hz	105
Figure 5.20 Effect of vibration duration on final fresh air content (different frequencies and peak accelerations)	106

Figure 5.21 Effect of vibration duration on final hardened air content (different frequencies and peak accelerations).....	106
Figure 5.22 Effect of vibration duration on final spacing factor (different frequencies and peak accelerations)	107
Figure 5.23 Rheological properties for the study of the effect of vibration acceleration	109
Figure 5.24 Effect of vibration acceleration on the freeze-thaw performance of rheological combination 4.....	109
Figure 5.25 Effect of vibration acceleration on the increase in the spacing factor of rheological combination 4.....	110
Figure 5.26 Effect of vibration acceleration on the decrease in the air content of rheological combination 4.....	110
Figure 5.27 Effect of vibration acceleration on the hardened spacing factor of rheological combination 4.....	111
Figure 5.28 Effect of vibration acceleration on the hardened air content of rheological combination 4.....	111
Figure 5.29 Effect of vibration acceleration on the freeze-thaw performance of rheological combination 1.....	112
Figure 5.30 Effect of vibration acceleration on the final spacing factor of rheological combination 1.....	113
Figure 5.31 Effect of vibration acceleration on the final air content of rheological combination 1	113
Figure 5.32 Rheological properties for the study of the effect of vibration frequency	115
Figure 5.33 Effect of vibration frequency on the freeze-thaw performance of rheological combination 4.....	115
Figure 5.34 Effect of vibration frequency on the final spacing factor of rheological combination 4.....	116
Figure 5.35 Effect of vibration frequency on the final air content of rheological combination 4	116
Figure 5.36 Effect of vibration frequency on the freeze-thaw performance of rheological combination 1.....	117

Figure 5.37 Effect of vibration frequency on the final spacing factor of rheological combination 1.....	118
Figure 5.38 Effect of vibration frequency on the final air content of rheological combination 1	118
Figure 5.39 Rheological properties for the study of the effect of vibration velocity.....	119
Figure 5.40 Effect of peak vibration velocity on the freeze-thaw performance of rheological combination 4.....	120
Figure 5.41 Effect of vibration velocity on the final spacing factor of rheological combination 4	120
Figure 5.42 Effect of vibration velocity on the final air content of rheological combination 4 .	121
Figure 5.43 Effect of peak vibration velocity on the freeze-thaw performance of rheological combination 1.....	122
Figure 5.44 Effect of vibration velocity on the final spacing factor of rheological combination 1	122
Figure 5.45 Effect of vibration velocity on the final air content of rheological combination 1 .	123
Figure 5.46 Rheological properties of rheological combination 4 of chemical admixture combination A for the study of the effect of air content before vibration	124
Figure 5.47 Effect of air content before vibration on the freeze-thaw performance of rheological combination 4 of chemical admixture combination A.....	125
Figure 5.48 Rheological properties of rheological combination 1 and 4 of chemical admixture combination C for the study of the effect of air content before vibration	126
Figure 5.49 Effect of air content before vibration on the freeze-thaw performance of rheological combination 1 and 4 of chemical admixture combination C	127
Figure 5.50 Effect of dynamic yield stress on the freeze-thaw durability	128
Figure 5.51 Effect of plastic viscosity on the freeze-thaw durability	128
Figure 5.52 Effect of dynamic yield stress on the final air content	129
Figure 5.53 Effect of dynamic yield stress on the final spacing factor.....	129
Figure 5.54 Durability factor versus spacing factor before vibration.....	131
Figure 5.55 Durability factor versus spacing factor after vibration.....	131
Figure 5.56 Durability factor versus fresh air content before vibration	132
Figure 5.57 Durability factor versus hardened air content before vibration.....	133

Figure 5.58 Durability factor versus hardened air content after vibration.....	133
Figure 5.59 Final length change versus spacing factor after vibration	134
Figure 5.60 Durability factor versus final length change	135
Figure 5.61 Final weight change versus spacing factor after vibration	136
Figure 5.62 Durability factor versus final weight change.....	136
Figure 5.63 Rheological properties for the immersion vibrator experiment	137
Figure 5.64 Freeze-thaw performance of rheological combination 4 (immersion vibrator experiment)	138
Figure 5.65 Freeze-thaw performance of rheological combination 3 (immersion vibrator experiment)	138
Figure 5.66 Rheological data for mixture 1 at a vibration frequency of 72.81 Hz and weight offset ID # 1	143
Figure 5.67 Rheological data for mixture 1 at a vibration frequency of 73.35 Hz and weight offset ID # 2	144
Figure 5.68 Rheological data for mixture 1 at a vibration frequency of 73.9 Hz and weight offset ID # 3	144
Figure 5.69 Rheological data for mixture 1 at a vibration frequency of 75 Hz and weight offset ID # 4	145
Figure 5.70 Rheological data for mixture 1 at a vibration frequency of 94.93 Hz and weight offset ID # 1	145
Figure 5.71 Rheological data for mixture 1 at a vibration frequency of 95.64 Hz and weight offset ID # 2	146
Figure 5.72 Rheological data for mixture 1 at a vibration frequency of 116.16 Hz and weight offset ID # 4	146
Figure 5.73 Rheological data for mixture 2 at a vibration frequency of 72.81 Hz and weight offset ID # 1	147
Figure 5.74 Rheological data for mixture 2 at a vibration frequency of 73.35 Hz and weight offset ID # 2	147
Figure 5.75 Rheological data for mixture 2 at a vibration frequency of 73.9 Hz and weight offset ID # 3	148

Figure 5.76 Rheological data for mixture 2 at a vibration frequency of 75 Hz and weight offset ID # 4	148
Figure 5.77 Rheological data for mixture 2 at a vibration frequency of 94.93 Hz and weight offset ID # 1	149
Figure 5.78 Rheological data for mixture 2 at a vibration frequency of 95.64 Hz and weight offset ID # 2	149
Figure 5.79 Rheological data for mixture 2 at a vibration frequency of 116.16 Hz and weight offset ID # 4	150
Figure 5.80 Rheological data for mixture 5 at a vibration frequency of 72.81 Hz and weight offset ID # 1	150
Figure 5.81 Rheological data for mixture 5 at a vibration frequency of 73.35 Hz and weight offset ID # 2	151
Figure 5.82 Rheological data for mixture 5 at a vibration frequency of 73.9 Hz and weight offset ID # 3	151
Figure 5.83 Rheological data for mixture 5 at a vibration frequency of 75 Hz and weight offset ID # 4	152
Figure 5.84 Rheological data for mixture 5 at a vibration frequency of 94.93 Hz and weight offset ID # 1	152
Figure 5.85 Rheological data for mixture 5 at a vibration frequency of 95.64 Hz and weight offset ID # 2	153
Figure 5.86 Rheological data for mixture 5 at a vibration frequency of 116.16 Hz and weight offset ID # 4	153
Figure 5.87 Vibration parameter versus average peak velocity at 6 in. deep inside mixtures 1, 2, and 5	155
Figure 5.88 Average vibration parameter for mixtures 1, 2, and 5 versus average peak velocity on the vibrating table	155
Figure 5.89 Average vibration parameter for mixtures 1 and 5 versus average peak velocity on the vibrating table	156
Figure 5.90 Rheological data for mixture 4 at a vibration frequency of 72.81 Hz and weight offset ID # 1	158

Figure 5.91 Rheological data for mixture 4 at a vibration frequency of 73.35 Hz and weight offset ID # 2	158
Figure 5.92 Rheological data for mixture 4 at a vibration frequency of 73.9 Hz and weight offset ID # 3	159
Figure 5.93 Rheological data for mixture 4 at a vibration frequency of 75 Hz and weight offset ID # 4	159
Figure 5.94 Rheological data for mixture 4 at a vibration frequency of 94.93 Hz and weight offset ID # 1	160
Figure 5.95 Rheological data for mixture 4 at a vibration frequency of 95.64 Hz and weight offset ID # 2	160
Figure 5.96 Rheological data for mixture 4 at a vibration frequency of 116.16 Hz and weight offset ID # 4	161

List of Tables

Table 3.1 Chemical and physical properties of cement	53
Table 3.2 Basic concrete mixture proportions	55
Table 3.3 Concrete mixture properties.....	56
Table 3.4 Mixture proportions of externally vibrated mixtures for target air content of 3.5% to 4.5%	58
Table 3.5 AEA dosages of mixtures used to study the effect of initial air content	58
Table 3.6 Mixture proportions of internally vibrated mixtures	59
Table 3.7 Concrete mixture proportions for the "rheology under vibration" study.....	59
Table 3.8 Quantities of mixtures' constituents for the "rheology under vibration" study.....	60
Table 5.1 Slump values of mixtures 1, 2, 3, 4 and 5.....	139
Table 5.2 Frequency and peak acceleration readings on the vibrating table	139
Table 5.3 Frequency and peak acceleration readings inside mixtures 1, 2, 4, and 5	140
Table 5.4 Rheological properties of mixtures 1, 2, and 5	142
Table 5.5 Vibration parameter (γ_v) for mixtures 1, 2, and 5	142
Table 5.6 Predicted rheological properties of mixture 4.....	157
Table 5.7 Predicted rheological properties of mixture 2.....	161

Acknowledgements

It is a pleasure and an honor to express my deepest gratitude to my family, friends, colleagues, teachers, committee members and supervisor whom I am extremely indebted for their friendship, kindness and support.

Initially, I would like to thank Allah for his mercy and blessings in the life he gave me and for the bestowment of Islam upon me and the people I love. Secondly, I would like to thank my beloved parents whom without their love, support and encouragement I would have never been able to reach whatever I have fulfilled so far in my life. My special thanks to my supervisor, Dr. Kyle Riding, for his patience, assistance and guidance over the past three and a half years which greatly contributed to the successful completion of this dissertation. Also, I would like to thank my committee members for their encouragement, support and valuable comments. I would like also to thank all honest members of the Department of Civil Engineering and the entire community of Kansas State University. Many thanks for the Federal Railroad Administration (FRA) for their financial support.

Dedication

To whom I am willing to sacrifice my life for theirs

Chapter 1 - Introduction

1.1. Background

Prestressed concrete railroad ties, such as those shown in Figure 1.1, are often used in the railroad industry on new track, heavy-haul rail lines, and high speed rail lines. These are usually made with large dosages of high-range water reducers (HRWR) in order to enable the use of low-water-cementitious-material-ratio (w/cm) concrete mixtures to achieve high early strengths necessary for increased form reuse and productivity. Even in plants that use very fluid concrete, these concrete mixtures are typically vibrated to consolidate the concrete and reduce the occurrence of bug holes on the concrete surface. However, vibration of low w/cm concrete with high dosages of chemical admixtures may cause air entrainment loss and reduced freeze-thaw durability.



Figure 1.1 Pre-stressed concrete railroad ties

Figure 1.2 shows the studied factors that contribute to the freeze-thaw performance of concrete. Chemical admixtures play an important role in forming the air void structure of concrete. Air-entraining admixtures (AEAs), for instance, are designed to create small well-spaced air bubbles inside concrete. Some HRWRs, on the other hand, produce unstable, relatively large air bubbles. The parameters of vibration (i.e., frequency, acceleration, and

duration) and the rheological properties of concrete determine the amount of liquefaction fresh concrete experiences. In other words, they determine the apparent viscosity at which the concrete flows. Apparent viscosity relates to the amount of air that escapes from fresh concrete during vibration. All mentioned factors help form the air void system of the final product. Air void parameters (i.e., air content, spacing factor, and specific surface) are the most influential factors for freeze-thaw resistance of concrete. Details regarding the relationship between these factors are described in Chapter 2.

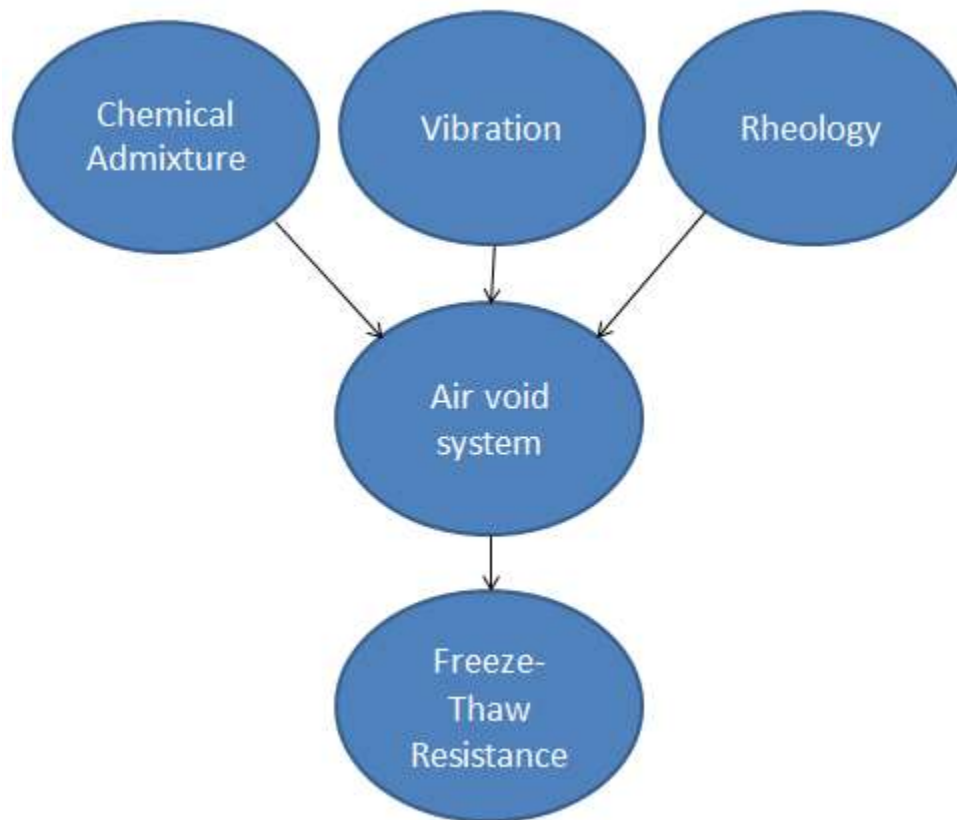


Figure 1.2 Factors contributing to freeze-thaw performance

1.2. Scope of Research

The objective of this research is to quantify the effects of vibration on the entrained air system and freeze-thaw durability of concrete containing low w/cm. The objective was fulfilled by examining:

1. The effects of time from mixing until vibration on air entrainment loss.
2. The effects of chemical admixture combinations on the air entrainment system and freeze-thaw durability.
3. The effects of vibration properties and concrete rheology on air entrainment loss and freeze-thaw durability.
4. Air entrainment requirements to achieve freeze-thaw durability.
5. The possibility of obtaining rheological properties of stiff concrete mixtures by measuring their rheology under vibration.

1.3. Organization of Dissertation

Chapter 2 gives theoretical backgrounds about freeze-thaw and each of the factors contributing to the freeze-thaw durability of concrete. It also talks about the existing knowledge related to the objective. Chapter 3 describes the materials characteristics and mix proportions used in this research. Chapter 4 details descriptions of the equipment used and the methods adopted to carry out the experiments necessary to fulfill the objective. Chapter 5 discusses the results obtained in this research. Chapter 6 provides a summary of the work done, concluding remarks and recommendations for future work.

Chapter 2 - Literature Review

2.1. Freeze-Thaw

Freeze-thaw damage of concrete is a significant cause of deterioration in cold climates. Concrete subjected to repeated cycles of freezing and thawing can result in excessive damage to the concrete, manifesting as internal cracking or surface scaling [1]. The most common theories attribute internal cracking damage to either freezing water inside the pores of concrete or hydraulic pressure caused by flowing water in the concrete pores during freezing. Because pore volume and size determine water content and permeability, they play an important role in the rate of freeze-thaw deterioration [1]. Pores are present in both aggregates and cement paste. Although aggregates generally comprise a majority of the concrete, they usually have low porosity. However, there are some types of aggregates that are susceptible to freeze-thaw damage due to their high porosity. If the aggregates are freeze-thaw resistant, the durability of concrete is a function of the air void distribution inside the cement paste. Pores are formed inside the cement paste during the mixing and hydration process. Water reacts with cement leaving behind voids that are not filled completely with the hydration products [1]. These voids are called capillary pores and they range in diameter from 5 nm to 1 μm . The size and amount of these pores decrease with increased degree of hydration. They also decrease with reduction in w/cm. Therefore, concrete mixtures with higher w/cm can be more susceptible to freeze-thaw damage [1]. Cement paste also contains pores that are smaller than the capillary voids. These pores are referred to as gel pores, and they are formed when water bonds on the surfaces of the hydrates [1]. Air voids are also introduced into the concrete through the mixing action. Pores of 1 to 10 mm in diameter are formed due to the entrapment of the air from the atmosphere while mixing [1].

Water freezing inside the cement paste occurs as a result of high humidity (i.e., high moisture absorption) and low temperatures. High humidity ensures the presence of water, while low temperatures freeze the water and cause damage from water flow and expansion [1]. The temperature at which ice forms varies depending on the size of the pores. Very small pores, such as gel pores, are highly pressurized, thereby preventing resident water from freezing under normal freezing temperatures (i.e., as low as -40°C). Large pores, such as entrapped and entrained air voids, are big enough to stay unsaturated and allow water to freeze without inflicting damage on the surrounding cement paste [1]. The entrained air voids are also typically designed to stay dry in order to attract the water during freezing. The capillary voids are believed to be the ones responsible for freeze-thaw damage in concrete. They have sizes that are big enough to cause ice formation under normal freezing temperatures and small enough to quickly become saturated with water [1].

There are several procedures that can be used to reduce freeze-thaw damage. The use of low w/cm concrete mixtures reduces concrete degree of saturation through self-desiccation and reduction in permeability to reduce the rate of water ingress [1]. Proper handling, placing and curing are also very important factors affecting freeze-thaw durability, especially salt scaling [2]. Scholer reported that many studies showed the significance of the construction practices when it comes to durability of concrete [3]. Extended mixing can also result in harmful effects on the air system and thus the freeze-thaw resistance of concrete [2]. Careful selection of constituent materials of concrete mixtures, especially sound aggregates, is also very crucial [4]. The most common and most effective technique for freeze-thaw protection is to add AEAs to the concrete mixtures. If the concrete contains sufficient amounts of well-distributed entrained air voids, then

freezing water in capillary pores can more readily flow to a larger void and freeze without causing damage.

2.1.1. Freeze-Thaw Mechanisms

As mentioned in section 2.1, there are two main types of freeze-thaw damage that can be observed in concrete in cold climates. One of them is surface scaling which is usually caused by the application of de-icer salts on the surface of the concrete during winter. This kind of damage is more common in concrete pavements [1]. Concrete railroad ties, however, are not usually subjected to the application of de-icer salts. Therefore, it is believed that the more common form of damage in concrete railroad ties is internal cracking. Many theories have been put forward to explain the mechanism of freeze-thaw internal damage. The most common ones are hydraulic pressure theory, osmotic pressure theory and Litvan's theory [1].

2.1.1.1. Hydraulic Pressure Theory

The hydraulic pressure theory was developed by Powers as he was trying to calculate the amount of air required to achieve freeze-thaw durability. His hypothesis attributes the freeze-thaw damage to the hydraulic pressure caused by the flow of water through the cement paste [5]. Due to the presence of dissolved chemicals in the water inside the capillary pores, the water freezes gradually as the temperature decreases. In saturated cement pastes, when the ice formation initiates inside capillary pores, it expands causing the unfrozen part of the water to flow to the nearest air void where it can freeze freely. The pressure imposed by the flow of the water is dependent on the porosity of the cement paste, the freezing rate and the distance traveled. The internal cracking occurs if the pressure exceeds the tensile strength of the cement paste [6]. Given the paste characteristics and freezing rate, it is possible to calculate the maximum distance water can travel before starting to cause damage. Extending this maximum

distance from the surface of each air void in all directions results in what Powers called the “sphere of influence” [1] (Figure 2.1). If the cement paste contains sufficient air voids that are well-spaced such that all spheres of influence are intersecting with each other, then the concrete is assumed to be freeze-thaw resistant. Therefore, the spacing between the air voids is the most crucial parameter according to this theory. Figure 2.1 illustrates the difference between bad and good air void distribution.

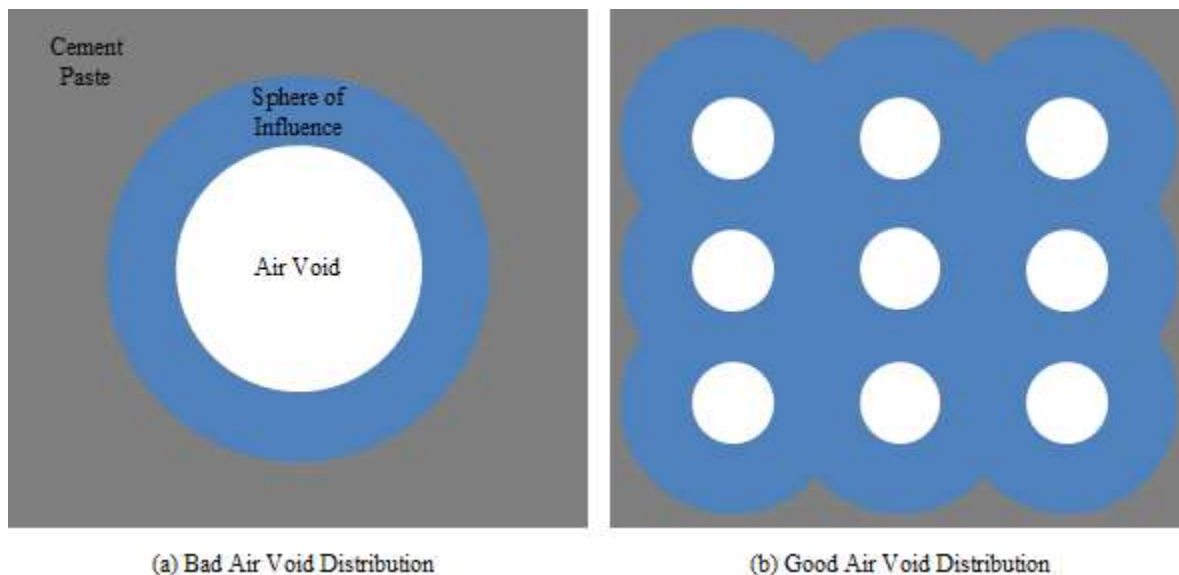


Figure 2.1 Bad versus good air void distribution

Powers also proposed an experimental method to estimate the average value of the maximum distance water has to travel to reach an air void in a concrete specimen. This value is called the spacing factor and is roughly an estimate of the average of half the distance between the surfaces of two adjacent air voids [1]. This method has been adopted by the American Society for Testing and Materials (ASTM) C457 [7]. It was discovered later by Powers that the hydraulic pressure theory is invalid due to experimental evidence which showed that the water actually flows into rather than from capillary pores. However, there were still many experimental evidences supporting many of this theory’s ideas such as the fact that the spacing between air voids is an important factor in determining freeze-thaw durability [1].

2.1.1.2. Osmotic Pressure Theory

Powers and Helmuth discovered that, during a freezing event, cement paste with a good air entrainment system can shrink due to the movement of the water to the capillary pores. They also found out that water trapped in smaller pores requires lower temperatures to freeze. Moreover, it was revealed that ice formation in the capillary pores was much smaller than what the thermodynamic laws suggest. Therefore, the osmotic pressure theory suggests that when the water temperature is sufficiently below 0 °C, water starts to freeze in some of the capillary pores which results in the ionic concentration increasing in the water solution. Ice continues to form until the water concentration is high enough to make the melting point equal to the current temperature [1]. Water of lower concentrations starts flowing from the gel pores to the capillary pores [5]. Consequently, the water concentration in the capillary pores reduces again causing additional ice buildup. According to this theory, damage occurs both due to water flow and ice formation [1]. Powers hypothesized that the role of air voids manifests in being a competitor to the capillary pores. It is observed that air voids normally have a little bit of water which would be the first to start freezing due to the larger size of these voids. Therefore, they would start attracting water from smaller pores. If there are sufficient air voids, they will be able to attract all water and protect the paste from freeze-thaw damage. However, according to this theory, there will never be complete protection due to the fact that there will always be capillary pores half-way between two air voids where water in close gel pores will be attracted to it [1]. This could either mean there is a flaw in this theory or there is no way to provide complete protection against freeze-thaw damage.

2.1.1.3. Litvan's Theory

Litvan developed a theory explaining the freeze-thaw mechanism in all porous materials [1]. His experiments showed that water does not freeze in the capillary pores when the temperature is below 0 °C. The water is instead supercooled resulting in drying caused by the high vapor pressure over supercooled water. If the cement paste is saturated, ice will form on all faces of the cement paste including the walls of the pores. The pressure of the water vapor over ice is, however, much lower than that over supercooled water inside the capillary pores. This pressure difference increases as the temperature decreases creating more imbalance. Equilibrium cannot be achieved unless the vapor pressure over supercooled water is equal to that over ice. This occurs if the water inside capillary pores freezes; however, this did not appear to happen in Litvan's experiments. The other way to achieve equilibrium is through the migration of water from capillary pores to empty air voids. If this migration occurs over long enough distances, freeze-thaw damage can happen due to forced movement of water [1]. Moreover, Litvan hypothesized that if the temperatures are very low and the freezing rate is very high, water might freeze during migration before reaching an air void causing very high internal stresses inside the cement paste, leading to freeze-thaw damage [1]. This theory explains well the role of air voids. If the air voids are sufficiently available and well-spaced, the migrating water will have a better chance reaching an air void before freezing while traveling short distances.

2.1.2. Freeze-Thaw Testing

There are many standardized tests available to evaluate the freeze-thaw durability of concrete and its constituents. These include, among others, the critical dilation test (was withdrawn from ASTM standard in 2003), rapid freezing and thawing test (ASTM C666) [8] and salt scaling test (ASTM C672) [9]. The most commonly used procedure in North America is ASTM C666 [8]. There are two different procedures that can be followed to carry out this test.

Both procedure A and procedure B require the thawing cycle to be in water. While procedure A asks for the freezing cycle to occur in water, procedure B freezes the specimens in air [8]. The evaluation of the performance of the concrete specimens under these tests is usually carried out through monitoring the expansion of concrete, weight fluctuations and the relative dynamic modulus of elasticity. These parameters are considered indicators of the state of the internal structure of concrete. Visual observation is also a common tool to examine the performance of concrete under freeze-thaw testing. This is especially crucial in the case of the salt scaling test [9].

2.1.3. Air Entrainment

One of the most important factors in determining the freeze-thaw durability is the spacing between air voids. Air entrainment can be achieved by adding AEAs to the concrete mixtures. These are surfactants consisting of hydrocarbon chains that possess hydrophilic heads and hydrophobic tails [10]. These chains surround air bubbles and stabilize them as shown in Figure 2.2. This stabilization caused by the AEA results in additional spherical well-distributed air voids that range from 0.01 to 1 mm in diameter [1].

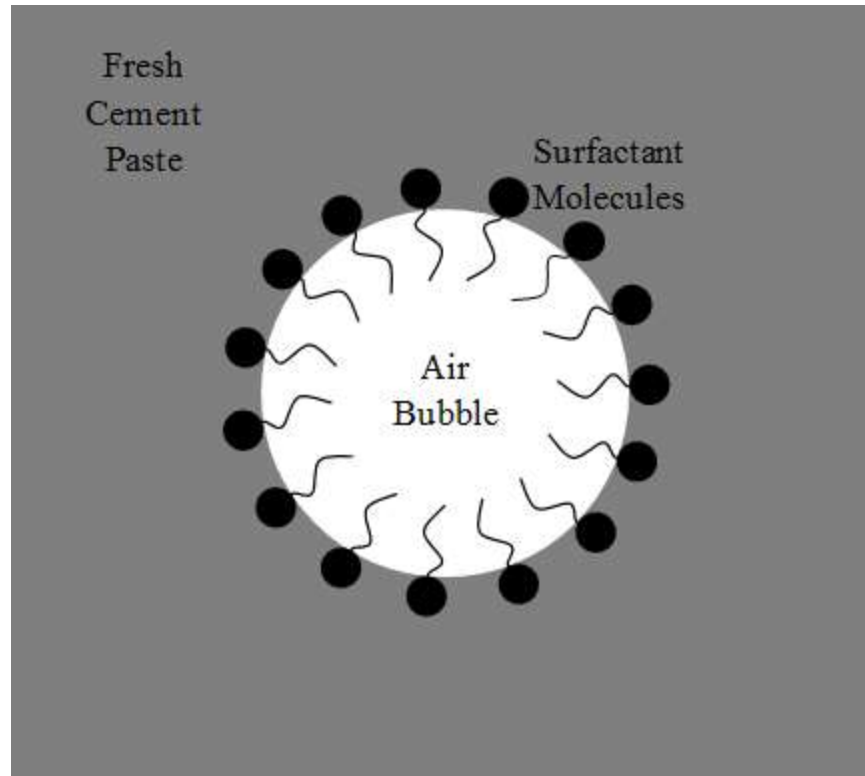


Figure 2.2 Air entrainment mechanism

The most commonly measured parameters of the air void system are the total air content, specific surface and spacing factor. Some recent studies also claim that other air parameters, such as total surface area of air voids [11], can be more representative of freeze-thaw performance. The claims, however, are not supported by sufficient experimental evidence and the explanations are often not convincing. AEAs are often used in concrete mixtures to increase the air content and achieve sufficiently small spacing factors. Air requirements for freeze-thaw resistance have always been a concern since the 1940s [1]. Powers suggested a maximum spacing factor of 0.25 mm necessary to ensure freeze-thaw durability [12]. In reality, Pigeon showed that this critical spacing factor value, for the same materials of the concrete mixture, is dependent on the particular freeze-thaw test. In other words, it depends on the freezing rate, the minimum temperature as well as the moisture condition [1]. This is expected since many studies showed that freeze-thaw performance highly depends on the freeze-thaw testing procedures and

conditions [13]. However, it is widely accepted that a spacing factor of 0.2 mm is sufficiently conservative for the vast majority of concrete mixtures [2].

ASTM C260 [14] contains requirements for AEAs that need to be met before the admixture can be used in concrete. While these requirements stress on certain limits for the most important air parameters (i.e. total air content, specific surface and spacing factor), they neglect a very important aspect of the air system inside concrete which is its stability with time. In other words, there are no specific requirements in ASTM pertaining to the effect of AEA and other chemical admixtures on the change of the effectiveness of the air system with time [1]. There are studies showing several factors that might affect the air system stability of air entrained concrete mixtures. Khayat and Assaad, for example, showed that higher cementitious materials content along with low w/cm can improve the stability of the air system of air entrained self-consolidating concrete (SCC). They also showed that viscosity-modifying admixtures (VMA) can enhance the stability of the air system as well [15]. Other studies showed, however, that VMAs might also decrease air entrainment [16, 17]. The issue of air stability is more pronounced when more than one chemical admixture is used in the concrete mixture (specifically HRWRs). HRWRs are chemical admixtures that are often used in concrete mixtures in order to increase their workability and reduce the w/cm so that high strength concrete can be obtained. They are widely used by concrete railroad tie manufacturers. HRWRs are known to entrain relatively large air bubbles in concrete which can result in larger than intended spacing factor values [9]. Piekarczyk showed through experiments that VMAs and HRWRs from different manufacturers can influence the SCC mixture differently even if they appear to have the same basic chemical composition [18]. She also showed that the admixture type used in the SCC mixture can greatly affect the spacing factor of air voids. Moreover, her results displayed that SCC with spacing

factors larger than the standard's recommended values can still perform well in freeze-thaw testing [19].

2.1.4. Measurement of Air Parameters

There are many tests that are used to measure the various parameters of the air void system inside concrete. For instance, total air content of fresh concrete can be measured using three different standardized methods: pressure method (ASTM C231) [20], volumetric method (ASTM C173) [21] and gravimetric method (ASTM C138) [22]. Air content is usually measured as percentage by volume of concrete. While typical values of total air content in non-air entrained concrete range between 1% and 3%, air entrained concrete can contain, depending on the design, more than 10% air [1]. The volumetric method works by measuring the volume of water needed to replace the air inside concrete via agitation [21]. While this method is not affected by the type of aggregates used, it is not necessarily very accurate due to the need for long periods of agitation. Consequently, this method usually underestimates the air content of concrete [1]. The air content can also be obtained through the gravimetric method by calculating the difference between the actual unit weight of concrete and the theoretical unit weight of concrete obtained from the weights and characteristics of each of the constituents of the concrete mixture [22]. This method, however, is known to be inaccurate because of the additive nature of errors in the material weights, specific gravities, and absorption properties [1]. The pressure method is by far the most widely used method for measuring air content of fresh concrete due to its relatively good precision and ease of use. This method is carried out by applying pressure to a fresh concrete sample, thereby compressing air voids inside the sample. All other constituents of concrete are assumed to be incompressible. The volume of the sample is consequently reduced by an amount equal to the volume of air inside the concrete. The total air content can then be

obtained by calculating either the volume change via a Type A air meter or the pressure change via a Type B air meter [20].

The spacing factor and specific surface of air voids are usually obtained from hardened concrete samples. Total air content can also be obtained from hardened samples as part of calculating the spacing factor and specific surface. It is usually not possible to measure these parameters in a 3D volume of concrete. However, it is common, through the science of stereology, to estimate the 3D air distribution using 2D, 1D and even 0D fields obtained from the same concrete [1]. This is usually done by saw-cutting a concrete prism or cylinder of which one surface is used to carry out the analysis. This surface is then well polished to ensure proper detection of all voids. The sample is then placed under an optical microscope of 50 x to 125 x magnification range [1]. Air parameters from a 2D field can be obtained by recording the diameters of all air voids intercepted on the surface of the specimen. This information along with the total surface occupied by air voids, cement paste and aggregates can then be used to get the required air parameters [1]. Calculations over a 1D field are carried out by scanning the surface of the specimen over a number of lines of traverse. The chords intercepting the air voids, cement paste and aggregates are then recorded and used to calculate the required air parameters [1]. The modified point count method of ASTM C457 [7] corresponds to the utilization of a 0D field of the concrete sample. It is carried out by making similar observations to the previous methods but this time over discretized points distributed along lines of traverse across the surface of the concrete specimen [7]. It is important to note that big entrapped air voids (i.e. larger than 1 mm in diameter) have a very big impact on the obtained value of spacing factor as per ASTM C457 Standard [1]. The fact that the calculations assume all voids to have the same size can result in a relatively large overestimation of the spacing factor if big voids are included in the calculations.

Therefore, many researchers think excluding big air voids results in a spacing factor value that is a better measure of freeze-thaw resistance [1].

The aforementioned hardened air void analysis via microscopical examination of concrete surfaces can prove to be very tedious and time consuming. Consequently, there have been many recent efforts attempting to computerize the process of hardened air void analysis. These methods usually involve scanning the concrete surfaces and devising computer programs capable of analyzing these images and executing the same ASTM C457 calculation procedures within short periods of time. Since it is very difficult for computers to distinguish between air voids, cement paste and aggregates, concrete surfaces are usually subjected to treatments prior to scanning. This often includes coloring the paste and/or aggregates with a stain and filling in air voids with a white or colored powder to give a color contrast between the air voids and rest of the concrete.

2.2. Concrete Vibration

Vibrations are oscillations that are typically emitted with certain frequencies. They can either be natural or man-made designed for certain applications [23]. Fresh concrete is usually subjected to high energy vibrations (i.e. vibrations with high frequencies and accelerations) in order to ensure proper consolidation. This is currently practiced in all concrete railroad tie plants. There are two types of waves that are usually associated with vibration. These are shear and compression waves [24]. Shear waves are oscillations in which particles or masses oscillate in a direction perpendicular to the direction of the propagation of the wave. Compression waves on the other hand excite particles to oscillate in the same direction as the propagation of the wave [24]. The extent to which compression and shear waves can travel through the medium is dependent on the compression and shear properties of the material, respectively. However,

compression properties (i.e. bulk viscosity for Newtonian fluids) can prove to be extremely difficult to obtain for complicated fluids such as fresh concrete. Only one attempt was found in the literature to estimate the compression properties of fresh concrete [25]. In this study, fresh concrete was approached as a solid rather than a fluid. In other words, bulk modulus instead of bulk viscosity was estimated using triaxial compression tests similar to the ones conducted for soils. In these tests, stresses were related to strains instead of strain rates which renders the obtained bulk modulus inapplicable for understanding compressional flow of fresh concrete. There are few rheometers capable of measuring the bulk viscosity of delicate viscous fluids such as the acoustic rheometer. An acoustic rheometer works by imparting successive sound waves (i.e. compression waves) into a fluid then measuring the speed and attenuation of these waves under different frequencies. From this information, compressibility and extensional viscosity of the fluid can then be obtained. Studying the compression properties through the propagation of sound waves is more common for viscoelastic materials such as polymers [26]. The main reason this area is not widely explored for viscous fluids in general is due to the lack of applications. Most applications are concerned about the regular flow of viscous fluids which can be fully understood by considering only the shear behavior while assuming incompressibility of the fluid [27]. Vibration, however, is one of the rare applications in which compression properties are very crucial. Shear waves are usually neglected, especially in the science of earthquake engineering due to the fact that they die very quickly relative to the compression waves [24]. This is due to the lower shear properties compared to the compression properties of all materials. This leads to the conclusion that compression properties are more important compared to shear properties when it comes to vibration. However, there is no existing rheometer capable of measuring the compression properties of concrete. It is generally assumed, like other fluids, that

the compression properties of fresh concrete are proportional to its shear properties. It is true that the rise of air bubbles in fresh concrete is dependent on its shear viscosity but that does not mean that shear waves are more important and that compression waves should be neglected. In fact, compression waves can also shear the fluid if more than one compression wave is imparted into the fluid from different directions which is the case for external vibrators of concrete.

When vibration is being discussed, vibration of solid masses is usually considered rather than attenuation of vibrations inside a continuum. In other words, it is more common to talk about single or multiple degrees of freedom discrete systems. This approach to vibration might be applicable to understand the mechanism of how vibrators work but cannot be used to capture the attenuation of vibration inside a fluid. For instance, consider Equation 2.1 for the forced vibration of single degree of freedom systems [28]:

$$m \frac{d^2x}{dt^2} + c \frac{dx}{dt} + kx = F(t) \quad \text{Equation 2.1}$$

Where:

m =Mass

x =Displacement

t =Time

c =A function of the mass, stiffness and damping factor

k = Stiffness

$F(t)$ =Time dependent force

There are many types of vibrators among which the most common are reciprocatory (linear) and rotary (i.e. harmonic) vibrators [23]. Fresh concrete is usually vibrated using steel rotary vibrators that are either applied internally (i.e. immersion vibrators) or externally (i.e. form vibrators or vibrating screeds). These vibrators force oscillations via a rotating imbalance

(i.e. by offsetting the center of rotation from the center of weights attached to the vibrating motor). This rotating imbalance will create harmonic waves (i.e. sinusoidal waves) of a certain frequency. It is possible to show that the solution for Equation 2.1 will also be a harmonic wave of the same frequency [29]. Therefore, the steel surface in contact with the concrete will emit sinusoidal waves that can be represented as shown in Equation 2.2:

$$x = x_0 \sin(2\pi ft) \quad \text{Equation 2.2}$$

Where:

x_0 =Amplitude of the wave proportional to the offset of the rotating imbalance

f =Frequency of the wave equal to the frequency of the vibrating motor.

Considering the immersion vibrator shown in Figure 2.3, it is possible to explain how this rotary movement can emit both compression and shear waves inside the fresh concrete.

Figure 2.4 shows a sketch of a cross section of a rotating vibrator, showing the offset between the center of mass (C) and the center of rotation (O). This offset will cause each point on the surface of the vibrator to move in a circular path with a radius equal to the offset. For a certain point (P) on the surface of the vibrator, one can decompose the rotation into two linear movements: one perpendicular to the surface and the other tangent to the surface. The perpendicular movement will cause a compression wave whereas the tangent one will cause a shear wave.



Figure 2.3 Immersion vibrator

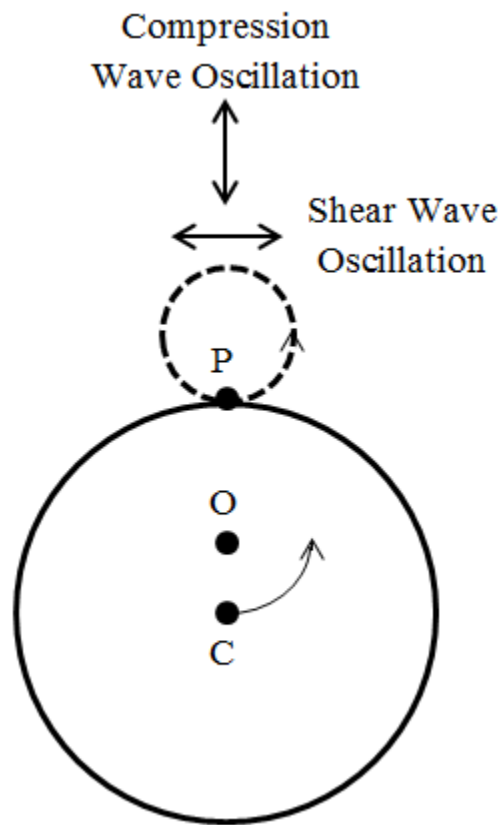


Figure 2.4 Immersion vibrator mechanism

A similar mechanism is also present in the table vibrator shown in Figure 2.5. This vibrator has a rotating motor attached to the bottom of its top plate. The motor will cause the table, including any steel forms attached to the top plate, to rotate. The circular movement of each surface of the steel forms can similarly be broken down into two linear movements creating shear and compression waves inside the concrete that is filling the form.

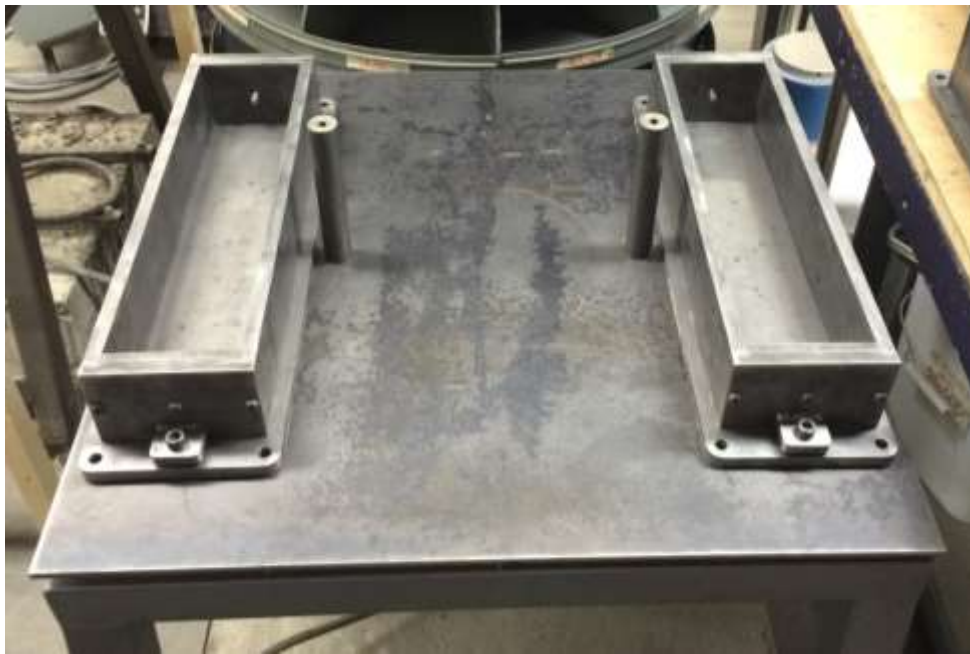


Figure 2.5 Table vibrator

Equation 2.1 is not applicable to understand the propagation of waves inside concrete and their effect on the apparent viscosity of fresh concrete. This is because Equation 2.1 deals with discrete masses rather than continuums. In the field of fluid-structure interaction, the term “acoustic radiation” is often encountered when vibration analysis is taking place [30]. This term refers to the sound waves (i.e. compression waves) that are emitted in the fluid during a vibration event of a structure in contact with a fluid. In these applications, the fluid is often considered inviscid [31] since shear properties are not important due to the fact that shear waves die very quickly inside fluids. This assumption, however, cannot be applied here since the reduction in

apparent viscosity of concrete caused by vibration is believed to be the cause for air bubble rise as discussed in a section 2.4. Attenuation of vibrations inside fresh concrete can only be understood through adopting the Eulerian approach to fluid mechanics. There are many books discussing the application of the differential equation of motion to the study of vibrations in continuous systems [29]. While these books often only discuss vibrations in solids, applying the same equation of motion to fluids is very similar as discussed in the next paragraph. The only difference is that, when it comes to the constitutive law (i.e. science of rheology), stresses are related to strain rates instead of strains. More details about the constitutive law can be found in section 2.3.

It is possible through conservation of mass and the divergence theorem to obtain the continuity equation for compressible fluids shown in Equation 2.3 [27]:

$$\frac{\partial \rho}{\partial t} + \vec{\nabla} \cdot (\rho \vec{v}) = 0 \quad \text{Equation 2.3}$$

Where:

ρ =Density

$\vec{\nabla}$ =Gradient vector

\vec{v} =Velocity vector

Conservation of linear momentum can be applied to obtain Equation 2.4 which is Cauchy's equation (i.e. equation of motion) for compressible fluids [27]:

$$\frac{\partial}{\partial t} (\rho \vec{v}) + \vec{\nabla} \cdot (\rho \vec{v} \vec{v}) = \rho \vec{g} + \vec{\nabla} \cdot (\sigma_{ij}) \quad \text{Equation 2.4}$$

Where:

$\vec{v} \vec{v}$ =Outer product of the velocity vector with itself

$\rho \vec{g}$ =Body force

σ_{ij} =Stress tensor

Equation 2.3 and Equation 2.4 are applicable for any type of fluid since no simplifying assumptions were made. These equations along with the vibration boundary conditions can be used to capture the attenuation of vibrations in fresh concrete. The only thing lacking is the relation between the stress tensor and the strain rate tensor (i.e. the partial derivatives of the velocities with respect to space). This relation depends on the type of the fluid and can be established through the constitutive law which will be discussed in section 2.3. Equation 2.4, however, can prove to be extremely difficult to solve without making simplifying assumptions. A reasonable assumption about the stress tensor is often made to simplify Cauchy's equation to the Navier-Stokes Equation 2.5 which is still considered almost as complex [27]:

$$\frac{\partial}{\partial t}(\rho \vec{v}) + \vec{\nabla} \cdot (\rho \vec{v} \vec{v}) = \rho \vec{g} + \vec{\nabla} \cdot (\tau_{ij}) - \vec{\nabla} p \quad \text{Equation 2.5}$$

Where:

p =Hydrostatic pressure

σ_{ij} =Deviatoric stress tensor

Additional assumptions are often made to obtain simpler forms of the equation of motion but these assumptions don't necessarily apply to fresh concrete under vibration. Such assumptions include incompressible flow, isothermal flow or Newtonian behavior of the fluid. In the case of vibration, compressibility of the flow might be crucial for the attenuation of compression waves. On the other hand, the assumption of isothermal flow or Newtonian behavior of the fluid is not applicable for concrete since it implies constant viscosity which is not the case for fresh concrete. It is therefore evident that the complexity of the equation of motion along with the difficulty of obtaining compression properties makes it very difficult to theoretically study the attenuation of vibration in fresh concrete.

2.3. Rheology

Rheology is one of the two essential foundations of a wide range of disciplines. Among these disciplines are hydraulics, fluid mechanics, strength of materials and plasticity. The other foundation for these disciplines is the science of mechanics [32]. Rheology can be defined as the science of deformation and flow of bodies including solids and fluids [33]. Deformation is the alteration of shape or size of bodies under the application of forces. In the context of rheology, an appropriate definition of flow would be the continuous change of the degree of deformation of bodies. Based on rheological properties, bodies can be classified under one of three major categories. These categories are solid, fluid, and plastic. A body is said to be solid if it undergoes deformation under the application of any inhomogeneous force system without undergoing flow no matter how large the applied force. On the other hand, if the body is a fluid, it will flow under the application of any inhomogeneous and anisotropic force system no matter how small the applied force. A plastic body, such as fresh concrete, however, can behave like both solids and fluids depending on the value of the applied force. If the applied force is above a certain critical value, called the yield value, the body will behave like a fluid; otherwise, it will act like a solid [32].

In molecular mechanics, the behavior of the body is determined by studying the properties of the molecules and the intermolecular forces rather than looking at the body as a continuum. In many other branches of science, however, it is more convenient to ignore the molecular structure and deal with the body as a continuum. Rheology is one of these sciences. One should keep in mind that the continuum approach is an approximation and in some cases can yield incorrect results. An example of such cases would be a dilute gaseous substance where there will be non-negligible volumes in which there are no gas molecules at all [32]. For fresh

concrete, however, the continuum approach is a good approximation since fresh concrete behaves more like a liquid where the molecules are always sufficiently close to one another.

2.3.1. Introduction to the Mathematics of Rheology

One of the most fundamental concepts that describe the kinematics of deformation and flow of bodies is the concept of strain and rate of strain [34]. Strains in materials are unitless measures of deformations that arise from the application of a force system [32]. Rotations and translations are types of movements that do not fall under deformation since they do not result in any change in shape or size of the body. Thus, such movements do not produce any strains in the body and therefore contribute only to rigid body motion [32]. There are two classes of deformations (strains) that a body can undergo. One is the volumetric strains class which is responsible for compression (decrease in volume) and dilation (increase in volume) caused by isotropic external pressure or tension respectively. This class of deformation alters the size of the body while leaving its shape intact. The other class of deformations is called the shearing strains class which alters the shape, but not the size, of the body [33]. The shearing strain between two points in a body is defined as one-half of the tangent of the angle (γ) formed between the line connecting the two points in the undeformed configuration and the line connecting the two points in the deformed configuration as shown in Figure 2.6. The shearing strain rate between two points in a body is the change in shearing strain with respect to time [32].

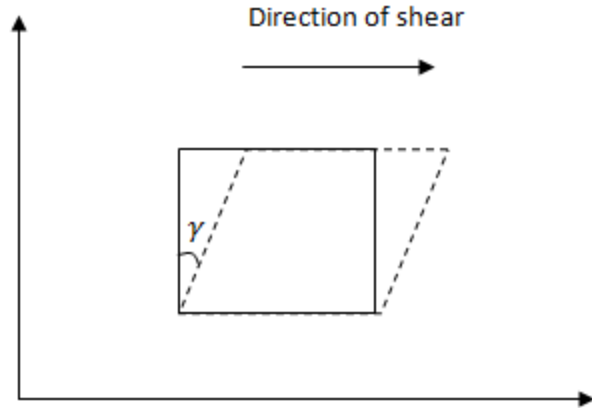


Figure 2.6 Simple shear of a two-dimensional body

The shearing strain (ϵ_{xy}) with respect to a point “P” at a time “t” for a 2-D body caused by shearing forces in both the x-direction and the y-direction is shown in Equation 2.6 [32]:

$$\epsilon_{xy}(P, t) = \frac{1}{2} \left(\frac{\partial u_x}{\partial y} + \frac{\partial u_y}{\partial x} \right) \quad \text{Equation 2.6}$$

Where:

u_x =Displacement in the x direction

u_y =Displacement in the y direction

The shearing strain rate (ϵ_{xy}^*) would then be as shown in Equation 2.7 [32]:

$$\epsilon_{xy}^*(P, t) = \frac{1}{2} \frac{\partial}{\partial t} \left(\frac{\partial u_x}{\partial y} + \frac{\partial u_y}{\partial x} \right) = \frac{1}{2} \left(\frac{\partial v_x}{\partial y} + \frac{\partial v_y}{\partial x} \right) \quad \text{Equation 2.7}$$

Where:

v_x =Velocity in the x-direction

v_y =Velocity in the y-direction

If the shear is to be applied in one direction then one of the velocity derivatives will vanish from Equation 2.7, resulting in what is known as simple shear. If, however, equal strain rates are considered then the aforementioned strain rate becomes as shown in Equation 2.8 producing what is called pure shear:

$$\varepsilon_{xy}^*(P, t) = \frac{\partial v_x}{\partial y} \quad \text{Equation 2.8}$$

Applying two equal shears in opposite directions results in a zero strain rate which corresponds to a rigid body rotation rather than deformation [32]. One can also define another quantity called vorticity (ω_z) which is a measure of the rate of rotation. It is shown in Equation 2.9 [32]:

$$\omega_z(P, t) = \frac{1}{2} \left(\frac{\partial v_x}{\partial y} - \frac{\partial v_y}{\partial x} \right) \quad \text{Equation 2.9}$$

One can now summarize the motions of a body as translations, rotations and strains which consist of volumetric strains and shearing strains. Rheological properties, however, are determined by examining only the volumetric and shearing strains, specifically, by looking at the relation between the stress and the rate of strain [32]. The general equation for the rate of strain tensor for 3-D bodies can be derived mathematically obtaining what is shown in Equation 2.10 [32]:

$$\varepsilon_{ij}^* = \frac{1}{2} (v_{i,j} + v_{j,i}) \quad \text{Equation 2.10}$$

Where:

ε_{11}^* , ε_{22}^* and ε_{33}^* =Volumetric rates of strain

ε_{ij}^* for $i \neq j$ =Shearing rates of strain

$v_{i,j}$ =Derivatives of velocities in the i^{th} direction with respect to the j^{th} direction

This rate of strain tensor takes care of all volumetric and shearing strains that 3-D bodies might undergo. However, it is possible to attribute all deformations in a body to volumetric strains alone by a certain change of coordinates. This change of coordinates can be carried out by solving the eigenvalue problem shown in Equation 2.11 [32]:

$$(\boldsymbol{\varepsilon}^* - \lambda \mathbf{I})\mathbf{n} = 0 \quad \text{Equation 2.11}$$

Where:

$\boldsymbol{\varepsilon}^*$ =Rate of shear tensor

\mathbf{I} =Identity tensor

λ =Eigenvalue

\mathbf{n} =Eigenvector

One can obtain from this system three eigenvalues ($\lambda_1, \lambda_2, \lambda_3$) which correspond to rates of volumetric strain in the new coordinate system that does not contain any rates of shearing strain. Associated with these eigenvalues, are three eigenvectors ($\mathbf{n}_1, \mathbf{n}_2, \mathbf{n}_3$) which determine the three orthogonal directions corresponding to the new coordinate system. The obtained eigenvalues are called the principal rates of strain while the eigenvectors are called the principal axes [34].

2.3.1.1. The Constitutive Relation

After looking at the deformations that can occur in bodies, it is possible to construct a relation between the rate of shear and the shearing stress by considering the internal forces in flowing fluids. Such relation becomes easy to establish by studying the flow of fluids through long slender tubes of circular cross section [32]. The relation between the rate of shear (ε_{ij}^*) and the shearing stress (τ_{ij}) is obtained to be as shown in Equation 2.12 [32]:

$$\varepsilon_{ij}^* = \frac{1}{8} \tau_{ij} \left(\frac{d\xi_{ij}}{d\tau_{ij}} + 3 \frac{\xi_{ij}}{\tau_{ij}} \right) \quad \text{Equation 2.12}$$

Where:

ξ_{ij} =Function of the shearing stress

ξ_{ij} is called the consistency variable since the relation between ξ_{ij} and τ_{ij} describes the consistency of the fluid. The relation between ξ_{ij} and τ_{ij} can be obtained empirically from experimental data [32].

For the classical case of incompressible Newtonian fluid, the relation turns out to be as shown in Equation 2.13 [32]:

$$\xi_{ij} = \frac{1}{\mu} \tau_{ij} \quad \text{Equation 2.13}$$

Where:

μ =Constant of proportionality called the viscosity

This yields the following relation, shown in Equation 2.14, between the rate of shear and the shearing stress which is normally called Newton's law of friction [32]:

$$\varepsilon_{ij}^* = \frac{1}{2\mu} \tau_{ij} \quad \text{Equation 2.14}$$

Stokes generalized Newton's law for compressible fluids by introducing volumetric rates of strain to accommodate both elongational and shear flows. However, after World War I, experimental studies showed that Stokes' law of fluid resistance did not apply successfully for all types of fluids. Several studies showed the existence of a class of fluids that exhibited stress-dependent viscosity such as fresh concrete. These fluids were later called non-Newtonian fluids [32].

2.3.1.2. Rheological Classification of Materials

There are several types of non-Newtonian fluids. Some fluids exhibit a decrease in viscosity with increase in shearing stress (Pseudo-plastic fluids) while others behave the opposite way (Dilatant fluids) [33]. In both of the aforementioned types of fluids, the viscosity approaches a limiting value as the shearing stress increases [32]. Some other bodies behave like an elastic solid if the applied shearing stress is less than the yield stress. If the shearing stress is greater than the yield stress, however, the body will flow like a viscous fluid. These types of bodies are called plastics or "Bingham plastics" [34].

By idealizing the behavior of real materials, one can end up with the rheological classification shown in Figure 2.7. This classification is based on the behavior of materials in shear. Figure 2.7 shows the rheological classification from the least consistent materials (Inviscid fluid), which cannot support shearing stress, to the most consistent materials (Rigid solid) which cannot be deformed under any applied shearing stress [32]. The arrows match materials that have some properties in common.

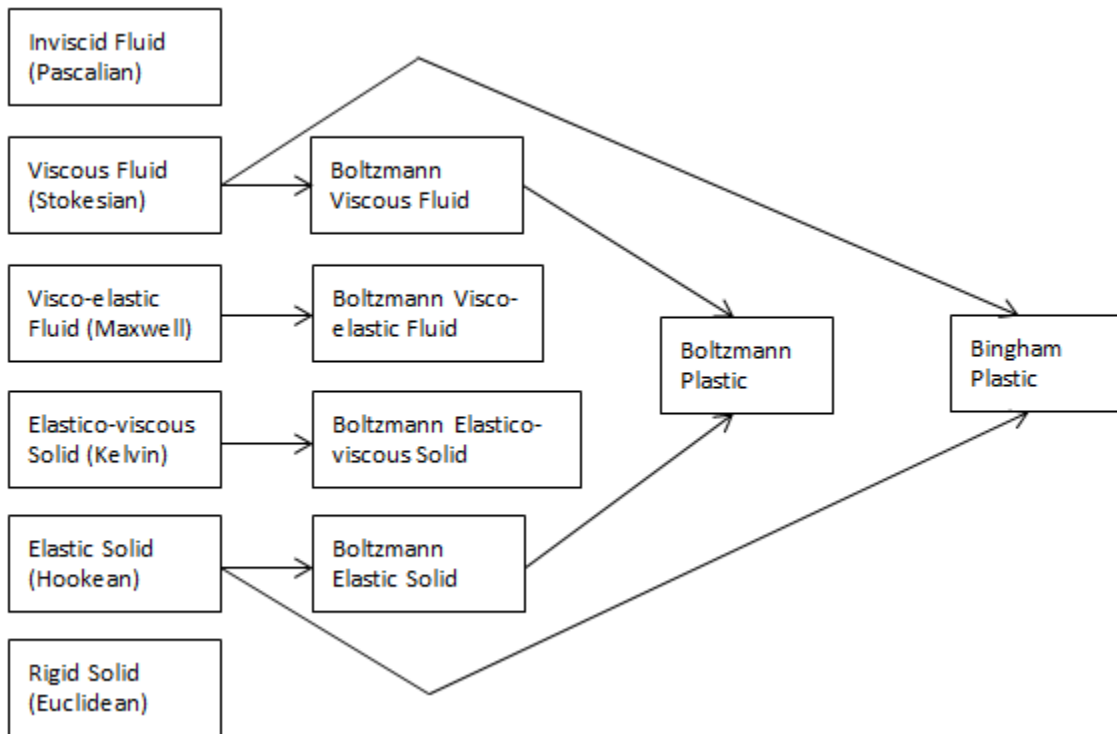


Figure 2.7 Rheological classification of bodies

The most common and convenient way to visualize the different types of behavior shown in Figure 2.7 is by analogy to the behavior of various mechanical models. For instance, the behavior of a viscous fluid is analogous to the behavior of the dashpot assembly shown in Figure 2.8 [35]. This analogy becomes apparent by comparing the rate of extension of the dashpot to the rate of shearing strain in the viscous fluid and the applied force on the dashpot to the shearing stress applied on the viscous fluid. In other words, while the rate of extension of the

dashpot is a function of the applied force, the rate of shearing strain in the viscous fluid is also a function of the applied shearing stress. One ends up with a Newtonian fluid if the function relating the rate of shearing strain to the applied shearing stress is linear. On the other hand, if the function is nonlinear then the resulting fluid is a non-Newtonian fluid exhibiting stress-dependent viscosity [32]. The model for the inviscid fluid is obtained by forcing the viscosity of the fluid in the dashpot to approach zero resulting in negligible resistance to extension [32].

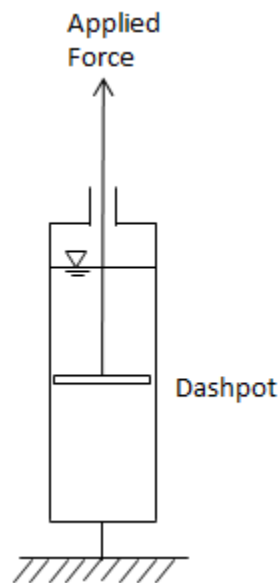


Figure 2.8 Mechanical model of a viscous fluid

The most suitable mechanical model for the elastic solid is the spring shown in Figure 2.9 [35]. In this model, the extension of the spring is analogous to the strain in the elastic solid while the applied force on the spring is analogous to the applied stress on the elastic solid. It is known that the extension in the spring is a function of the applied force. Similarly, the strain in the elastic solid is a function of the applied stress. The removal of the applied force from the spring results in an instantaneous reversion to its unstretched position which matches what happens in the elastic solid after removal of the applied stress. The obtained elastic solid will have a constant modulus of elasticity if the function relating the strain to the applied shear is linear;

otherwise, the obtained elastic solid will have varying modulus of elasticity [32]. The model of the rigid solid is obtained by forcing the stiffness of the spring to approach infinity resulting in an inextensible spring [32].

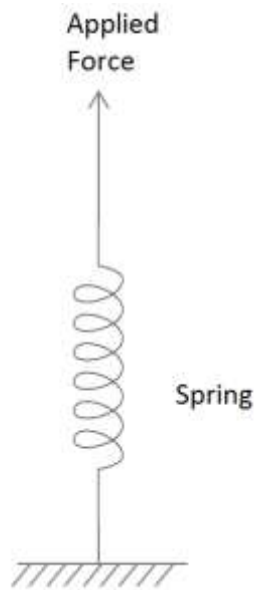


Figure 2.9 Mechanical model of an elastic solid

By placing a spring and a dashpot in series (Figure 2.10), one can obtain a mechanical model simulating the behavior of visco-elastic fluids [32]. It is clear from Figure 2.10 that the application of any force will result in a continuous deformation of the model due to the continuous extension of the dashpot. This indicates that such model is indeed suitable to simulate fluids. The application of a constant force to this assembly results in an initial sudden extension caused by the instantaneous elongation of the spring followed by a continuous extension produced by the dashpot. This is the exact phenomenon that appears in visco-elastic fluids [32]. There are another two phenomena that visco-elastic fluids exhibit. These are stress relaxation and the recoil phenomenon. Stress relaxation happens as time progresses while the system is under the constant force in which the dashpot gets pulled and the spring contracts maintaining a constant elongation of the entire system. This process continues until the spring contracts to its

equilibrium position after which the internal deformation process stops and the force relaxes completely. After this point, the fluid is said to have reached steady state condition where it flows exactly like a viscous fluid (i.e. the spring no longer has an effect). As a result, it is very hard to distinguish between viscous and visco-elastic fluids using steady state experiments. The recoil phenomenon happens when the applied force is released before the termination of the internal deformation process. This release while the spring is under tension results in the contraction of the spring producing a compression force on the dashpot which in turn contracts the dashpot leading to an overall contraction of the system, hence, the name “recoil” [32].

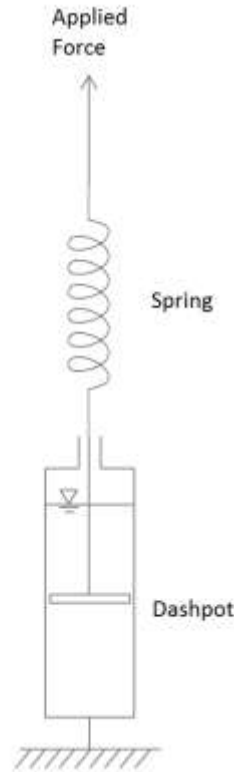


Figure 2.10 Mechanical model of a visco-elastic fluid

The mechanical model analogous to the elastico-viscous solid can be obtained using a spring and a dashpot arranged in parallel as shown in Figure 2.11 [32]. Due to the presence of the spring, it is clear that the system will exhibit a certain maximum extension that depends on the applied force and the stiffness of the spring. This indicates that such model is indeed suitable to

simulate solids. This model exhibits a phenomenon called “creep” which can also be seen in elastic-viscous solids. Applying a certain force will result in a gradual increase in extension of the system, which depends on the viscosity of the fluid inside the dashpot, up to a certain maximum extension determined by the stiffness of the spring. Releasing the applied force will in turn gradually recover the initial configuration of the system [32].

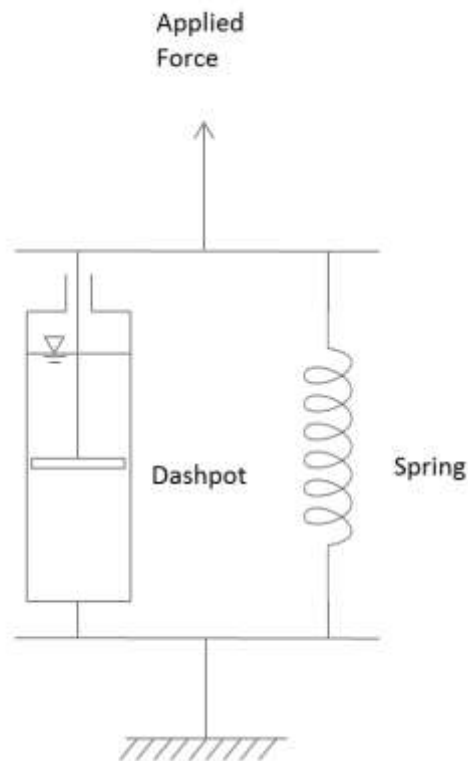


Figure 2.11 Mechanical model of an elasto-viscous solid

The mechanical model for Bingham plastics can be obtained by introducing static friction in the system as shown in Figure 2.12. The stiffness of the spring in this model is defined as a step function that takes a value approaching infinity when the applied force is more than or equal to the static friction between the block and the solid surface. If the applied force is less than the static friction, the block will not move and the extension in the system will only be caused by the spring producing an elastic solid deformation. The spring, however, will act as a rigid (inextensible) connection when the applied force exceeds the static friction resulting in the

movement of the block. Consequently, the extension in the system will be caused by the dashpot independently resulting in a viscous fluid flow. The static friction in this model is analogous to the minimum stress (yield stress) in plastics required to shear the material and produce a flow.

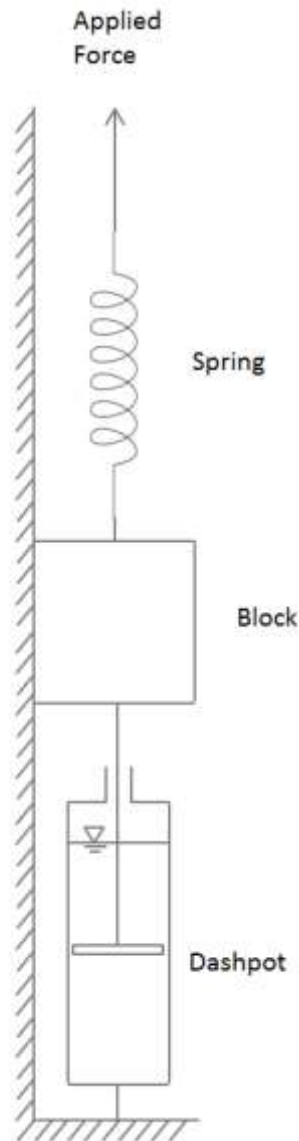


Figure 2.12 Mechanical model of a Bingham plastic

The mechanical models for the Boltzmann materials shown in Figure 2.7 are identical to the aforementioned models except that the characteristics of Boltzmann materials depend on the past shearing history of the materials. In other words, these materials exhibit time-dependent behavior even under the same applied force (i.e. the same rate of shearing stress in fluids or the

same shearing stress in solids). This means that the viscosity of the fluid in the dashpot and the stiffness of the spring can change with time [32]. For instance, Boltzmann fluids are said to exhibit thixotropy if their viscosity decreases with time under load and they are said to exhibit antithixotropy if their viscosity increases with time [32].

2.3.2. Rheology and Vibration of Fresh Concrete

For all practical purposes, fresh concrete is often considered a Bingham plastic [36]. However, in reality, fresh concrete behaves more like a Boltzmann plastic which exhibits changes in the rheological characteristics depending on the past shearing history of the concrete. This means that fresh concrete exhibits changes in shearing stress with time even at a constant rate of shearing strain. This property can be ignored when studying vibration in concrete since vibration is usually applied for some time, thereby causing the shear stress of concrete to reach a steady-state condition. There is also the debate about whether fresh concrete is actually a plastic. However, this has not been verified yet due to the fact that, unlike most rheometers of other fluids, concrete rheometers cannot operate at extremely small strain rate values. Nevertheless, considering the high strain rates vibration usually cause, the assumption of Bingham plastic is reasonable for studying concrete under vibration.

A brief mathematical explanation of a Bingham plastic can be inferred from Figure 2.13 by comparing it to a Newtonian fluid such as water. As can be observed from Figure 2.13, any small application of a shear stress would result in a shear rate causing flow of a Newtonian fluid. This is not the case for a Bingham plastic. A certain yield stress has to be exceeded for the Bingham plastic to start flowing. The ratio of the applied shear stress to the rate of shearing strain is the viscosity and is constant in the case of Newtonian fluids. Bingham plastics, however, have varying viscosities. The slope of the straight line that defines the relation between the

shearing stress and the rate of shearing strain is referred to as the plastic viscosity for a Bingham plastic. In case of Newtonian fluids, the plastic viscosity is equal to the viscosity [32]. In Bingham plastics, the lower the plastic viscosity the higher the rate at which viscosity decreases with increasing rate of shearing strain. The main function of vibration is to induce a high enough shearing strain rate to make the concrete move at a low enough viscosity in order to allow it to fill the voids and consolidate properly.

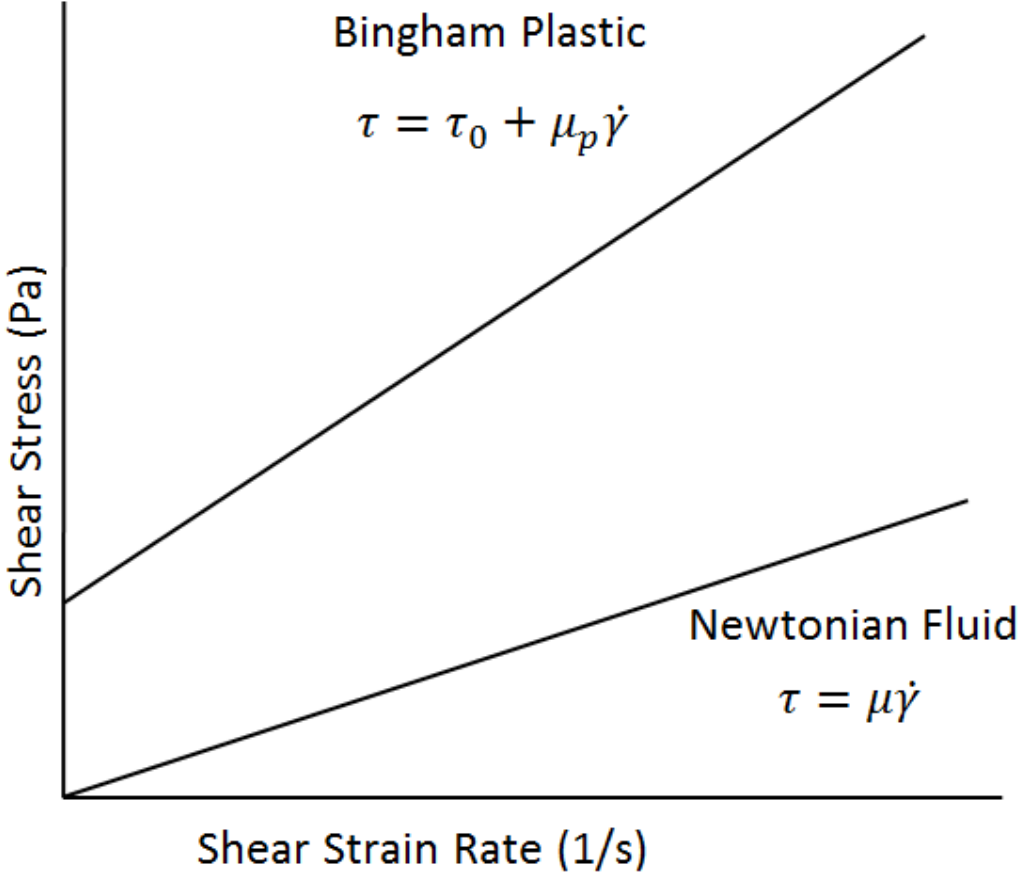


Figure 2.13 Bingham plastic versus Newtonian fluid

Aside from vibration, there are many factors that can affect the rheological properties of fresh concrete. These factors include paste volume, coarse and fine aggregates fraction, HRWR type and dosage [37]. Also, the gradation and moisture content of both coarse and fine aggregates play an important role in determining the fresh properties of concrete. Therefore, it is

necessary to use well-graded aggregates [38]. The rheological properties of fresh concrete are usually controlled through adjustment of the w/cm, mixture water content, superplasticizers (SP), viscosity modifying admixtures (VMA), or through the use of fine supplementary cementitious materials [18]. The packing density of particles also plays an important role in determining the rheological properties of fresh concrete [39].

There have been a lot of studies, for a wide range of applications, conducted on the rheology and vibration of concrete. For instance, Chidiac and his colleagues attempted a very unique effort to study the effect of the rheological properties of fresh concrete on the mechanical properties and durability of hardened concrete [40]. The potential durability of hardened concrete was assessed by its surface transport properties, namely, the air permeability and the sorptivity. The yield stress and plastic viscosity were obtained mathematically from the measured flow properties of fresh concrete which are slump, slump flow and slump time [40]. Better measurements of the rheological properties of fresh concrete could have been obtained if a concrete rheometer was used instead of depending on the empirical tests of rheology. Their results showed no obvious correlation between the rheological properties and the durability of concrete as well as the tensile strength of the concrete cover. Despite the fluctuation of the data, the results also showed that the general trend is that higher yield stress and plastic viscosity values lead to higher compressive strength [40]. This is logical since the w/cm is lower in this case. The effect of rheological properties on the pulse velocity showed that higher pulse velocity (i.e. higher modulus of elasticity and higher density) can be obtained by assuring high values of yield stress and plastic viscosity [40].

Toutou and Roussel attempted to study the influence of suspended grains on the rheological properties of concrete by considering fresh concrete as a suspension of grains of

various sizes in a continuous fluid phase [41]. The rheometric tests were conducted on cement based suspensions by examining four different scales defined by the authors as the saturating fluid scale (a nano-silica suspension), the cement paste scale, the mortar scale and the concrete scale. The testing apparatus for the first three scales was a Couette type viscometer whereas it was a concrete rheometer (BTRHEOM) for the concrete scale [41]. The use of different rheometric apparatuses was necessary due to the presence of very large grains in fresh concrete that prevents the applicability of using the Couette type viscometer [41]. This variability in the apparatuses brings doubt about whether linking the first three scales to the concrete scale would be reasonable or not. Nevertheless, Toutou and Roussel carried out their experiments on all scales and obtained (for each scale) shear stresses as functions of shearing rates for given fractions of solid volume [41]. The nano-silica suspension seemed to behave as a Bingham fluid and its yield stress was obtained following that assumption. On the other hand, the mortar and cement paste suspensions experienced shear thickening. The data obtained for the concrete suspension was able to be fitted correctly using the Bingham model and the yield stress was obtained accordingly. The general trend observed in the results showed that the yield stress increases as we move from the first scale to the last scale indicating that as we increase the maximum granular size the yield stress increases with the concrete scale being the highest. This observation, however, had some exceptions for low fractions of solid volume. Results also showed that yield stress increases rapidly as the gravel volume fraction increases.

The rheology of concrete is not only meant to be used for studying air voids and workability of concrete but can also be utilized to study the segregation of concrete under vibration. Teranishi and his colleagues investigated the effect of the rheological properties of fresh concrete on the sinking behavior of coarse aggregate in concrete under vibration [42]. The

results did not show consistent proportionality between the rheological properties and segregation [42]. The most apparent reason seems to be the fact that the theoretical formulation did not account for the interaction between aggregates which is believed to be certainly happening. It was also clearly evident from their results that the higher the volume of coarse aggregate the lower the segregation of concrete.

Another interesting study is the investigation of the transmission of vibrations in fresh concrete which was carried out using two-dimensional dynamic viscoplastic finite element method (VFEM) by Kitaoji and his colleagues [43]. Their study not only involved vibration via a surface vibrator and an internal vibrator but also included the investigation of the effect of obstacles on the transmission of vibration. The authors assumed Bingham behavior of fresh concrete in their analysis and consequently used yield stress and plastic viscosity parameters as inputs in their model. It was observed from their results that the agreement between the analytical and experimental results is absent except for the trivial fact that the acceleration of vibration decreases as we move away from the source of vibration [43]. This poor correlation could be attributed to a possible disagreement between the rheological properties of the actual concrete and the ones inputted into the model. Another possibility could be the fact that the concrete was modeled as a single homogenous material whereas it might have been more accurate to model it as a suspension of aggregate particles in mortar. Many other simulations were carried out by the authors to examine the various parameter intended to be investigated. The general conclusion was that the higher the Bingham parameters the higher the damping of the vibration and the lower the effect of obstacles on the transmission of vibrations [43].

Banfill and his colleagues also attempted to predict the radius of action of internal poker vibrators in fresh concrete using the mathematics of wave propagation [44]. They were able to

show mathematically and confirm experimentally that there is an inner liquefied zone (closer to the source of vibration) where the flow is mainly controlled by shear waves. This zone is created due to the strong vibrations that inflict an applied shear exceeding the yield shear stress of fresh concrete. On the other hand, an outer solidified zone (further from the source of vibration), where the flow is mainly controlled by compressive waves, is created by the weak vibrations that fail to overcome the yield shear stress of fresh concrete. The radius of action, as defined by them, is the distance from the source of vibration to the interface between the two regions [44]. Their mathematical and experimental results agree relatively well and confirm that the peak velocity of the poker vibrator governs the efficiency of vibration since the radius of action increased with increased peak vibrator velocity while holding the properties of fresh concrete constant. Moreover, their results show that the radius of action also increases with decreasing yield stress and increasing plastic viscosity of fresh concrete while holding the characteristics of the poker vibrator constant [44].

There were few researches that attempted to study the effect of vibration on the air system and freeze-thaw durability of concrete. In a paper published in 2001, Hover discussed the importance of vibration frequency when it comes to freeze-thaw durability [45]. He emphasized the fact that higher vibration frequencies can produce exponentially higher vibration energies capable of severely liquefying the concrete to the point where small air bubbles might get lost. He also pointed at the fact that very high vibration frequencies might cause small air bubbles to vibrate at their resonant frequency resulting in their explosion [45]. Pigeon and Malhotra looked at the freeze-thaw resistance of air-entrained and non-air-entrained roller-compacted high-volume fly ash concrete [46]. They prepared cylindrical samples that were vibrated laterally while applying a compressive force on the concrete. The w/cm ranged from 0.27 to 0.42 while

the air content values before vibration ranged from 3.6% to 5.2%. Despite the fact that the spacing factor values were 0.25 mm for air-entrained concrete and 0.3 to 0.4 mm for non-air-entrained concrete, all samples showed good freeze-thaw resistance under ASTM C666 Method A test. One of the non-air-entrained samples experienced reduction in the durability factor (DF) but was able to pass the test successfully [46]. In another research, Zhang and Gao studied the effect of high-frequency vibration on the air parameters and freeze-thaw performance of air-entrained concrete [47]. The vibration was carried out using a 200 Hz-frequency 50 mm-diameter immersion vibrator that was immersed in the center of the specimen at a depth of 15 cm. The air content before vibration was around 6%. Freeze-thaw testing was performed according to JTG E30-2005. Results showed a gradual decrease in the final air content as the vibration duration increased, reaching about 2% at a 2-minutes vibration. The spacing factor decreased then increased to about 0.35 mm at a 2-minutes vibration. Their main conclusion was that long periods (i.e. more than 1 minute) of high frequency vibration resulted in lower freeze-thaw resistance [47]. Another similar study was published a year later and showed the same conclusion [48].

2.3.3. Rheology under Vibration

There have been some studies attempting to measure the rheological properties of fresh concrete under vibration. For instance, a paper published in 1988 by Tattersall and Baker presented a study about the rheological properties of concrete during vibration [49]. The apparatus used in this study was constructed by mounting the bowl of a two-point workability test on an electromagnetic vibrating table. Rheological measurements were carried out twice for each fresh concrete sample one before vibration and the other during vibration [49]. The authors did not mention any usage of a retarding agent which is believed to lead to an inconsistent

comparison between data obtained from the unvibrated concrete and data obtained from the vibrated concrete since the rheological properties of fresh concrete change with time. Nevertheless, results showed that unvibrated concrete, similar to previous studies, seemed to behave as a Bingham fluid [49]. The concrete under vibration, however, showed a behavior very similar to a power law pseudo-plastic fluid with zero yield stress. In some cases, the curve for concrete under vibration seemed to be below the curve of unvibrated concrete for any shearing rate indicating that vibration increases the flowability of fresh concrete no matter what the shearing rate is. In some other cases, the curve for concrete under vibration crossed that of unvibrated concrete pointing to the fact that vibration might actually reduce workability under high shearing rates. Another conclusion obtained from this study is the fact that the efficiency of vibration is mainly controlled by the peak velocity of vibration. The authors also stated that the concrete under vibration could be regarded as a Newtonian fluid only if very low shear rates are considered [49].

Juradin also tried to determine the rheological properties of fresh concrete during vibration and published her work in 2012 [50]. She developed a vibration rheometer which can measure the yield stress and plastic viscosity of mixtures under vibration. The vibration was induced via a vibrating table that vibrates the sample altogether. She assumed that the concrete behaves similar to a Bingham fluid. The setup of the vibration rheometer made it very difficult to obtain an analytical solution for the yield stress and plastic viscosity. Thus, constants of the vibration rheometer were obtained experimentally by examining two materials of known rheological properties [50]. Such step is questionable and might yield wrong results about the rheological properties of fresh concrete since two reference materials is too little to cover all possible values of yield stresses and plastic viscosities. The doubt increases further knowing that

these reference materials, unlike concrete, are fine grained. As a result, Juradin failed to test actual concrete samples and tested mortar instead. Her results for the mortar, contrary to the concrete results obtained in this dissertation, show that higher acceleration of vibration results in an increase in yield stress and a decrease in plastic viscosity [50].

Krstulovic and Juradin previously tried to model the fresh concrete behavior under vibration by numerically obtaining the yield stress, the plastic viscosity and the dynamic forces [51]. They also performed lab experiments on two different fresh concrete specimens in order to validate their model and make sure there is good correlation between the two. For the experimental part, they developed a vibration rheometer where the specimen, the main parts of the apparatus and the source of vibration form a unique oscillatory system whose parameters can be measured with sufficient precision. Due to the fact that fresh concrete changes its chemical and physical properties with time, the authors struggled to obtain two fresh concrete specimens with exactly similar chemical and physical properties. Consequently, they decided to make two separate concrete mixtures with exactly similar proportions and test them after the lapse of the exact same amount of time from the initiation of the mixing [51]. A better and more accurate way to do it would be to obtain the two specimens from one single concrete mixture which contains a retarder in order to preserve its chemical and physical properties. Cement paste specimens were also tested and compared with the theoretical values. For the modeling part, they used the D'Alambert principle and derived a very complex solution of the oscillation of a modified Bingham model under forced vibration. The extreme complexity of their solution arises from the discontinuous deformation of their model which produces a system of nonlinear implicit equations that need to be solved numerically [51]. The comparison between the experimental and the numerical results did not seem to be very promising.

2.3.4. Methods for Measuring the Flow of Concrete

Measuring the rheological properties of concrete is of utmost importance in today's civil engineering industry due to several reasons. One would be that concrete is usually placed in its fresh plastic condition where its flow is an important factor for its placement. Knowing the rheological properties would help identify the flow properties of fresh concrete and thereby devise the necessary procedures to properly place concrete. Some applications require pumping concrete to very high elevations. In this case, rheological properties become very crucial to facilitate such a task. Another reason would be to predict how much vibration would cause segregation of concrete. Unfortunately, no existing method in the literature is available for prediction of rheological properties of fresh concrete from its constituents due to its complex composition [52]. Consequently, it is necessary to measure the rheological properties of fresh concrete after mixing using one of the many standard tests available in the literature. However, even these tests have a limited prediction power of the rheological properties and can only partially measure the intrinsic flow properties of fresh concrete. This limitation is due to the wide range of particle sizes available in fresh concrete and other chemical issues such as hydration and the existence of charged particles [52]. There are many methods available in the literature that are used to characterize the flow properties of fresh concrete. Some of which provide only a single factor which does not fully characterize the rheology of concrete. There are, however, other tests that provide two factors rather than one [52].

2.3.4.1. One-Parameter Rheometric Tests

The vast majority of the available standard tests provide only one parameter about the flow properties of concrete that can be linked either to the yield stress or plastic viscosity [52]. Due to its simplicity the slump test is one of the most widely used tests. It is also one of the

oldest tests used to measure the consistency of fresh [52]. This test can be found in ASTM C143 Standard [53]. The slump test is performed by filling a truncated metal cone (open from both sides) with fresh concrete, and then lifting the cone within an approximate 5-seconds period. The drop in the height of the concrete is then measured and reported as the slump value of the concrete [53]. Unfortunately, the slump test cannot differentiate between concrete mixtures that are too stiff to allow a drop in the concrete height. Also, for concrete mixtures with very high slumps, a modified slump test is used which measures the spread of the concrete instead of its drop. This test can be found in ASTM C1611 [54]. The K-Slump test is also an ASTM standard test that can be found in ASTM C1437 [55]. It was widely used in the concrete industry even before it became a standard [52]. This test mainly consists of a probe that is inserted in the fresh concrete allowing a portion of the concrete to flow into the hollow center of the probe through the perforated exterior of the probe. A measuring rod placed in the other end of the probe measures how much concrete was able to flow into the probe [55]. The higher the amount of concrete the easier its placement is. This test is only suitable for concretes with low yield stresses since the probe is not inserted that deep into the concrete. There are other tests that work by dropping an object with a certain force and observing the depth of penetration of that object into the fresh concrete [56]. Similar to the slump test, these tests can be used as quality control tests to detect any changes in the composition of the delivered concrete. They can also be used to estimate the setting time of concrete [52].

Remolding tests are meant to measure the capability of concrete to change shape under vibration [52]. These tests work by placing fresh concrete through an open-ended truncated cone into a cylinder attached to a vibrating system. After the cone is removed, the duration of time needed for concrete under vibration to remold itself into the shape of the cylinder is recorded

[52]. The biggest advantage of these tests is the fact that they simulate the placement of concrete in the field [52]. Fritsh test also measures the ability of concrete to consolidate under vibration [52]. It is carried out by pouring the fresh concrete in a container with a vibrator and then placing a lid on top of the concrete sample. After the vibrator is switched on, the settling curve is obtained by monitoring the height of the lid with time [57]. There is also the flow cone test that was originally devised for measuring the flow of oil well cement slurries but was later adapted for use with concrete [52]. This test is conducted using a funnel of certain dimensions which restrict the size of the aggregates to 20 mm. Ten liters of fresh concrete are poured through the funnel and the duration needed for a given volume of concrete to pass through the orifice is recorded [58]. This test is also not very useful for very stiff mixtures and those having large maximum aggregate sizes [52]. A similar test is the Oriment apparatus which can accommodate larger aggregate sizes due to the applicability of changing the diameter of tube used in the test [59]. The tuning tube viscometer is an instrument capable of measuring the viscosity of fluids. This instrument consists of a tube of certain diameter and length where the fluid of interest is inserted and a ball of a certain size is then dropped in the fluid. The velocity of the ball is then measured between two points that are a certain distance apart. Balls of different sizes are used to obtain several readings after which the Stokes equation is used to calculate the viscosity of the fluid [60]. The tuning tube viscometer can be used to measure the viscosity of cement paste and mortar but not concrete due to restriction caused by the large size of aggregates [60]. However, cement pastes and mortars are known to exhibit changing viscosities so using this test on them might not yield representative results. There are also filling ability tests that measure the easiness at which fresh concrete can fill forms [52]. There are many other one-parameter rheometric tests available in the literature. However, like the aforementioned tests, they can only give relative

parameters as opposed to some of the two-parameter rheometric tests that can give directly the yield stress and plastic viscosity.

2.3.4.2. Two-Parameter Rheometric Tests

Despite the vast majority of rheometric apparatuses being one-parameter test devices due to their simplicity, there are some rheometric apparatuses that can obtain two parameters for fresh concrete relating to the yield stress and the plastic viscosity of concrete. However, the two parameters are usually not directly related to yield stress and plastic viscosity [52]. Designing rheometric devices that can directly measure yield stress and plastic viscosity of fresh concrete is often very difficult due to several possible reasons such as the large size of coarse aggregates and their tendency to segregate [52]. For normal fluids where the particle sizes are very small, coaxial cylinders is the most common geometry of the rheometers used to measure them. The dimensions of these cylinders are chosen such that the flow gradient between the shearing surfaces is linear. For concrete, however, such linearity is very difficult to achieve due to the presence of coarse aggregates that have very large sizes [52].

The modified slump test is a modification of the traditional slump test to allow for correlation to plastic viscosity in addition to yield stress [52]. In addition to obtaining the final slump height, this test requires the measurement of the speed at which the height of concrete drops. The speed is calculated by recording the duration it takes the top of the concrete to travel down 100 mm. The yield stress and plastic viscosity can then be estimated from the final slump and the 100 mm slump time, respectively using empirical equations [52]. Similar to the one-parameter rheometric tests, this test does not seem to facilitate direct analytic calculations of yield stress and plastic viscosity. The first test to allow for calculation of yield stress and plastic viscosity is the Tattersal two-point test [61]. The test is performed by pouring a fresh concrete

sample of certain volume into a bucket after which an impeller of certain size and geometry is inserted into the concrete sample. The impeller is rotated at several rotational speeds and the resisting torque by the concrete sample is recorded at each speed. The fundamental parameters of rheology can then be calculated from the obtained graph of torque versus speed which is supposed to be linear since concrete behaves like a Bingham fluid for all practical values of rotational speeds [61]. The main issue with this instrument is obtaining the calibration parameters which are extremely difficult to determine [52]. The calibration parameters are obtained by running the test on Newtonian and non-Newtonian fluids of known rheological properties. However, due to the large size of the container along with the complicated nonlinear flow during the test, the obtained calibration parameters can be very different depending on the calibrating fluids. Modifications were made later to automate data recording. The rheometer is now available as the BML Viscometer and the IBB Concrete Rheometer. The principle is still the same but differences can be in the impeller shape, size or motion [36]. A similar rheometer is the ICAR rheometer which was used in this study.

The BTRHEOM rheometer is a rheometer which utilizes the parallel plate principle. It might be one of the most suitable instruments for directly measuring the rheological properties of concrete even under vibration. It is made of a bucket with a jagged bottom, where the fresh concrete sample is placed, and a rotating top wheel resting on top of the concrete sample. For each rotational speed of the top wheel, a shearing strain rate and shearing stress can be obtained. Therefore, a graph of shear stress versus shear strain rate can be obtained which can be used to get the rheological properties of the concrete [62]. The contact between the shearing wheel and the entire concrete surface along with the geometry of this apparatus assures linear flow gradient which in turn guarantees accurate values of shear rates and shear stresses. The major

disadvantage of this test, which is also available in the other tests, is the inapplicability of shearing concrete mixtures with high yield stress and plastic viscosity values [52]. Another rheometer that utilizes the coaxial cylinders principle and permits direct calculation of yield stress and plastic viscosity is the Bertta apparatus. The apparatus consists of two concentric cylinders where the fresh concrete sample is placed in between. The outer cylinder rotates in an oscillatory mode with a frequency and amplitude chosen by the operator. The induced torque is then recorded in the inner cylinder and the rheological parameters are directly obtained as functions of frequency [52]. The main issues with this test is the restriction of 13 mm on the maximum size of aggregate and the fact that the ratio between the outer and inner diameters is 1.45 which does not guarantee a linear flow gradient, indicating possible incorrectness in the obtained values of yield stress and plastic viscosity [33]. Until now, there has been no rheometer capable of directly measuring rheological properties for very stiff mixtures.

2.4. Bubble Rising

Air bubbles rise in fresh concrete due to the buoyancy force. The larger the air bubble the larger its buoyancy force and therefore, the faster it will rise and escape from the surface of the concrete [63]. Under static conditions, a certain air bubble will start rising only if its buoyancy force exceeds the yield stress of concrete. At that moment, the air bubble will start exerting a shearing strain rate on the concrete which makes the concrete surrounding the air bubble move with a certain viscosity. This viscosity is what determines the resistance to air bubble rising. For stiff concrete mixtures, the shearing strain rate induced by the air bubble (if any) is not high enough to make the surrounding concrete flow with a low enough viscosity that would allow the air bubble to move fast enough to be able to escape. Therefore, unless the concrete is fluid enough, air bubbles will not escape under static conditions. Vibration induces a certain shearing

strain rate resulting in the flow of fresh concrete at a certain viscosity. This viscosity that the concrete achieves during vibration results in reduced resistance to air bubble rising. Therefore, bubbles with large enough sizes will start rising fast enough to be able to escape the surface of the concrete. Consequently, the amount of air loss during vibration in different concrete mixtures will highly depend on the rheological properties of each mixture. Figure 2.14 shows a comparison in the behavior of two different Bingham plastics under vibration. A certain vibration acceleration and frequency will result in a shearing strain rate which is represented by the vertical red line in Figure 2.14. This particular shearing strain rate will make these two different Bingham plastics flow at two different viscosities represented by the slopes of the blue dashed lines in Figure 2.14. Therefore, for this particular example, Bingham plastic 1 will flow at a higher viscosity compared to Bingham plastic 2 which means that the air loss from Bingham plastic 2 will in theory be larger than the air loss from Bingham plastic 1.

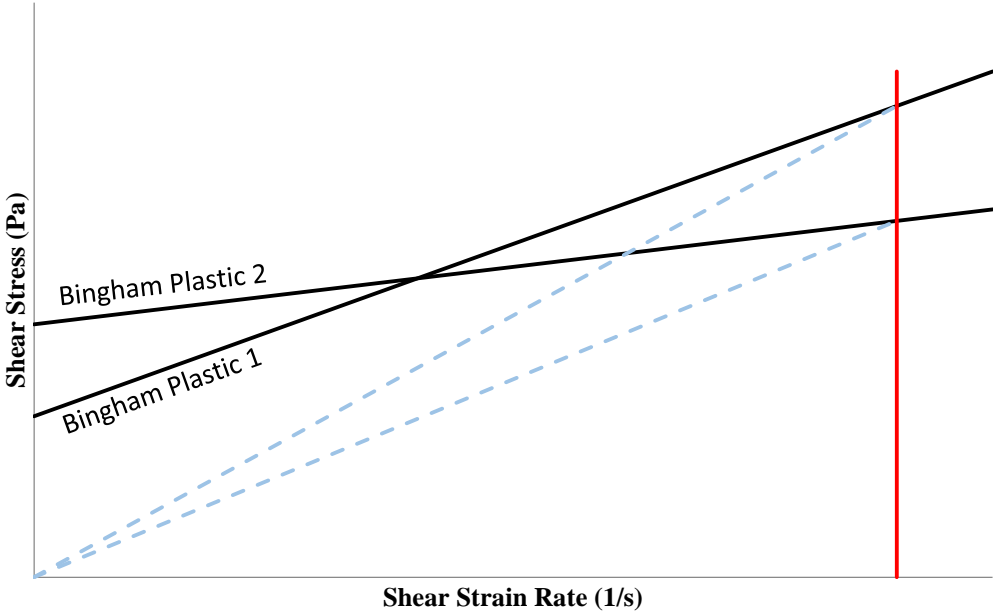


Figure 2.14 Behavior of two different Bingham plastics under vibration

For the same concrete mixture, viscosity decreases as the strain rate caused by vibration increases since fresh concrete is typically a shear-thinning material. Lower viscosity means less drag force [27] resisting the rise of air bubbles to the surface of fresh concrete. Therefore, more bubbles are expected to be lost if stronger vibration is applied. While bubble rising is assumed to be complicated due to the complex nature of concrete mixtures, it is possible to illustrate the concept of bubble rising by considering Newtonian fluids and very small spherical air bubbles. As shown in Figure 2.15, there are typically three forces acting on an air bubble inside a viscous fluid. These are the weight (negligible for air), buoyant force and drag force [64].

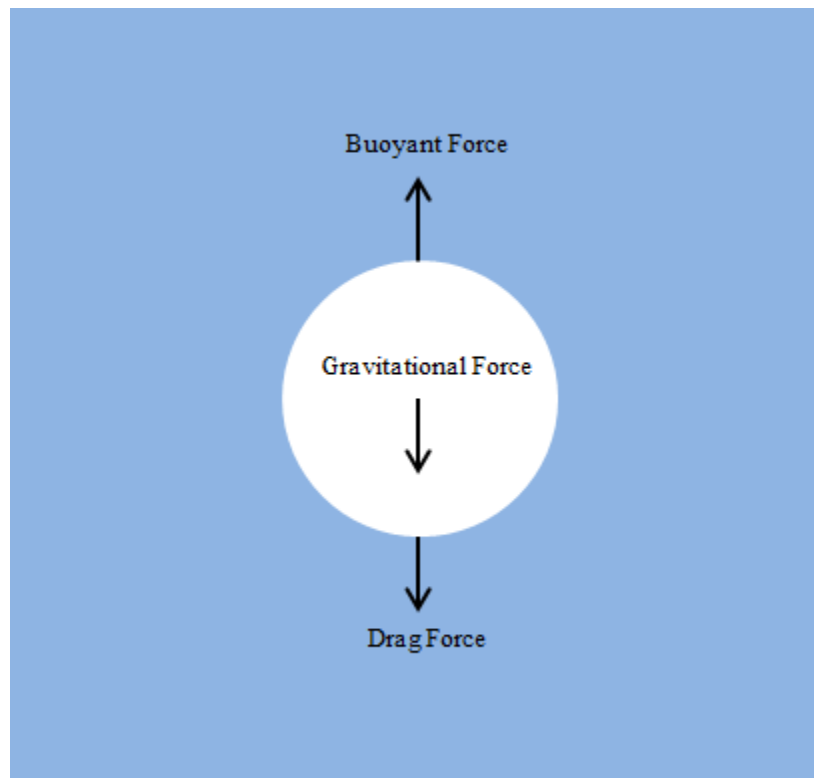


Figure 2.15 Bubble rise mechanism

It is possible to obtain the terminal velocity of rising air bubbles by applying equilibrium under some simplifying assumptions. The terminal velocity can be calculated from Equation 2.15 [64]:

$$v = \frac{2 \rho_c}{9 \mu} g r^2$$

Equation 2.15

Where:

v =Terminal velocity of the rising air bubble

ρ_c =Density of fresh concrete

μ =Apparent dynamic viscosity of fluid

g =Gravitational acceleration

r = Radius of air bubble

It can be observed from Equation 2.15 that the speed of air bubble rising is also a function of the size of the air bubble. Larger air bubbles escape faster than smaller ones. This is good news because smaller air voids are much more important for concrete when it comes to freeze-thaw resistance as discussed in section 2.1.

Chapter 3 - Materials

3.1. Material Characterization

All concrete mixtures were prepared in the laboratory using ASTM C150 Type III cement, a natural siliceous sand, and a limestone coarse aggregate. Table 3.1 shows the cement physical and chemical properties. The coarse aggregate had a specific gravity of 2.69 and absorption of 0.39% while the fine aggregate had a specific gravity of 2.66, absorption of 0.74% and fineness modulus of 3.02. Figure 3.1 and Figure 3.2 show the particle size distribution of coarse and fine aggregates, respectively. The size of the mixture ranged from 0.9 to 2.7 ft³ depending on the purpose of the test. The mixture proportions varied depending on the targeted rheological properties. The following admixtures were used: a lignosulfonate-based low-range water reducer (LRWR), two different polycarboxylate-based HRWRs, and synthetic, wood rosin, tall oil and vinsol resin AEAs.

Table 3.1 Chemical and physical properties of cement

Property	Value
Silicon dioxide (%)	22.03
Ferric oxide (%)	3.41
Aluminum oxide (%)	4.18
Calcium oxide (%)	63.45
Magnesium oxide (%)	1.96
Sulphar trioxide (%)	3.21
Loss on ignition (%)	1.45
Insoluble residue (%)	0.25
Free lime (%)	0.96
Sodium oxide (%)	0.16
Potassium oxide (%)	0.49
Equivalent alkalies (%)	0.48

C ₃ S (%)	48.8
C ₂ S (%)	26.4
C ₃ A (%)	5.3
C ₄ AF (%)	10.4
Blaine Fineness (cm ² /g)	5920

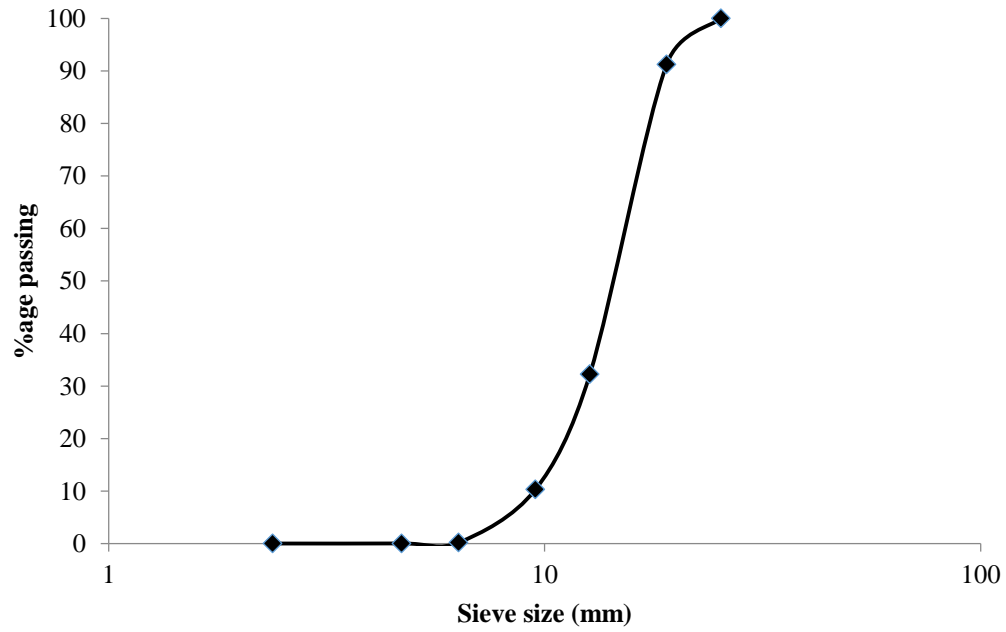


Figure 3.1 Particle size distribution of coarse aggregate

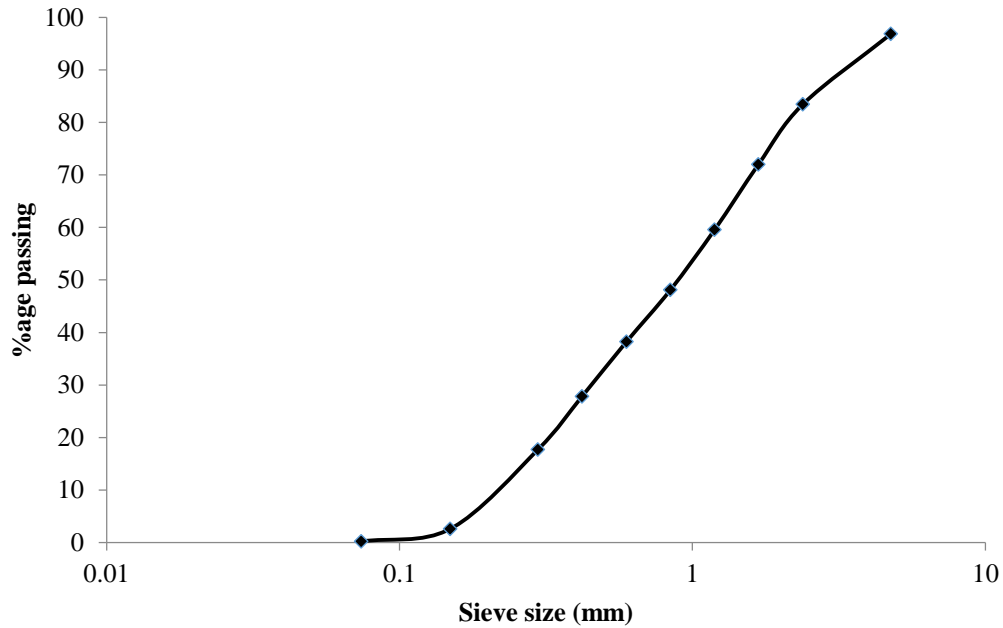


Figure 3.2 Particle size distribution of fine aggregate

3.2. Mixture Proportions

3.2.1. Stability of Air Void System

In this part of the study, the size of mixtures ranged from 2.1 to 2.7 ft³ depending on the number of times the air content was measured. The mixture proportions for all of these mixtures were the same except for the mixture without any water reducers (WR), as shown in Table 3.2.

The admixture dosages were also different for each mixture.

Table 3.2 Basic concrete mixture proportions

Material	Weight (lb/yd ³)	
	No WR	Mixtures Containing WR
Cement	834.90	887.04
Water	358.45	270.07
Rock (SSD)	1677.63	1,778.25
Sand (SSD)	852.66	896.67

The rheological properties of the mixtures were varied by using different LRWR, HRWR and AEA dosages. The LRWR used was a lignosulfonate-based admixture. A polycarboxylate-

based HRWR admixture was used. For the AEA, synthetic, wood rosin, and tall oil admixtures were used. Details about all mixtures used in this study can be found in Table 3.3. The air content values shown in Table 3.3 were taken after mixing but before vibration.

Table 3.3 Concrete mixture properties

Peak Vibration Acceleration	AEA	Dosage (Oz/100 lb of Cement)	WR	Dosage (Oz/100 lb of Cement)	Temp. (°F)	Unit Weight (lb/ft ³)	Air Before Vibration (%)	Slump (in)
3g	Synthetic	1.8	None	N/A	76	137.24	7.8	8
	Synthetic	1.3	HRWR	7	75.4	140.56	9	6.5
	Synthetic	0.6	HRWR	7.5	73.3	142.72	7.5	6.25
	Synthetic	0.6	LRWR + HRWR	4.5+3.5	68.4	143.12	7.8	2.875
	Synthetic	0.6	LRWR + HRWR	4.5+4.5	75.9	141.56	8	4.5
	Synthetic	0.6	LRWR + HRWR	5+5	75	141.64	8.5	8
	Synthetic	0.5	LRWR + HRWR	5+4.5	66.1	-	7.4	4.5
	Synthetic	0.5	LRWR + HRWR	5+5	74.6	-	8.5	6.75
	Wood Rosin	0.6	HRWR	7.5	72.2	-	7.4	9.25
	Wood Rosin	0.8	HRWR	7	74.2	-	6.2	6
	Tall Oil	1	HRWR	7	77.3	-	9.5	4.5
	Wood Rosin	0.9	HRWR	7	74	144.84	5.6	6
	Tall Oil	0.6	HRWR	7.25	74.9	143.36	7	5.5
	Tall Oil	0.65	HRWR	7.25	75.5	144.32	6.2	4
10g	Synthetic	0.6	HRWR	7.5	75.4	139.12	9.5	6.5
	Synthetic	0.5	LRWR + HRWR	5+5	77.1	-	6.9	4.5
	Tall Oil	0.65	HRWR	7.5	76.4	-	7	4
	Wood Rosin	1.1	HRWR	7.5	76.1	-	6.2	5.5

3.2.2. Freeze-Thaw Durability of Externally Vibrated Concrete

The size of each mixture used to study the freeze-thaw durability of externally vibrated concrete was 1.1 ft³. Concrete mixtures of different rheological properties were used in this study. They ranged from low yield stress and plastic viscosity mixtures to high yield stress and plastic viscosity mixtures that had a target 4 in slump. The rheological properties were varied by changing the w/cm and volume fraction of coarse and fine aggregates. The HRWR dosage for a particular HRWR admixture was kept constant in these mixtures in order to study the effect of admixtures type rather than dosages. Two types of polycarboxylate HRWRs were used. Synthetic and vinsol resin AEAs were used. Mixtures with HRWR1 and vinsol resin AEA were labelled as combination A. Mixtures with HRWR1 and synthetic AEA were labelled as combination B. Mixtures with HRWR2 and synthetic AEA were labelled as combination C. Table 3.4 shows the quantities of the constituent materials in each mixture used in this part of the study. Each of the four mixtures were designed to have considerable differences in terms of rheological properties. The HRWR dosages of combination C were significantly higher than those of combination A and B in order to obtain similar rheological properties among the different combinations that could not be achieved using the same dosage. It can also be observed that the AEA dosages are also different among the various combinations and mixtures. This was done to obtain the desired initial fresh air content since mixtures with different AEA type, HRWR type and rheological properties require different AEA dosages. Mixtures which have the same rheological combination number are designed to have the same rheological properties. Generally, rheological combination 1 would always have the highest yield stress and plastic viscosity while rheological combination 4 would have the lowest yield stress and plastic viscosity. Also, rheological combination 2 tend to have higher yield stress compared to

rheological combination 3 which tells us that, for approximately the same w/cm, increasing the sand volume fraction increases the yield stress while increasing the rock volume fraction reduces it.

Table 3.4 Mixture proportions of externally vibrated mixtures for target air content of 3.5% to 4.5%

Admixture Combination	Rheological Combination	AEA Dosage (oz/cwt)	HRWR Dosage (oz/cwt)	w/cm	Paste (% Vol.)	Rock (% Vol.)	Sand (% Vol.)
A	1	1.44	7.67	0.29	28.8	32.4	32.8
	2	0.48	7.67	0.30	29.3	21.7	44.0
	3	0.72	7.67	0.31	29.6	36.7	27.8
	4	0.48	7.67	0.33	30.5	31.6	31.9
B	1	0.07	7.67	0.29	28.8	32.4	32.8
	2	0.07	7.67	0.30	29.3	21.7	44.0
	3	0.07	7.67	0.31	29.6	36.7	27.8
	4	0.07	7.67	0.33	30.5	31.6	31.9
C	1	0.38	13.43	0.29	28.8	32.4	32.8
	2	0.01	13.43	0.32	29.8	21.6	43.6
	3	0.48	13.43	0.32	29.9	36.5	27.7
	4	0.19	13.43	0.33	30.7	31.5	31.9

The AEA dosages shown in Table 3.4 are for the most frequently used mixtures where the initial air content was intended to be constant. These dosages were changed for some mixtures in order to study the effect of initial air content and are shown in Table 3.5.

Table 3.5 AEA dosages of mixtures used to study the effect of initial air content

Admixture Combination	Rheological Combination	Target Air Content (%)	AEA Dosage
B	4	3	0.02
		5	0.1
C	1	4	0.77
		5.5	1.53
	4	4	0.48

		5.5	1.06
		7	1.44

3.2.3. Freeze-Thaw Durability of Internally Vibrated Concrete

In this study, rheological combinations 3 and 4 of chemical admixture combination B (Table 3.4) were used. Two mixtures of each rheological combination category were tested. The AEA dosages were changed to have one high and one low air content for rheological combinations 3 and 4. Table 3.6 shows the mixture proportions used for these mixtures.

Table 3.6 Mixture proportions of internally vibrated mixtures

Admixture Combination	Rheological Combination	AEA Dosage (oz/cwt)	HRWR Dosage (oz/cwt)	w/cm	Paste (% vol.)	Rock (% vol.)	Sand (% vol.)
B	3	0.07	7.67	0.31	29.6	36.7	27.8
		0.14	7.67	0.31	29.6	36.7	27.8
	4	0.07	7.67	0.33	30.5	31.6	31.9
		0.14	7.67	0.33	30.5	31.6	31.9

3.2.4. Rheology under Vibration

The size of each mixture used to study the rheological properties of fresh concrete under vibration was 0.9 ft³. Five concrete mixtures of different rheological properties were used in this study. No chemical admixtures were used. Rheological properties were varied by changing the w/cm. A hydration controlling admixture was used in all mixtures in order to allow for extended periods of testing while maintaining constant rheological properties. Table 3.7 shows the mixture proportions of all five mixtures while Table 3.8 shows the weights of the constituents.

Table 3.7 Concrete mixture proportions for the "rheology under vibration" study

Mixture ID	w/cm	Paste (% vol.)	Rock (% vol.)	Sand (% vol.)
1	0.4	34.1	32	32.4
2	0.5	38.8	29.7	30
3	0.36	32.2	33	33.4

4	0.38	33.1	32.5	32.9
5	0.43	35.5	31.3	31.7

Table 3.8 Quantities of mixtures' constituents for the "rheology under vibration" study

Mixture ID	Water (lb/yd ³)	Cement (lb/yd ³)	Rock (SSD) (lb/yd ³)	Sand (SSD) (lb/yd ³)
1	336.31	800	1446.25	1441.23
2	415.1	800	1339.67	1335.02
3	304.79	800	1488.88	1483.71
4	320.55	800	1467.57	1462.47
5	359.94	800	1414.27	1409.36
Mixture ID	Water (kg/m ³)	Cement (kg/m ³)	Rock (SSD) (kg/m ³)	Sand (SSD) (kg/m ³)
1	199.52	474.62	858.03	855.05
2	246.27	474.62	794.79	792.04
3	180.82	474.62	883.32	880.25
4	190.17	474.62	870.67	867.65
5	213.54	474.62	839.05	836.14

Chapter 4 - Methodology

4.1. Equipment and Common Tests Description

4.1.1. Concrete Mixing

Concrete mixing was carried out according to ASTM C192 in a horizontal pan-style mixer. All constituent materials were preconditioned to laboratory temperature. The water was divided into two portions; a $1/3$ and a $2/3$ portions. The WR was added to the $1/3$ portion while the AEA was added to the $2/3$ portion. This was done in order to prevent interactions between chemicals prior to mixing. The mixing started by adding the coarse and fine aggregates along with the $2/3$ portion of the water to the mixer. The constituents were then mixed for 3 minutes after which the cement and the $1/3$ portion of water was added gradually while mixing. The mixing continued for another 3 minutes followed by 3 minutes of resting. Finally the mixer was run for another 2 minutes before using the obtained mixture (Figure 4.1) to measure the concrete's temperature, slump, unit weight, fresh air content and rheological properties.



Figure 4.1 Concrete after mixing

4.1.2. Rheology

The rheological properties were measured for each mixture using an ICAR Rheometer. For this test method, the sample container shown in Figure 4.2 was filled with concrete up to the top of the plastic strips attached to the inside wall of the bucket. These strips help in eliminating slippage of the concrete at the wall of the bucket during the test. A vane (Figure 4.3 (a)) was then inserted into the concrete as shown in Figure 4.3 (b). The concrete was then sheared via the rotating vane. The torque developed by the resistance of concrete to the rotational motion of the vane was measured by the rheometer. This rheometer is capable of performing two tests, the stress growth test and the flow curve test. Assuming Bingham plastic behavior of fresh concrete, the stress growth test was used to measure static yield stress (i.e. yield stress without prior shearing history) while the flow curve test was used to measure the concrete dynamic yield stress (i.e. yield stress after breaking the thixotropic effect) and plastic viscosity. During the stress

growth test, the vane was rotated using a slow constant speed while recording the increase in torque with time. Once the value of the torque started decreasing, the maximum torque was considered to have been reached. The static yield stress was obtained from the maximum torque. For the flow curve test, a pre-shear period was performed prior to the actual testing. The vane was rotated at a high speed during this period in order to minimize the effects of thixotropy and to reach a steady state condition. After pre-shearing, the rheometer started registering data. The torque versus speed data were obtained by recording the developed torques in the vane corresponding to several vane rotational speeds. A line was fit to the measured torque vs rotational speed resulting in an equation that can be used to obtain the dynamic yield stress and the plastic viscosity of the Bingham model [65].



Figure 4.2 Rheometer concrete container



(a)



(b)

Figure 4.3 ICAR rheometer a) electronic equipment with vane and b) in concrete sample

4.1.3. Vibration

Depending on the measurement, table vibrators (Figure 4.4) or an immersion vibrator (Figure 4.5) were used to vibrate the concrete. Both of these vibrators' types used were rotary vibrators that produced sinusoidal shear and compression waves. The immersion vibrator has a fixed frequency of 230 Hz whereas the table vibrators had the option of changing frequency and amplitude. The small table vibrator was used for low frequencies of 30 to 110 Hz. The large table vibrator was used for high frequencies of 120 to 180 Hz. The table vibrators were custom-made at the Kansas State University lab. Each vibrating table had a control unit attached to digitally control the frequency (Figure 4.6). The vibrating motor was attached to the bottom of the table top as shown in Figure 4.7. The vibration acceleration was adjusted by changing the offset of the weights on the vibrating motor (Figure 4.8). A huge concrete block was placed in the bottom of the vibrating table (Figure 4.9) in order to insure the stability of the table during

vibration. The freeze-thaw molds were rigidly attached to the top of the table using bolts at each of the four corners of the mold (Figure 4.10). The freeze-thaw molds used had dimensions of 16 X 4 X 3 in. The pot of the fresh air test was fixed to the vibrating table by bolting a steel arch (Figure 4.11) on the steel rods coming from the top of the table (Figure 4.4) which securely held the handles of the air pot. The large vibrating table after bolting the necessary equipment on its top is shown in Figure 4.12. The small vibrating table, however, could only fit either two freeze-thaw molds or one freeze-thaw mold and one air pot as shown in Figure 4.13. The acceleration of vibration was measured using a three-axis submersible accelerometer. In the case of the immersion vibrator, the accelerometer was placed at several distances away from the vibrator. In the case of the table vibrators, the vibration acceleration was taken at the middle of the mold. The duration of vibration was either 30 seconds, 2 minutes or 4 minutes.



Figure 4.4 Large vibrating table



Figure 4.5 Immersion vibrator



Figure 4.6 Control unit for the large vibrating table



Figure 4.7 Vibrating motor attached to the bottom of the table top



Figure 4.8 Vibrating motor weights inside the motor for the small vibrating table



Figure 4.9 Concrete block at the bottom of the large vibrating table



Figure 4.10 Freeze-thaw molds at the top of the large vibrating table



Figure 4.11 ASTM C231 concrete air content container bolted to the top of the large vibrating table



Figure 4.12 The large vibrating table with two freeze-thaw specimen molds and ASTM C231 specimen container bolted to the table top



Figure 4.13 The small vibrating table during vibration

4.1.4. Freeze-Thaw Testing

Freeze-thaw testing was performed using an automated freeze-thaw machine (Figure 4.14) that can fit up to 80 prisms. All prisms went through 300 cycles of freezing and thawing or until the durability factor (DF) dropped below 60% according to ASTM C666 Method A. Initial concrete prisms' dimensions were measured prior to initiation of the test. Weight, length change and resonant frequency of each prism were taken before the initiation of testing and after each 30 to 36 freeze-thaw cycles. The sample was considered to have failed once the durability factor reached 60% or lower.



Figure 4.14 Freeze-thaw machine

Prior to freeze-thaw testing, concrete prisms were cured in limewater for 14 days then brought down to 40 ± 3 °F before taking initial measurements. Five hour freeze-thaw cycles were used in this study starting with 225 minutes of freezing from 40 ± 3 °F to 0 ± 3 °F followed by 75 minutes of thawing from 0 ± 3 °F to 40 ± 3 °F. The samples were protected from loss of moisture at all times. The following calculations were made each 30 to 36 cycles in order to assess the performance of the specimens. Equation 4.1 was used to calculate the relative dynamic modulus of elasticity. Equation 4.2 was used to calculate the durability factor (DF). Equation 4.3 was used to calculate the length change.

$$P_c = \frac{n_1^2}{n^2} \times 100 \quad \text{Equation 4.1}$$

Where:

P_c =Relative dynamic modulus of elasticity after “c” cycles of freeze-thaw (%)

n =Relative dynamic modulus of elasticity after “c” cycles of free-thaw (%)

n_f =Fundamental transverse frequency after “c” cycles of freeze-thaw (Hz)

$$DF = \frac{PN}{300} \quad \text{Equation 4.2}$$

Where:

P =Relative dynamic modulus of elasticity after “N” cycles of freeze-thaw (%)

N =Number of cycleas at which the test is terminated

$$L_c = \frac{(l_2 - l_1)}{L_g} \times 100 \quad \text{Equation 4.3}$$

Where:

L_c =Length change after “c” cycles of freeze-thaw (%)

l_1 =Length comparator reading after 0 cycles of freeze-thaw (in.)

l_2 = Length comparator reading after “c” cycles of freeze-thaw (in.)

L_g =Length of specimen (in.)

4.1.5. Hardened Air Void Analysis

The hardened samples from before and after vibration and the freeze-thaw prisms were saw-cut using the electric saw shown in Figure 4.15. One in. thick samples were obtained from each specimen for hardened air void analysis. These samples were then polished prior to scanning and image processing. Scanning of polished samples was performed at a resolution of 4800 dpi. A modification of the Peterson method [66] was adopted for scanning and image processing. The goal of image processing was to obtain a black and white image where the white was the air voids and the black was everything else. This image was then used along with the paste content value obtained from the mixture design to calculate air content and spacing factor.

This was done using a software that utilizes the principles of the linear traverse method of ASTM C457.



Figure 4.15 Electric saw

Figure 4.16 shows a saw-cut sample prior to polishing. Polishing was performed using the polishing machine shown in Figure 4.17. The two motors on the left and right of the machine were used to rotate the samples while the polishing wheel was rotated in the opposite direction. The different magnetic polishing discs were placed on top of the metal polishing wheel shown in Figure 4.17. The bucket shown at the top of Figure 4.17 was used to ensure a continuous stream of water for lubrication was applied on the polishing disc during the polishing operation. The polishing procedures began by applying a solution made of 80% acetone and 20% lacquer to the surface of the concrete that was to be polished in order to strengthen the paste and preserve the air voids during polishing. After the solution dried, the sample was fixed to a plastic cylinder

(Figure 4.18) using hot glue. This assembly was then placed on the polishing disc and connected to the two motors using rubber bands as shown in Figure 4.19. As shown in Figure 4.19, this procedure allowed four samples to be polished at the same time. Polishing was performed using progressively finer-grit discs: 80-grit, 1200-grit and 2200-grit discs respectively (Figure 4.20). The purpose of these discs was to level the specimen, remove the macro-scratches and remove the micro-scratches, respectively. An example of a polished specimen is shown in Figure 4.21. Prior to scanning, an orange powder was applied to the polished surface in order to fill all the voids with a machine-distinguishable color. The sample was then scanned. An example of a scanned sample after the colored powder was applied is shown in Figure 4.22. The scanned image after application of the colored powder was then processed in Photoshop in order to convert the orange color into white and the rest of the sample into black, resulting in the final black and white image (Figure 4.23). This image was then analyzed using a software to obtain the air content and the spacing factor using Equation 4.4 through Equation 4.6.

$$A = 100 \left(\frac{T_a}{T_t} \right) \quad \text{Equation 4.4}$$

$$p = 100 \left(\frac{T_p}{T_t} \right) \quad \text{Equation 4.5}$$

$$\bar{L} = \begin{cases} \frac{T_p}{4N} & \text{for } \frac{p}{A} \leq 4.342 \\ \frac{3T_a}{4N} \left[1.4 \left(1 + \frac{p}{A} \right)^{\frac{1}{3}} - 1 \right] & \text{for } \frac{p}{A} > 4.342 \end{cases} \quad \text{Equation 4.6}$$

Where:

A =Air content (%)

p =Paste content (%)

\bar{L} =Spacing factor

N =Total number of air voids intersected

T_t = Total length of traverse

T_a = Traverse length through air

T_p = Traverse length through paste



Figure 4.16 Saw-cut sample



Figure 4.17 Polishing machine



Figure 4.18 A concrete sample fixed to the plastic cylinder



Figure 4.19 Polishing machine during operation



Figure 4.20 Polishing discs (left to right: 80-grit, 1200-grit, 2200-grit)

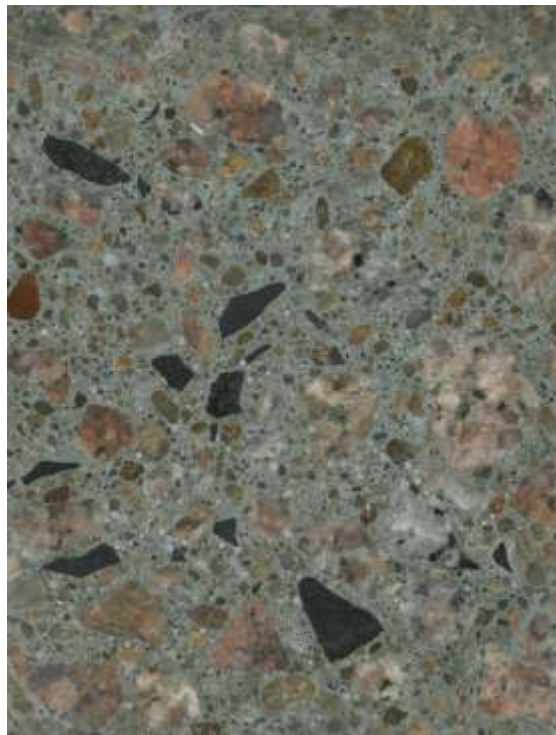


Figure 4.21 Polished sample

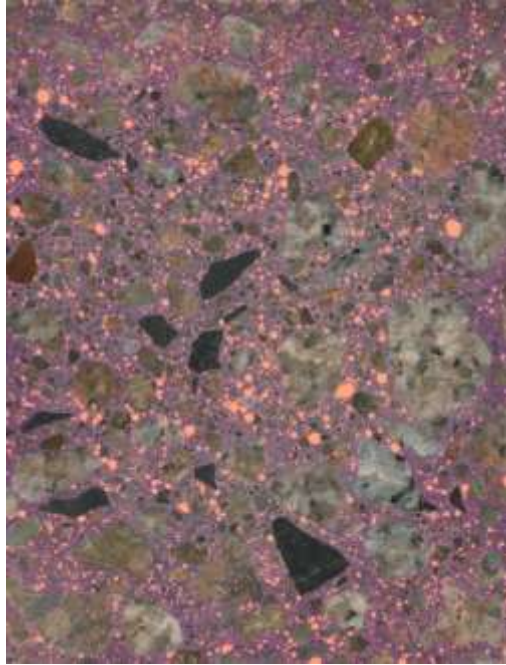


Figure 4.22 Scanned image with orange powder

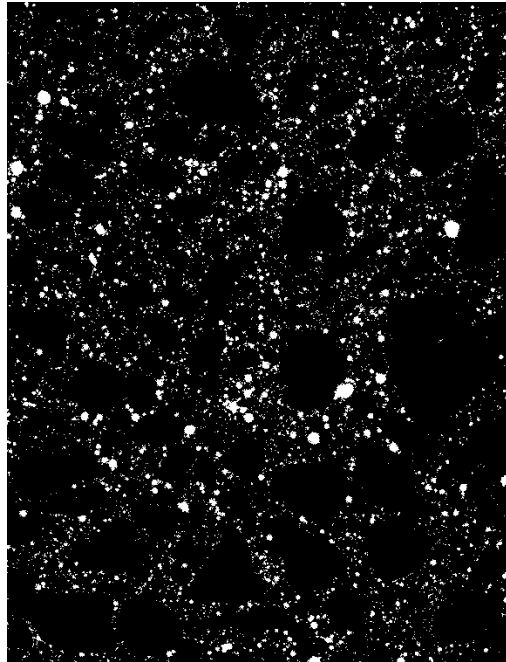


Figure 4.23 Black and white image

4.2. Specific Methods

4.2.1. Stability of Air Void System

The procedures for each test started with mixing the concrete after which the rheological properties were immediately measured. Temperature, slump, unit weight and air content before vibration was measured after finishing the rheology test. The fresh air content was measured using ASTM procedures of rodding and tamping according to ASTM C231. The small table vibrator was then used to vibrate the air pressure test container and freeze-thaw prism molds filled with concrete. The vibration was done at several times after the start of mixing; each time for new concrete molds and air pressure tests. Fresh air content was taken after each vibration. The concrete samples obtained from the molds were used for freeze-thaw testing. Each vibration period was carried out at a frequency of 75 Hz for 2 minutes. Two different peak vibration accelerations were used. Tests were done at a peak acceleration of either 3g or 10g. All measurements reported for the durability factor and hardened air parameters presented in section 5.1 are the average of two specimens.

4.2.2. Freeze-Thaw Durability of Externally Vibrated Concrete

After mixing, rheological properties were immediately measured using the ICAR rheometer. Temperature, Unit weight and fresh air content before vibration were measured after finishing the rheology test. The fresh air content was measured using ASTM procedures of rodding and tamping according to ASTM C231. A hardened concrete sample was also obtained before vibration in order to measure hardened concrete air void parameters before vibration. A table vibrator was then used to vibrate molds filled with concrete. Molds were vibrated for either 30 seconds or for 4 minutes. Some of the concrete prisms obtained from the molds were later used for hardened air void analysis while others were used for freeze-thaw testing followed by

hardened air void analysis. The frequency of vibration ranged from 33 Hz to 160 Hz and the peak acceleration ranged from 4 g to 25 g. After freeze-thaw testing, the prisms were saw-cut, polished then scanned. The scans were then used for hardened air void analysis. All measurements for the durability factor and hardened air parameters presented in section 5.2 are the average of two specimens.

4.2.3. Freeze-Thaw Durability of Internally Vibrated Concrete

Experiments to determine the freeze-thaw durability of internally vibrated concrete were performed using 85 in. long concrete beams that are 3 x 4 in. in cross section. After mixing, rheological properties, temperature, unit weight and fresh air content before vibration were measured. The fresh air content was measured using ASTM procedures of rodding and tamping according to ASTM C231. Concrete in these experiments was consolidated using an immersion vibrator at one end as shown in Figure 4.24. The vibration was then executed for 30 seconds. The first sample is expected to experience the highest acceleration whereas the last one is expected to experience almost no vibration. After hardening as shown in Figure 4.25, the long beams were saw-cut into 5 specimens using a hand-held gas saw as shown in Figure 4.26. These specimens were then subjected to freeze-thaw testing according to ASTM C666 method A.

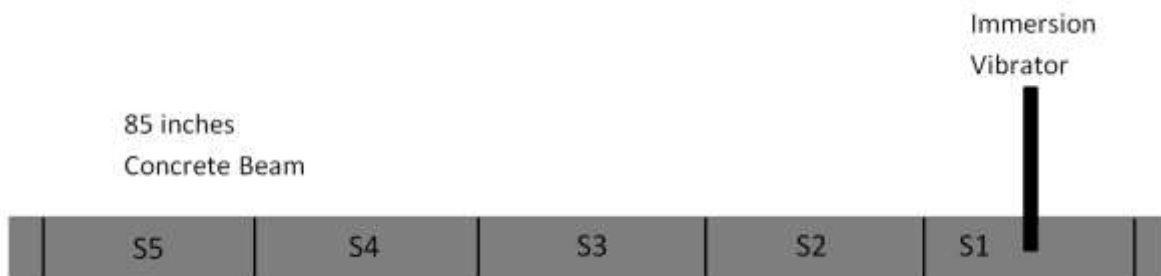


Figure 4.24 Immersion vibrator placement



Figure 4.25 Long beam after hardening



Figure 4.26 Saw-cutting long beams

4.2.4. Rheology under Vibration

In some applications, low slump concrete mixtures are used. These mixtures are also vibrated and can be exposed to freeze-thaw damage [1]. However, most existing concrete rheometers do not have the capability to measure the rheological properties of stiff concrete mixtures (i.e. typically mixtures having a slump value below 3 in.). Therefore, it has been attempted in this dissertation to try estimating the rheological properties of stiff mixtures from their properties under vibration. Due to the similarity in the behavior, under certain assumptions, between fresh concrete and granular suspensions (i.e. both exhibit Bingham plastic properties), it is assumed that the rheological properties of fresh concrete under vibration can be modelled using the same Equation 4.7 for vibrated granular suspensions [67]:

$$\tau = \frac{(G\gamma_c + \eta_H f_b \gamma_c) \dot{\gamma} + \eta_H \dot{\gamma}^2}{\dot{\gamma} + f_b \gamma_c} \quad \text{Equation 4.7}$$

Where:

τ =Shear stress

$\dot{\gamma}$ =Shear strain rate

G , γ_c , and η_H =Material properties

f_b =Vibration parameter

It is easy to see that Equation 4.7 can be reduced to Equation 4.8 if the vibration parameter is set to zero (i.e. no vibration):

$$\tau = G\gamma_c + \eta_H \dot{\gamma} \quad \text{Equation 4.8}$$

Equation 4.8 is very similar to the Bingham plastic equation where $G\gamma_c$ is analogous to the yield stress and η_H is analogous to the plastic viscosity. Figure 4.27 illustrates the behavior of granular suspensions both without and under vibration. It can be observed that, under vibration, granular suspensions cease to be a plastic and start to behave like a shear thinning non-

Newtonian fluid which is typically modelled by a power-law relationship. However, such a relationship is unrealistic in this case since the slope of the curve would be infinite at a zero strain rate. Vibrated materials should be flowing at a certain apparent viscosity which requires a finite slope at a zero strain rate. Therefore, Equation 4.7 is more suitable to model vibrated granular suspensions since it exhibits a finite initial slope and is asymptotic to the original Bingham model of the un-vibrated material at high strain rates. It can also be observed from Figure 4.27 that granular suspensions under vibration behave like Newtonian fluids at low strain rates and like Bingham plastics at high strain rates.

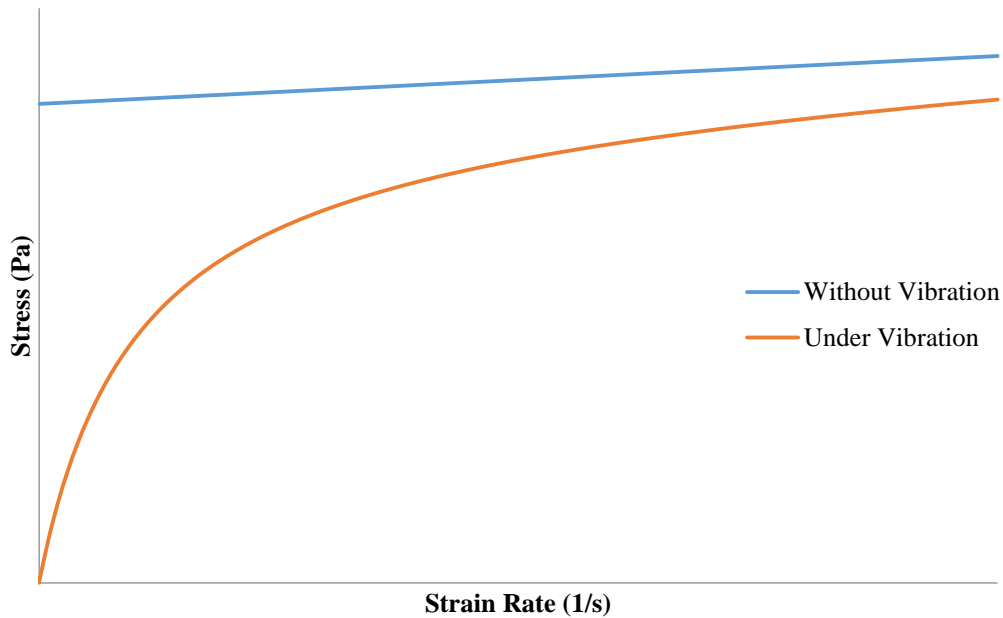


Figure 4.27 Rheological behavior of granular materials

In this study, rheology tests using the ICAR rheometer were performed during vibration. This was done for each mixture at different vibration configurations (i.e. different frequencies and peak accelerations). The rheology tests were also performed without vibration for applicable mixtures (mixture 1, 2 and 5). The rheometer bucket was bolted to the vibration table as shown in Figure 4.28. A wooden frame was used to hold the rheometer as shown in Figure 4.29.

Vibration parameters were measured both on the table itself and inside the concrete using an accelerometer as shown in Figure 4.30 and Figure 4.31 respectively. The vibration parameters inside the concrete were measured in the center of the rheometer pot at 1, 3, 6, 8 and 10 in. deep from the surface of the concrete. The height of the entire concrete sample was 12 in..



Figure 4.28 The rheometer bucket bolted to the top of the small vibrating table



Figure 4.29 The rheometer bolted to a wooden frame



Figure 4.30 Measuring vibration parameters on the vibrating table using an accelerameter



Figure 4.31 Measuring vibration parameters inside concrete using an accelerometer

The rheological data obtained without vibration were fitted using the Bingham

Equation 4.9:

$$\tau = \tau_0 + \mu_p \dot{\gamma} \quad \text{Equation 4.9}$$

Where:

τ =Shear stress

$\dot{\gamma}$ =Shear strain rate

τ_0 =Yield stress

μ_p =Plastic viscosity

The rheological data obtained during vibration were fitted using Equation 4.10 which is analogous to Equation 4.7:

$$\tau = \frac{(\tau_0 + \mu_p \gamma_v) \dot{\gamma} + \mu_p \dot{\gamma}^2}{\dot{\gamma} + \gamma_v} \quad \text{Equation 4.10}$$

Where:

γ_v =Vibration parameter

It was assumed that the slope of the tangent line of Equation 4.10 at $\dot{\gamma}=0$ is equal to the average apparent viscosity of the concrete mixture developed due to the given vibration.

Therefore, the intersection of this tangent line with the Bingham Equation 4.9 obtained from data without vibration was assumed to be at a point corresponding to the strain rate value that the vibration is imposing on the mixture. This is illustrated in Figure 4.32.

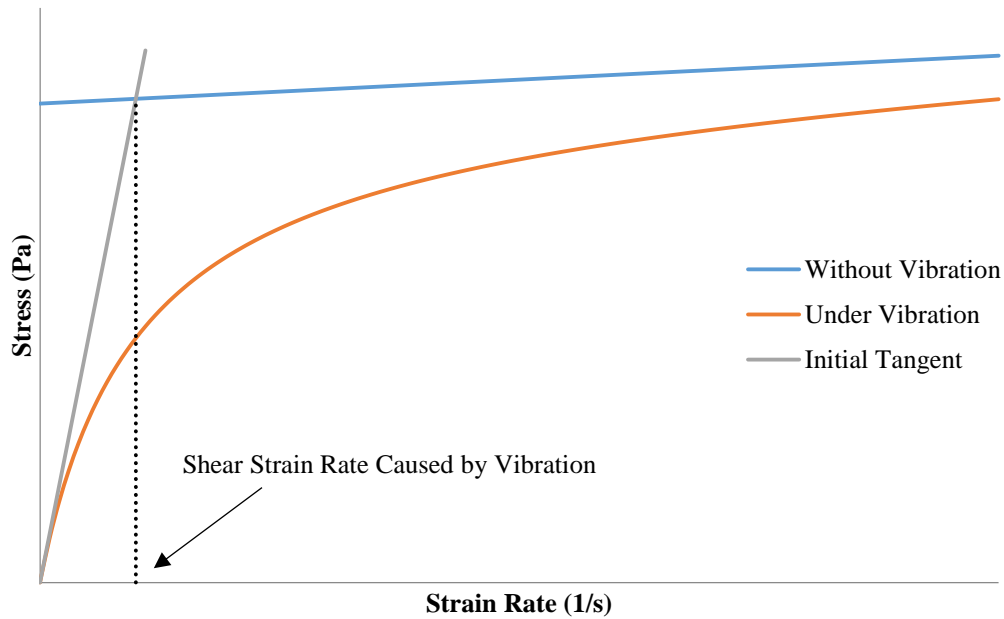


Figure 4.32 Point of intersection between the initial tangent to the "under vibration" curve and the "without vibration" line

By differentiating Equation 4.10, it is found that the slope of the tangent line at $\dot{\gamma}=0$ is as shown in Equation 4.11:

$$\text{Slope of initial tangent} = \frac{\tau_0}{\gamma_v} + \mu_p \quad \text{Equation 4.11}$$

Therefore, the equation of this tangent line is represented by Equation 4.12:

$$\tau = \left(\frac{\tau_0}{\gamma_v} + \mu_p \right) \dot{\gamma} \quad \text{Equation 4.12}$$

The strain rate at the point of intersection between Equation 4.8 and Equation 4.12 can then be found to be as shown in Equation 4.13:

$$\left(\frac{\tau_0}{\gamma_v} + \mu_p\right)\dot{\gamma}_i = \tau_0 + \mu_p\dot{\gamma}_i \xrightarrow{\text{Implies}} \dot{\gamma}_i = \gamma_v \quad \text{Equation 4.13}$$

Where:

$\dot{\gamma}_i$ =Shear strain rate at point of intersection (i.e. shear strain rate caused by vibration)

This indicated that the strain rate caused by vibration is actually equal to the vibration parameter γ_v . The yield stress and plastic viscosity parameters were obtained experimentally for mixtures 1, 2 and 3 by fitting Equation 4.9 to the data obtained without vibration. These parameters were then used to obtain the vibration parameter experimentally for mixtures 1, 2 and 5 at each vibration configuration by fitting Equation 4.10 to the data obtained during vibration. A linear correlation between the vibration parameter and peak vibration velocity was then established. This correlation was used to obtain the vibration parameters corresponding to each peak vibration velocity applied to mixture 4. The vibration parameter was then used to obtain the yield stress and plastic viscosity parameters experimentally for mixture 4 at each vibration configuration by fitting Equation 4.10 to the data obtained during vibration. The yield stress and plastic viscosity of mixture 4 was then taken to be the average of the obtained parameters from all vibration configurations.

Chapter 5 - Results and Discussions

5.1. Stability of Air Void System

Looking at the mixtures that contained the HRWR, the LRWR and the synthetic AEA, one can observe from Figure 5.1 the different rheological properties of these mixtures. All of these mixtures had similar plastic viscosity. The mixtures in Figure 5.1 and Figure 5.2 are labeled with their admixtures' dosages (i.e. HRWR dosage / LRWR dosage / AEA dosage in oz/cwt).

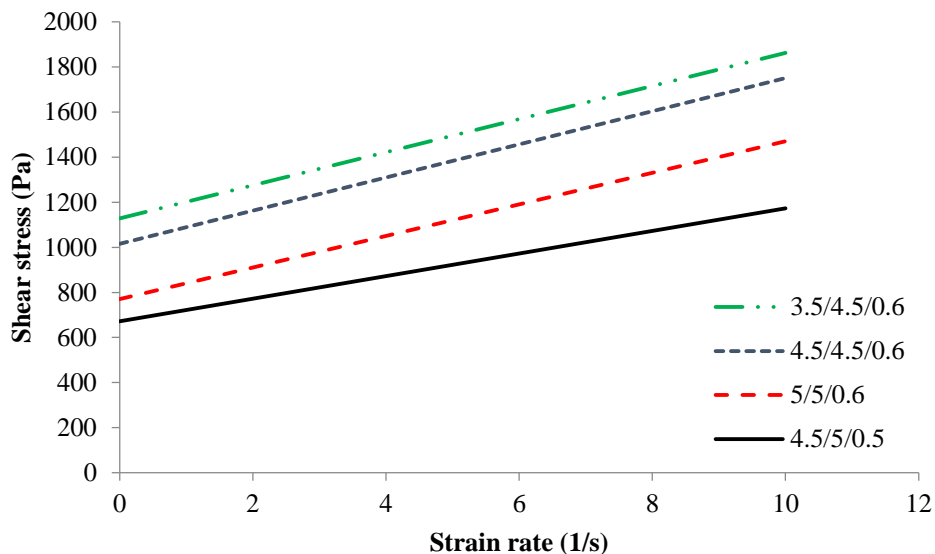


Figure 5.1 Rheological properties of HRWR + LRWR + synthetic AEA mixtures that experienced 3 g of vibration

Figure 5.2 shows the percentage air loss due to the 3g vibration at different times from the start of mixing. It can be observed that the air content in concrete became more unstable with time causing increased air loss due to vibration. The maximum percentage air loss was found to be around 55% for mixtures 3.5/4.5/0.6 and 4.5/4.5/0.6 at 100 minutes from the start of the mixing. The relation between the percentage air loss and time seemed to be somewhat linear

which makes it applicable to predict air loss with time. It can also be noted from Figure 5.2 that the rate at which air loss increased with time was similar for all mixtures. This could give an indication that mixtures with the same set of admixtures tend to have the same air system stability once air loss begins. Figure 5.1 and Figure 5.2 show that mixtures with higher yield stress (i.e. stiffer mixtures) tend to lose more air with time than mixtures with lower rheological properties (i.e. more fluid mixtures). The air loss was also higher in mixtures with lower HRWR, contradicting the notion that polycarboxylate admixtures bear primary responsibility for the loss of air void stability. This may be because the mixtures with the higher yield stress should also stiffen faster and increase the pressure acting on the bubbles during vibration, possibly causing them to go into solution and form larger bubbles after reemerging from solution or fracturing the shell formed around the air bubble by the AEA and hydration products [68, 69].

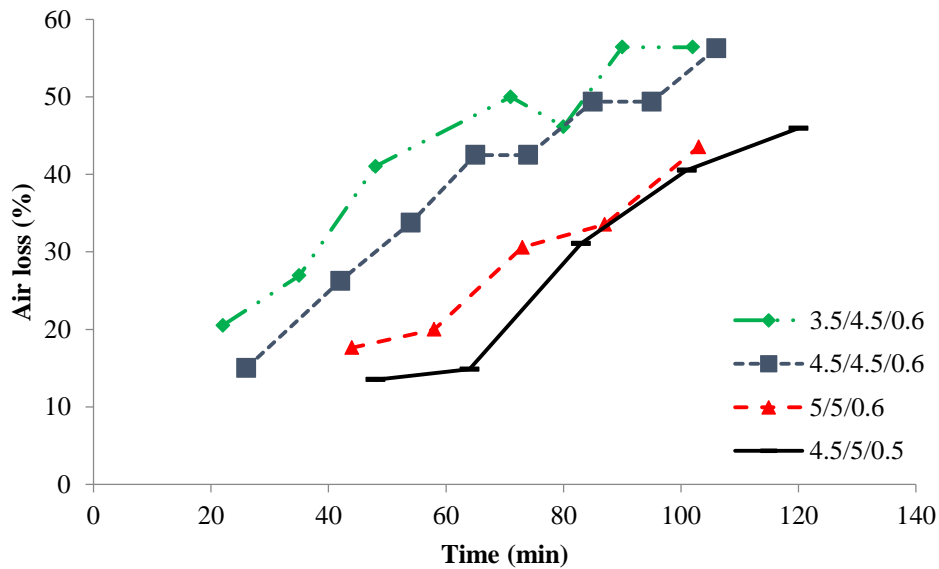


Figure 5.2 Air loss versus time for HRWR + LRWR + synthetic AEA mixtures that experienced 3 g of vibration

Figure 5.3 and Figure 5.4 show the results obtained for the set of mixtures that contained the HRWR and the wood rosin AEA. The mixtures in Figure 5.3 and Figure 5.4 are labeled with

their admixtures' dosages (i.e. HRWR dosage / AEA dosage in oz/cwt). Just like the previously described experiments, this set of experiments also showed increased instability of the air system with time (Figure 5.4). Maximum air loss was observed to be around 45% at about 100 minutes from the start of mixing. This set also showed the linear relation between percentage air loss and time. Moreover, the rate at which air loss increased with time was similar for all mixtures which further confirmed the observation that mixtures with the same set of admixtures tended to have the same rate of air loss once air loss began. Figure 5.3 and Figure 5.4 show that mixtures with higher viscosity lose similar amounts of air with time, probably because the similar dosages of HRWR gave similar slump retention with time. Changes in the plastic viscosity or AEA dosage did not appear to have a significant effect on the air loss rate.

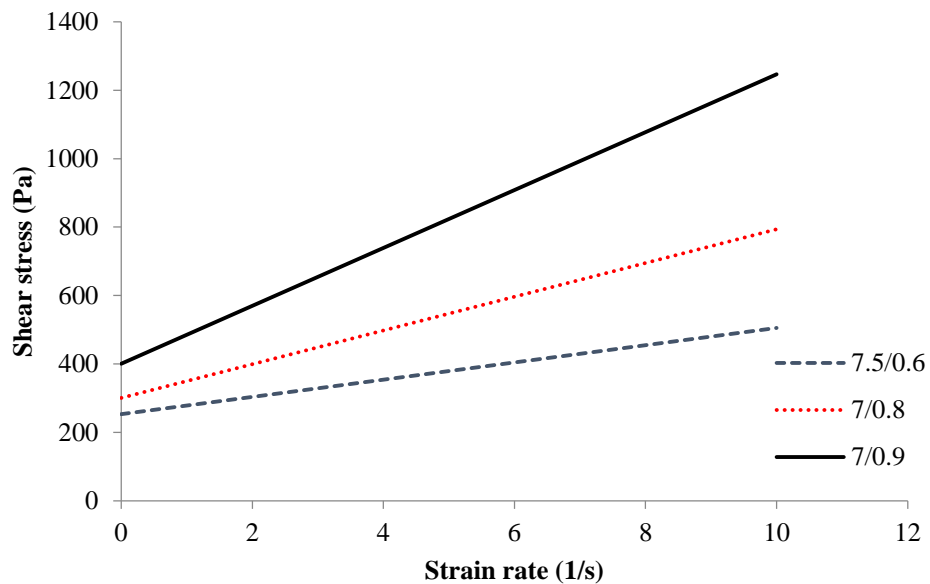


Figure 5.3 Rheological properties of HRWR + wood rosin AEA mixtures that experienced 3 g of vibration

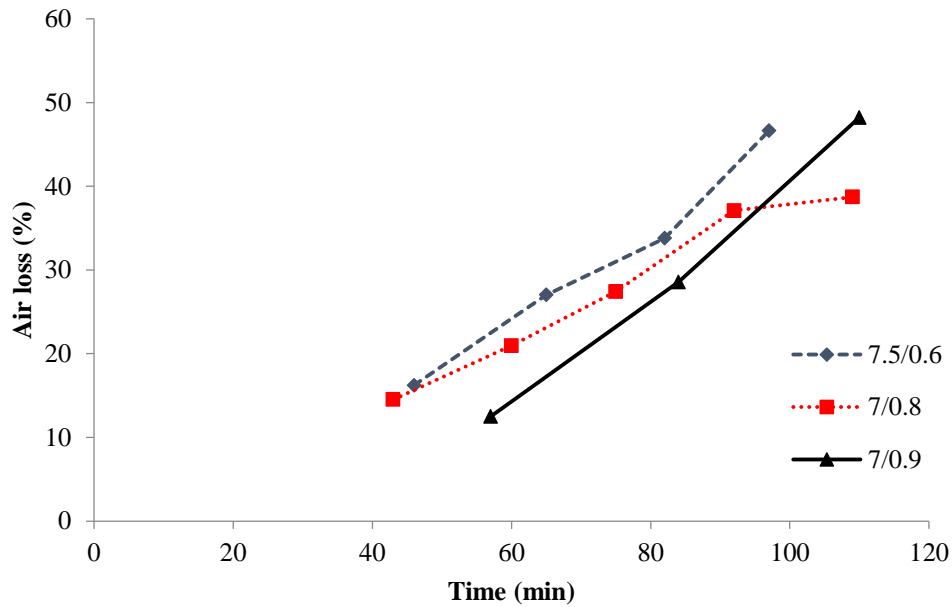


Figure 5.4 Air loss versus time for HRWR + wood rosin AEA mixtures that experienced 3 g of vibration

Figure 5.5 through Figure 5.8 show two other sets of mixtures made to examine the effects of AEA type. The first set (Figure 5.5 and Figure 5.6) consisted of mixtures that contained the HRWR and the synthetic AEA, while the second set (Figure 5.7 and Figure 5.8) consisted of mixtures that contained the HRWR and the tall oil AEA. The mixtures in Figure 5.5 through Figure 5.8 are labeled with their admixtures' dosages (i.e. HRWR dosage / AEA dosage in oz/cwt). Similar to the previous sets, these sets also showed the trend of increased air loss with time. In the case of the synthetic AEA, the mixture with the lower yield stress lost more air. This is probably because the mixture that used more AEA either stabilized more bubbles with shells containing AEA, or the shells produced were of higher quality when more AEA was used. Clearly the mechanisms that contribute to air void instability are complex and dependent on many variables. The synthetic and tall oil-based AEA experienced similar rates of air loss with time.

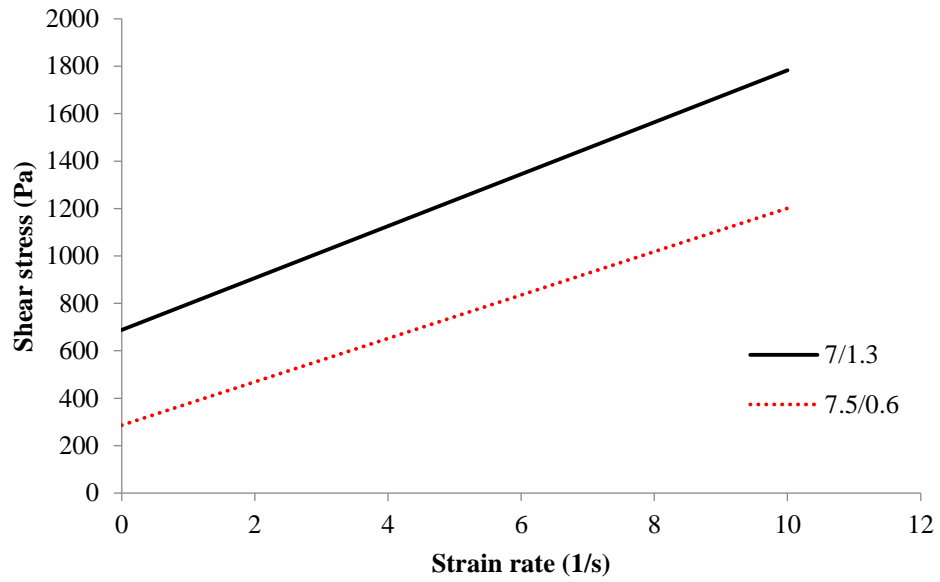


Figure 5.5 Rheological properties of HRWR + synthetic AEA mixtures that experienced 3 g of vibration

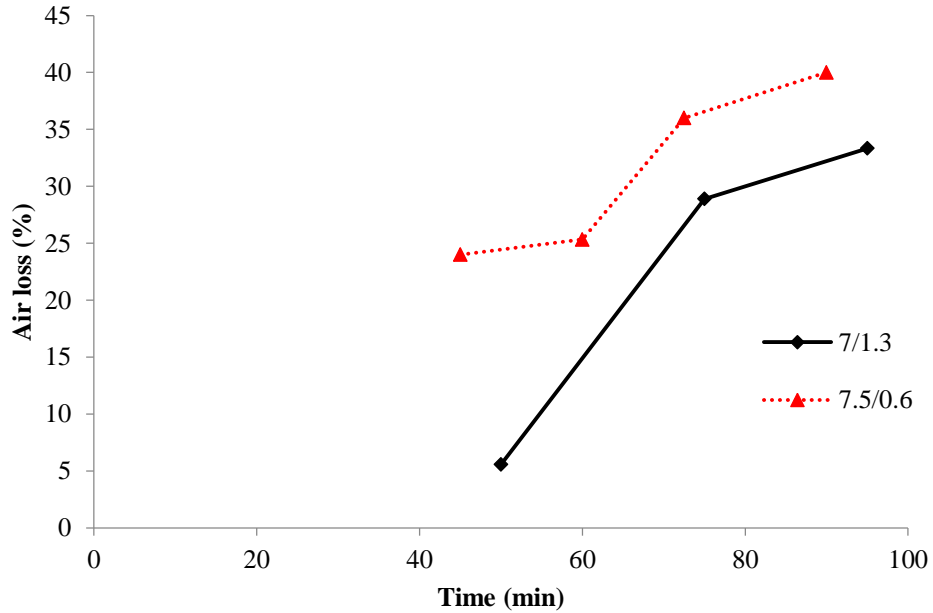


Figure 5.6 Air loss versus time for HRWR + synthetic AEA mixtures that experienced 3 g of vibration

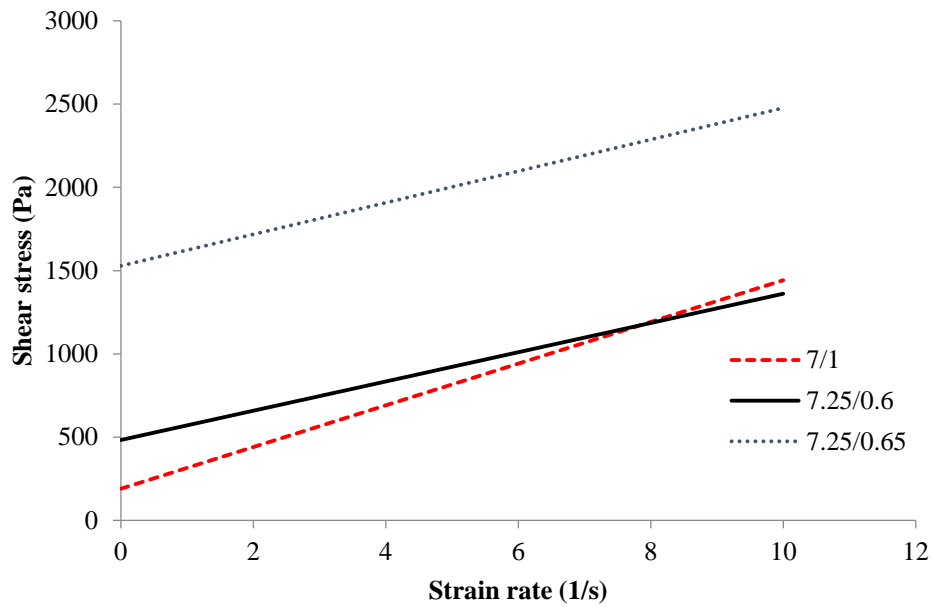


Figure 5.7 Rheological properties of HRWR + tall oil AEA mixtures that experienced 3 g of vibration

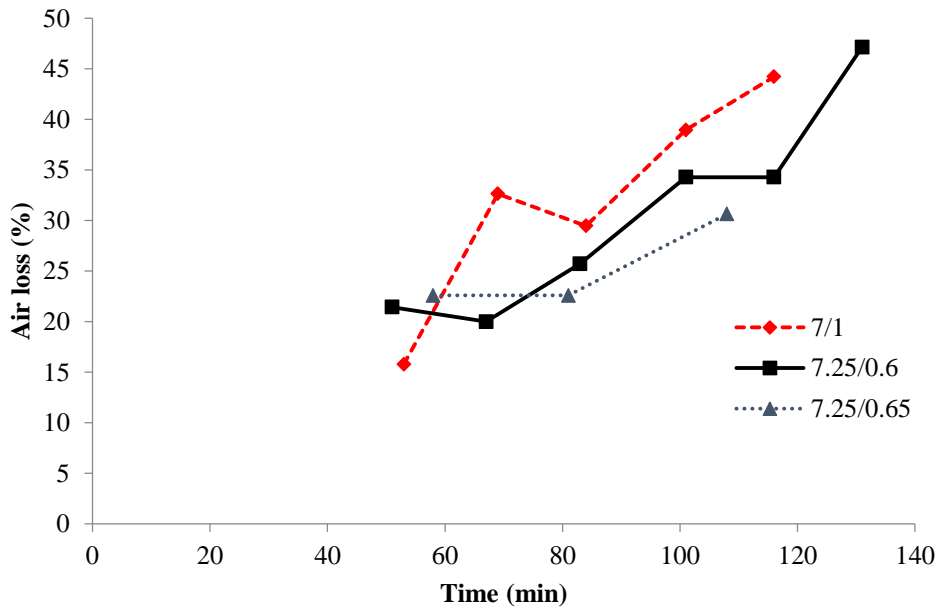


Figure 5.8 Air loss versus time for HRWR + tall oil AEA mixtures that experienced 3 g of vibration

In an attempt to compare the effect of different admixtures combinations on the stability of the air system of concrete while isolating the effect of rheological properties, mixtures with

similar rheological properties were grouped together for comparison. Figure 5.9 and Figure 5.10 display the results for this group. It can be observed from Figure 5.9 that the rheological properties were not exactly the same since it is practically very hard to obtain mixtures with similar rheological properties, especially if different materials are used in each mixture. However, the shown properties were considered to be fairly close to each other. The first observation from Figure 5.10 is the fact that the mixture with no HRWR took longer to begin to show air void instability. This could be because of the higher w/cm required to achieve similar yield stress as the mixtures with HRWR, and should have better slump retention with time. The synthetic AEA + HRWR mixture experienced slightly higher air loss by percentage. However, the difference was small. Looking at the slope of percentage air loss versus time (Figure 5.10), it can be observed that the tall oil AEA + HRWR mixture and the synthetic AEA + HRWR mixture had slightly smaller slopes compared to the other two. However, the difference was not enough to say that it is significant.

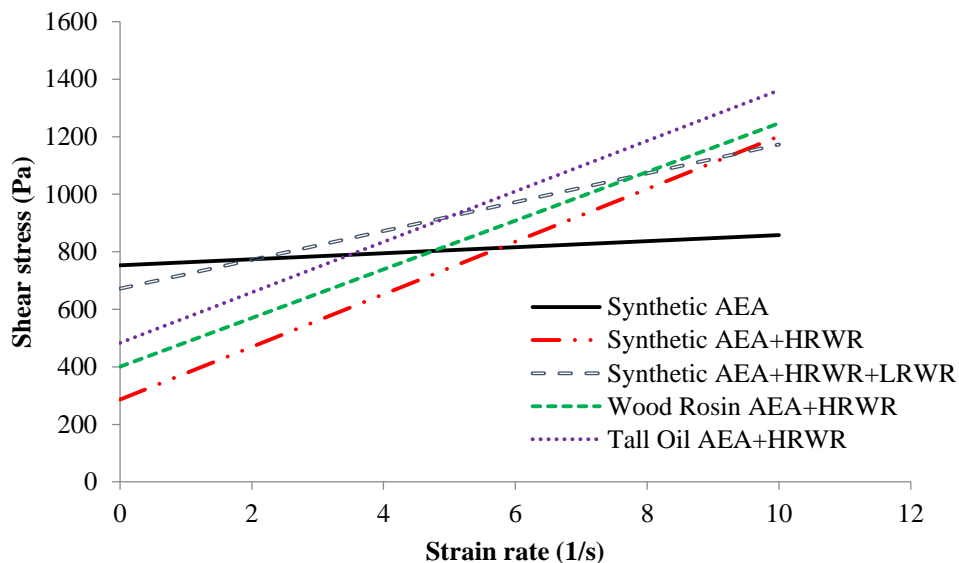


Figure 5.9 Rheological properties of selected mixtures that experienced 3 g of vibration

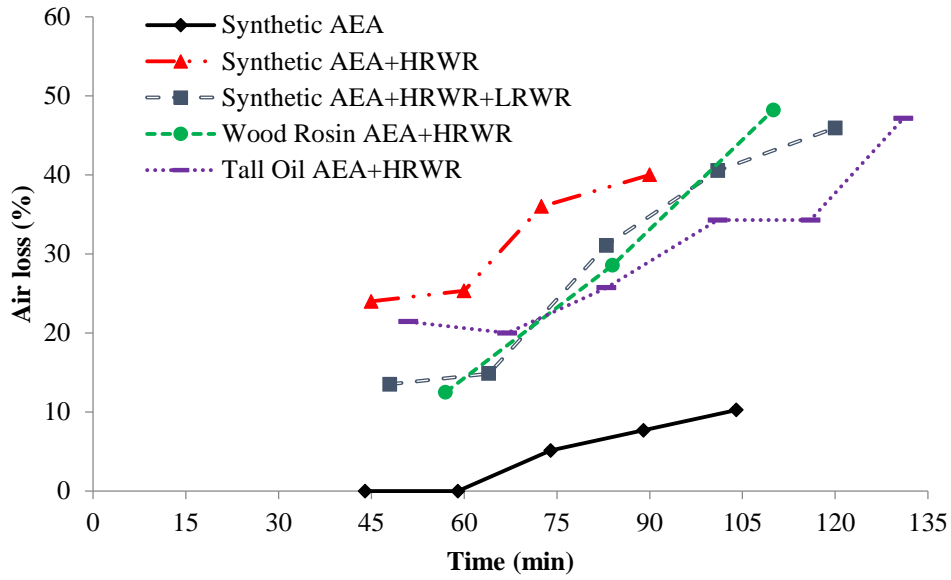


Figure 5.10 Air loss versus time for selected mixtures that experienced 3 g of vibration

A similar group was constructed for the case of concrete mixtures vibrated using 10 g of vibration acceleration (Figure 5.11 and Figure 5.12). This group yielded similar results to the previous group. The AEA type appeared to have little effect on the rate of air loss with time before vibration.

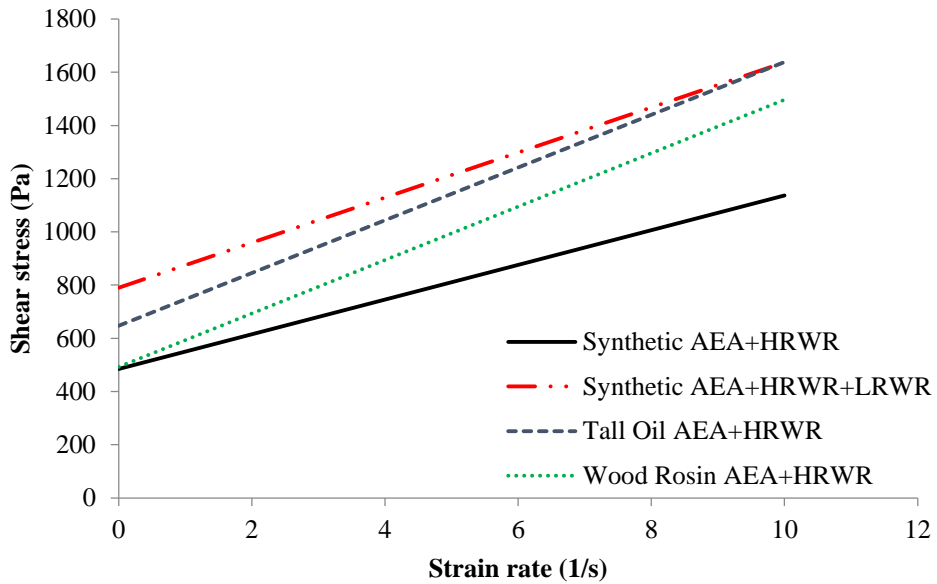


Figure 5.11 Rheological properties of selected mixtures that experienced 10 g of vibration

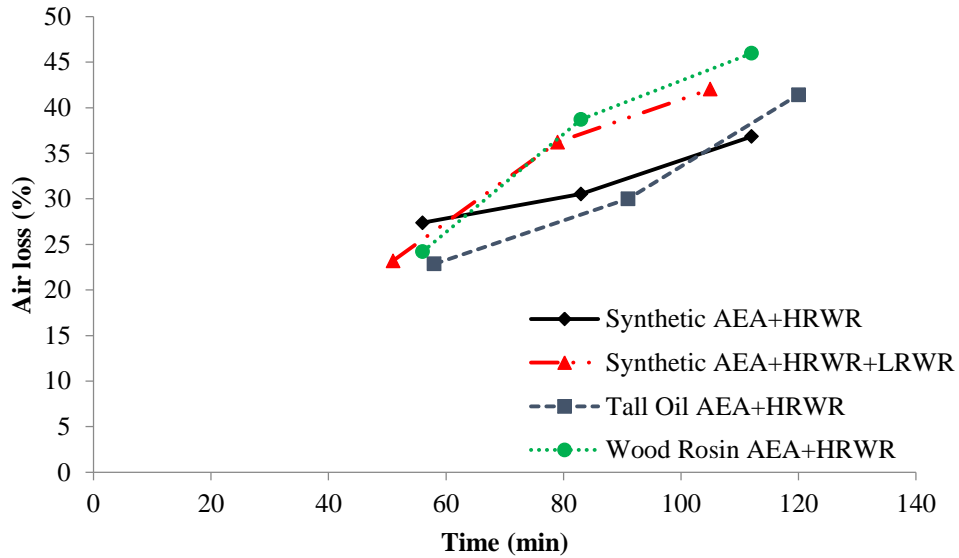


Figure 5.12 Air loss versus time for selected mixtures that experienced 10 g of vibration

Figure 5.13 and Figure 5.14 show the results for two tall oil AEA + HRWR mixtures vibrated at two different vibration accelerations. These results show the effect of the vibration acceleration on the percentage air loss. It is evident that vibration at higher acceleration (i.e. higher vibration energy) resulted in similar air void stability with time.

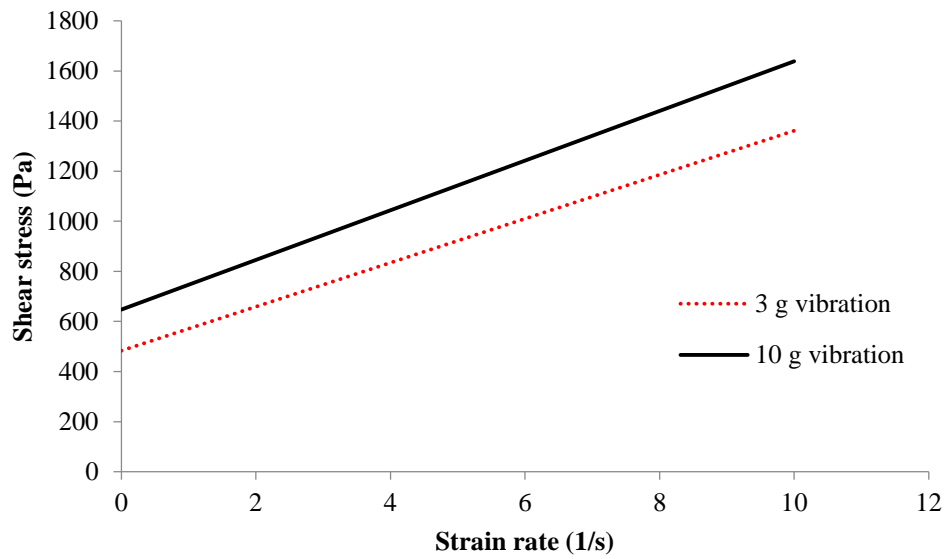


Figure 5.13 Rheological properties of tall oil AEA + HRWR mixtures (10 g versus 3 g vibrations)

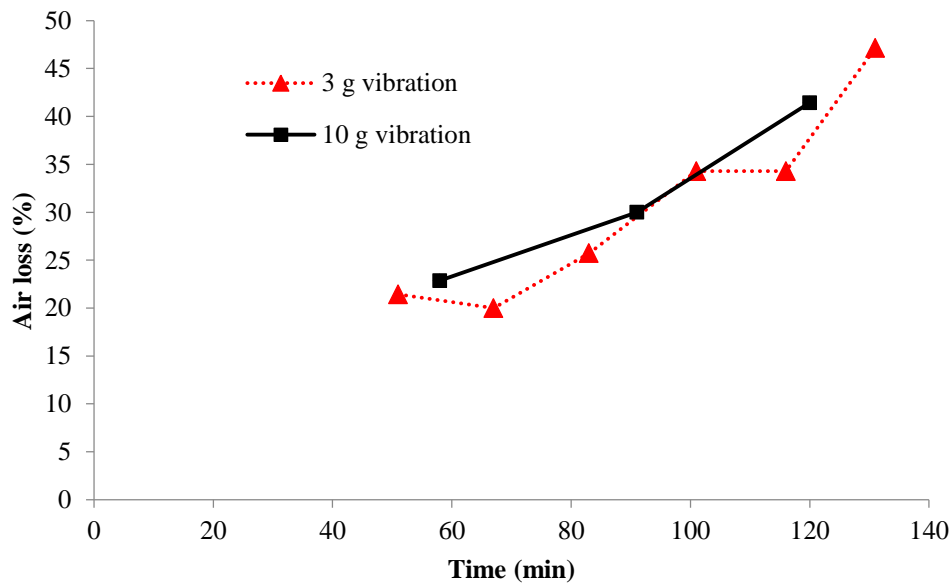


Figure 5.14 Air loss versus time for tall oil AEA + HRWR mixtures (10 g versus 3 g vibrations)

As shown in Figure 5.15, all the specimens in this study were able to pass freeze-thaw testing even after losing 55% of the initial air content. This is most probably due to the fact that

the initial air content was fairly high in all mixtures. Even after vibration, almost all specimens retained final air contents above 3% (Figure 5.16). There are, however, some specimens that experienced some decrease in the relative dynamic modulus of elasticity, although they still passed. These specimens had the lowest initial air content (5.45%) among all specimens. Their durability factors were found to be 82%, 62% and 76% corresponding to spacing factors of 0.0087, 0.0089 and 0.0099 in., respectively. These spacing factors were higher than the recommended maximum limit by the American Concrete Institute (ACI). The freeze-thaw testing showed that even though the mixtures tested experienced large air losses as a percentage of the air content before mixing, this did not necessarily translate into performance issues.

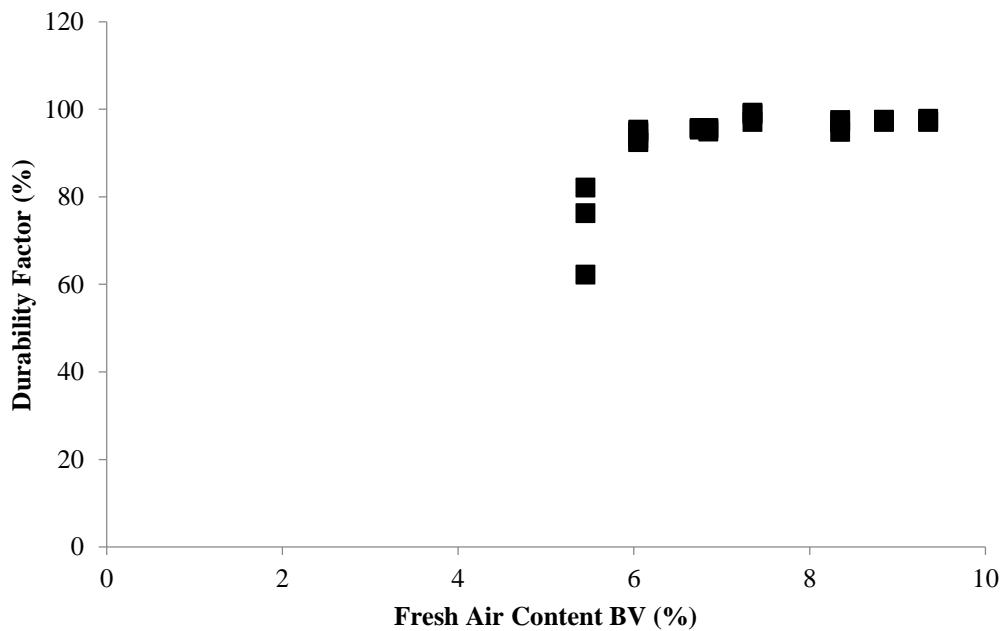


Figure 5.15 Durability factor versus fresh air content before vibration (effect of admixtures on the air system)

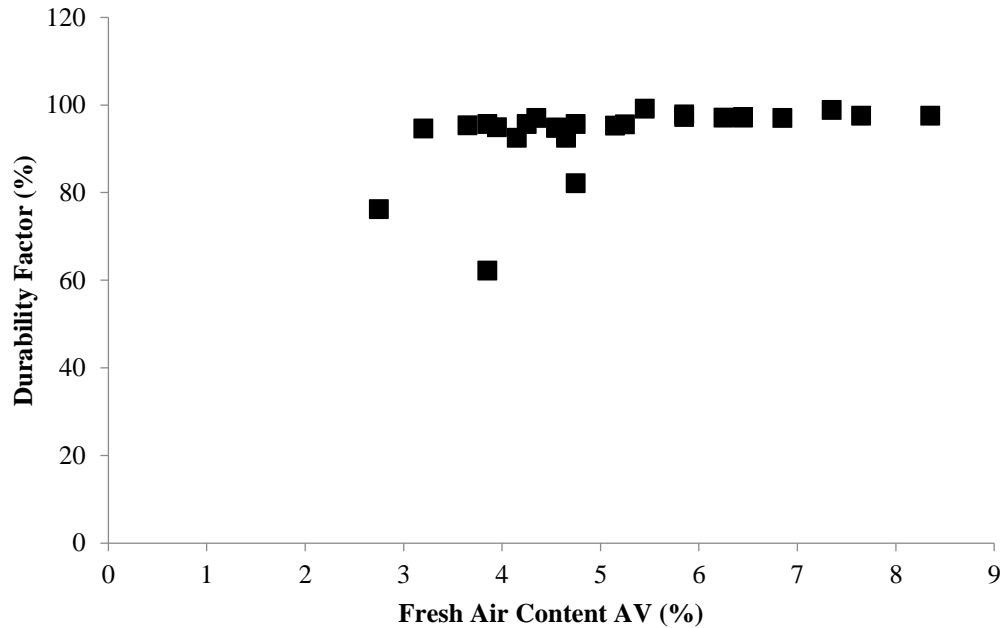


Figure 5.16 Durability factor versus fresh air content after vibration (effect of admixtures on the air system)

5.2. Freeze-Thaw Durability of Externally Vibrated Concrete

5.2.1. Effect of Vibration Duration

In order to isolate the effect of the vibration duration and the admixture combination, some of the concrete mixtures were vibrated at the same frequency (75 Hz) and peak acceleration (8 g) for different amounts of time. The average of the fresh air content before vibration for this set of experiments was 4.23% which is normally considered to be sufficient for freeze-thaw durability. The average for the hardened air content before vibration, however, was lower at 3.53%. It is usually observed that the hardened air content was slightly lower than the fresh air content for each test. This could be due to loss of large air bubbles during the hardening period.

Figure 5.17 illustrates the effect of vibration duration on the freeze-thaw performance. It can be observed from the figure that all mixtures, with the exception of two, performed almost the same way whether vibrated for 30 seconds or 4 minutes. This is true despite the fact that

Figure 5.18 indicates that the final spacing factor value was slightly higher in the case of 4 minutes vibration. However, the difference on average was only around 0.001 in. On the other hand, there was a notable difference in terms of the amount of total air loss (Figure 5.19). The air loss due to 4 minutes vibration was 0.5% to 1.5% more than the air loss due to 30 seconds vibration. This big difference in air loss compared to the small difference in durability performance indicates that extended vibration will impacts the larger bubbles more than the small bubbles that are essential for freeze-thaw resistance. Therefore, spacing factor was only marginally affected which explains the similarity in durability factor values. Another thing that can be observed from Figure 5.17 is the fact that admixture combination C performed very poorly compared to combinations A and B. This was true despite the fact that corresponding mixtures had comparable rheological properties and initial air content. This indicates that admixture combinations can play a critical role in the freeze-thaw performance of the resulting system once vibration is used. The durability factor results were supported by the high final spacing factor values shown in Figure 5.18. This particular admixtures' combination could be producing larger than desired air bubbles resulting in a poor air structure. Alternatively, the chemicals could be producing a very unstable shell around the air bubbles that could be easily destroyed under vibration.

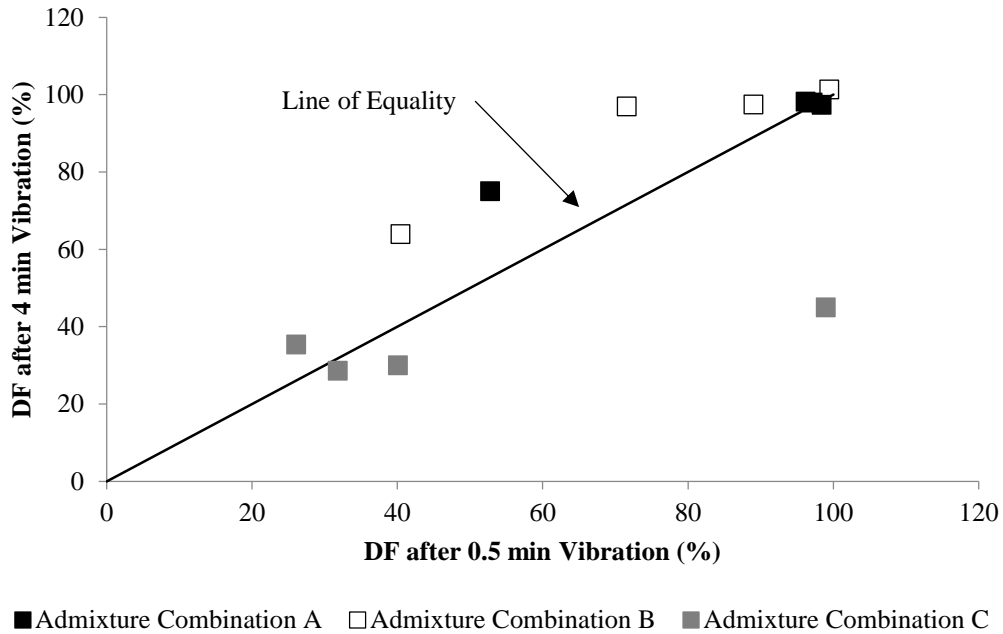


Figure 5.17 Effect of vibration duration on the durability factor with vibration acceleration of 8g at 75 Hz

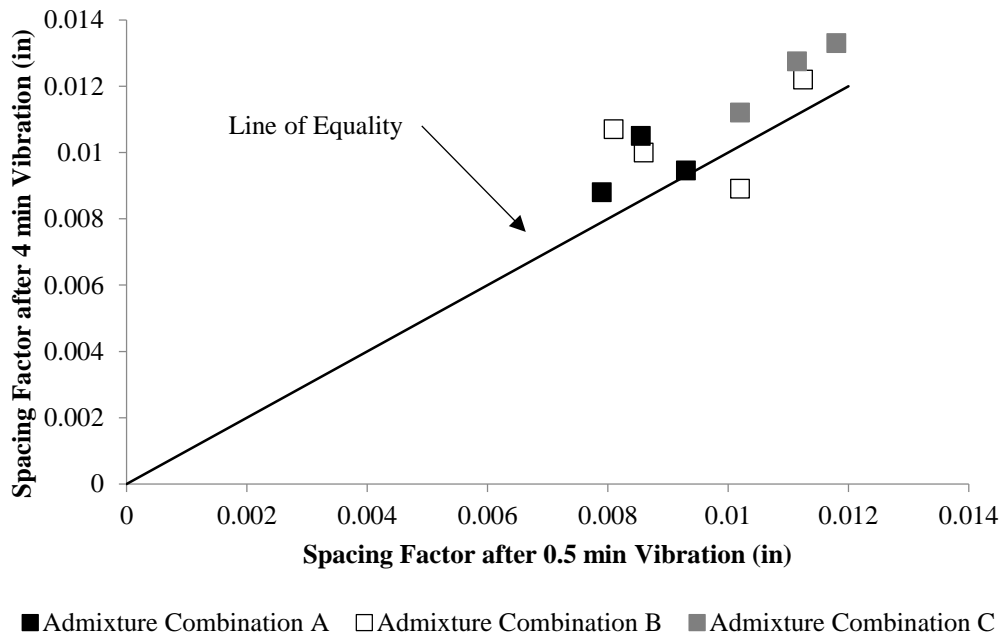


Figure 5.18 Effect of vibration duration on final spacing factor with vibration acceleration of 8g at 75 Hz

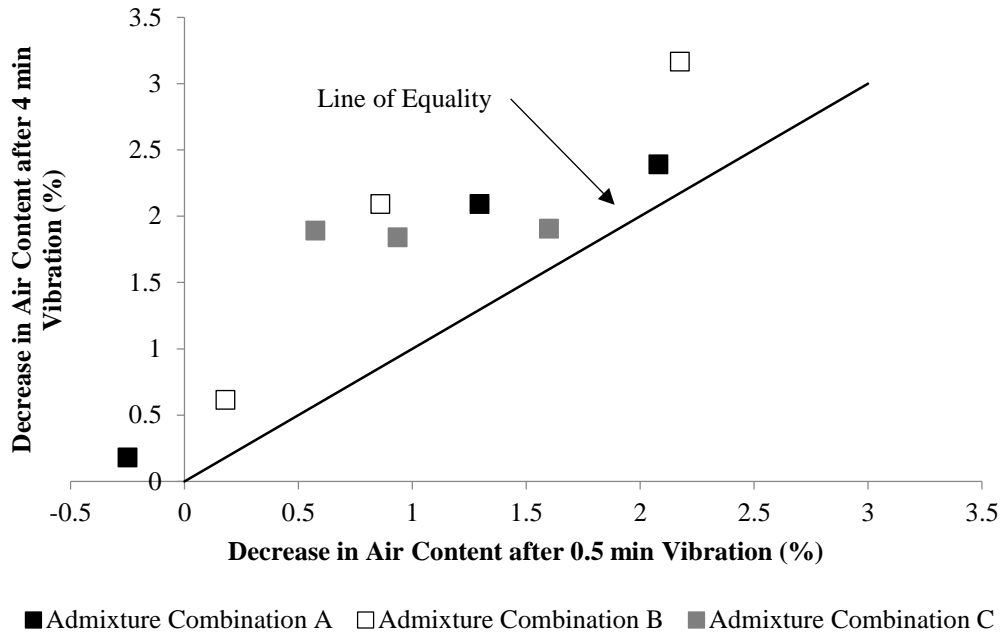


Figure 5.19 Effect of vibration duration on decrease in air content with vibration acceleration of 8 g at 75 Hz

In order to determine if different vibration frequencies and peak accelerations would affect the air void system and freeze-thaw durability differently than 8g of acceleration at 75 Hz, the effect of vibration duration was measured for results from mixtures that were vibrated at different frequencies (75, 110 and 160 Hz) and peak accelerations (8, 15 and 20 g) for chemical admixture combinations A and B. From Figure 5.20 and Figure 5.21, both the final fresh and hardened air content values supported the previous results that 4 minutes vibration resulted in a significantly higher air loss. The difference in air loss was as high as 3% in some cases. However, Figure 5.22 suggests that the difference in the final spacing factor is, in most cases, very marginal. These results support the previous conclusions that extended vibration periods will result in loss of large air bubbles rather than small ones.

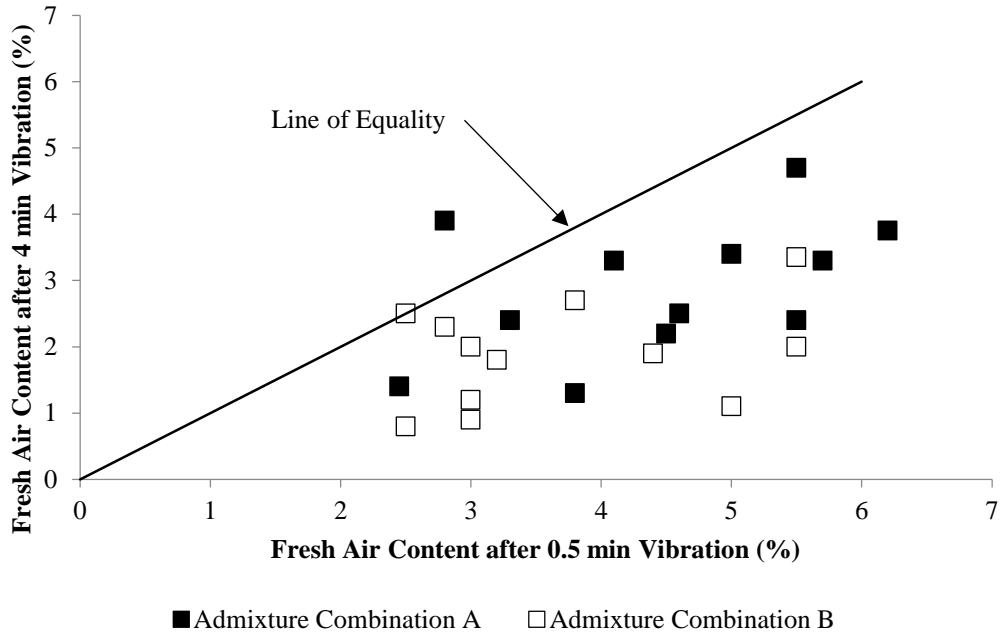


Figure 5.20 Effect of vibration duration on final fresh air content (different frequencies and peak accelerations)

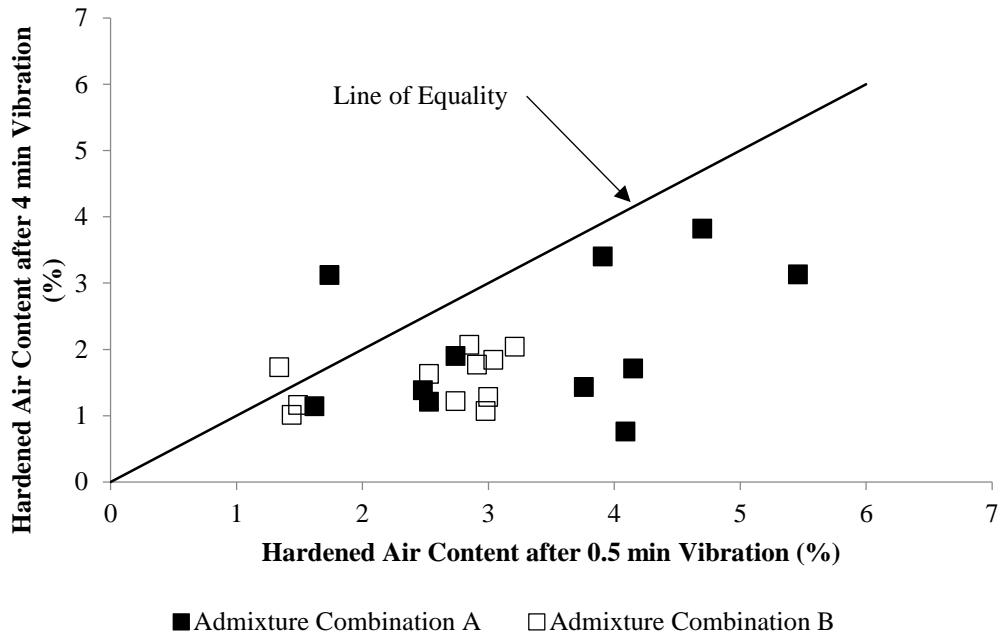


Figure 5.21 Effect of vibration duration on final hardened air content (different frequencies and peak accelerations)

observed that the batches, which underwent peak accelerations of 15 g and higher, experienced deterioration which led to failure in the case of 15 and 20 g peak accelerations. However, it cannot be ascertained that samples vibrated at 8 g are not susceptible to damage since the air content before vibration for this particular case was more than 1% higher than those vibrated at higher accelerations. The interesting thing to be observed from Figure 5.24 is that 25 g peak acceleration caused less deterioration (i.e. no failure) compared to lower peak accelerations. This occurred despite the fact that the batch vibrated at 25 g had lower air content (Figure 5.24), yield stress and plastic viscosity (Figure 5.23) compared to the batch vibrated at 20 g. This could be just a natural experimental variation. Nevertheless, considering the deterioration of the specimens regardless of failure, one can conclude that for very fluid mixtures vibration acceleration above a threshold amount can contribute to freeze-thaw damage. Looking at the air void parameters, Figure 5.25 and Figure 5.26 show the effect of peak acceleration on the increase in spacing factor and the decrease in air content, respectively. Looking at the final spacing factor (Figure 5.27) and final air content (Figure 5.28), some conclusions can be made. Figure 5.27 indicates that the final spacing factor increased with the increase in peak acceleration. However, this increase was very small (around 0.001 in between the 8 g and the 25 g specimens). Figure 5.28 shows that the final air content decreased with increase in peak acceleration. The total air content after vibration was similar for concrete vibrated at 8g or higher. This is most likely because vibration at 8g or higher for 4 minutes removed most of the air from the concrete.

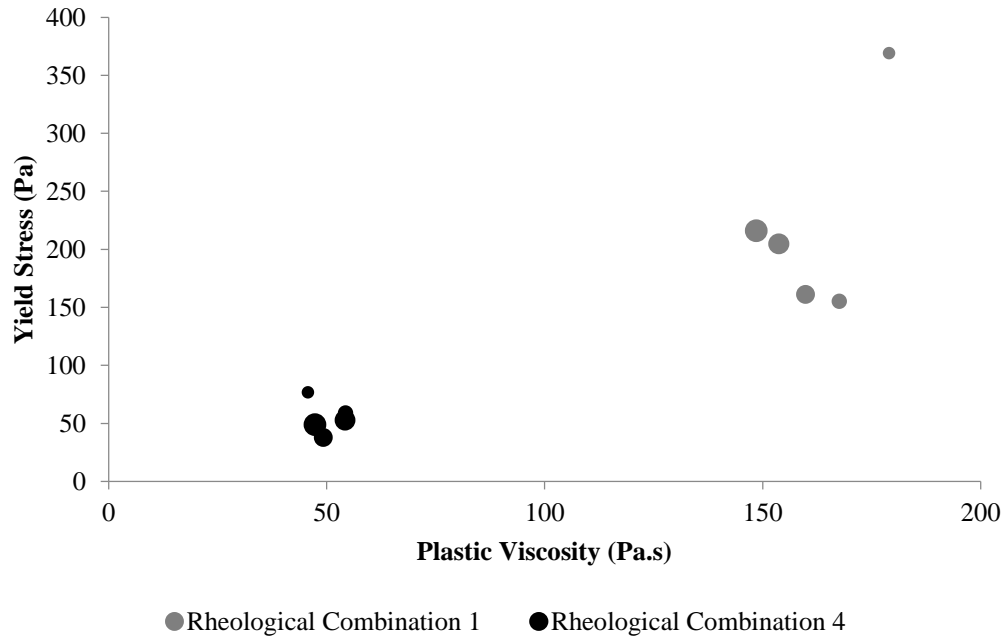


Figure 5.23 Rheological properties for the study of the effect of vibration acceleration

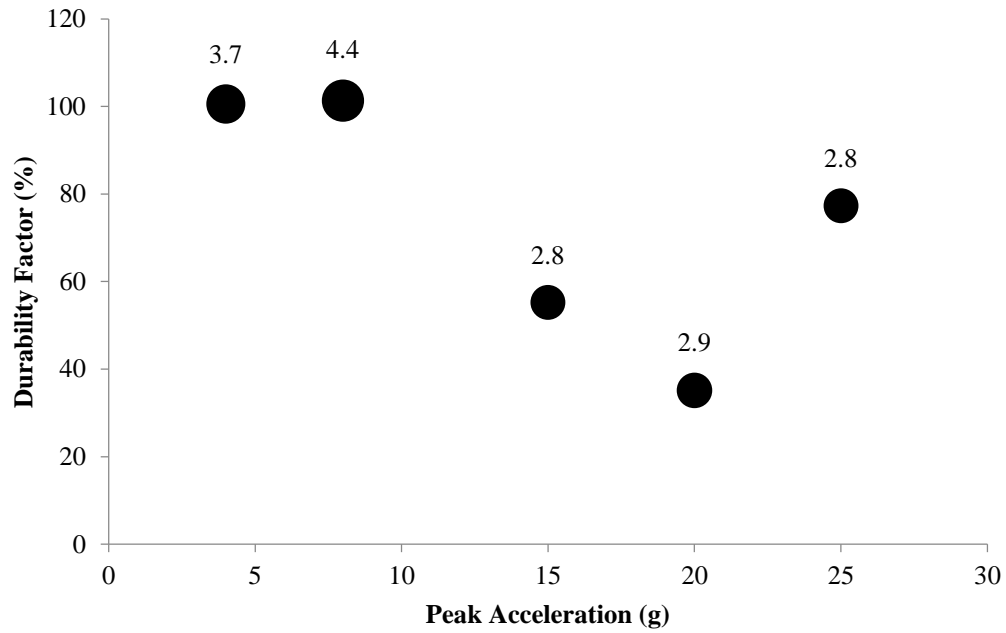


Figure 5.24 Effect of vibration acceleration on the freeze-thaw performance of rheological combination 4

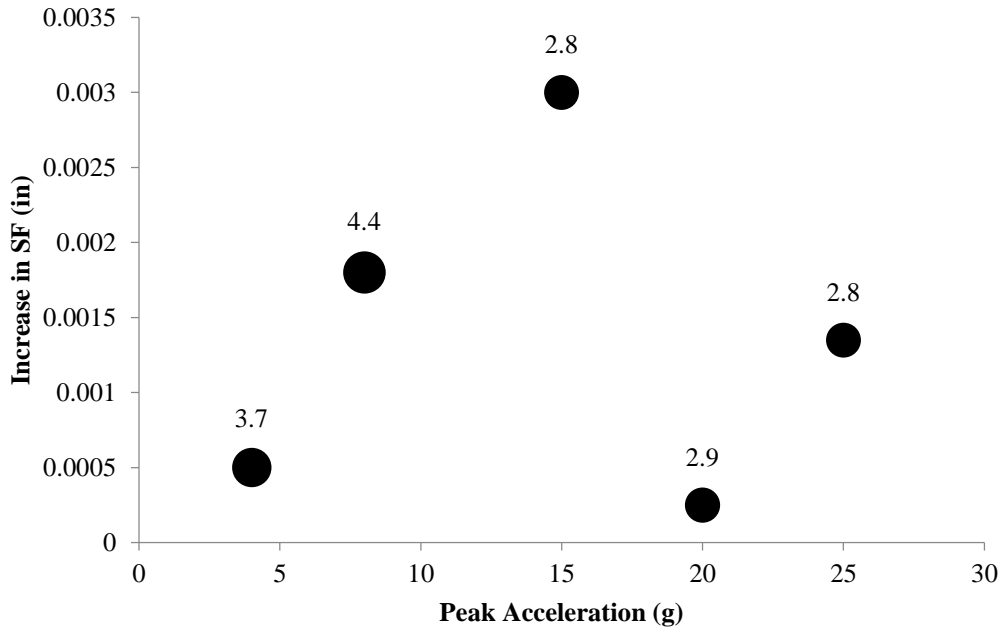


Figure 5.25 Effect of vibration acceleration on the increase in the spacing factor of rheological combination 4

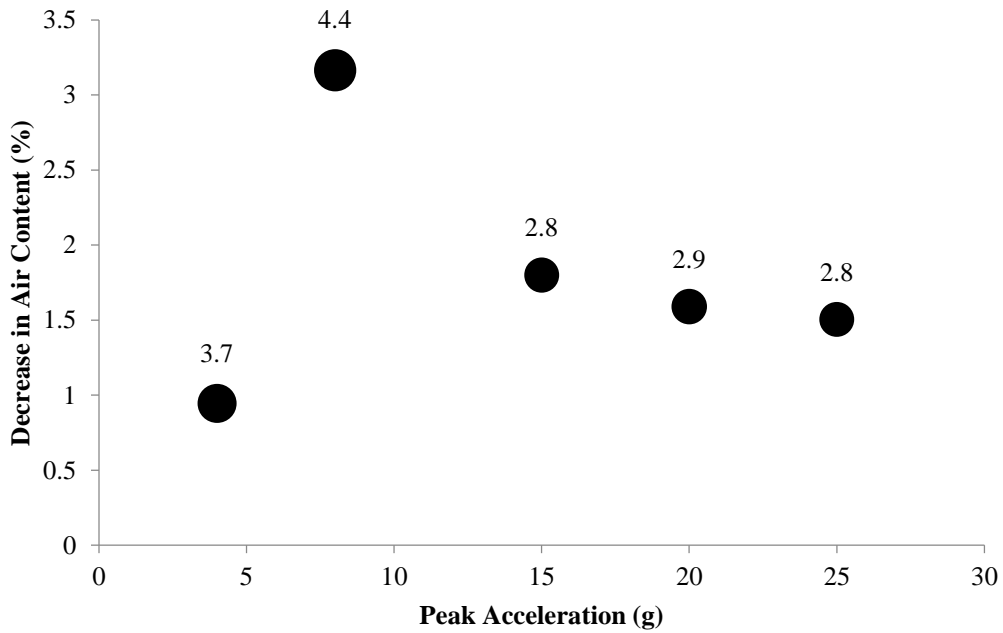


Figure 5.26 Effect of vibration acceleration on the decrease in the air content of rheological combination 4

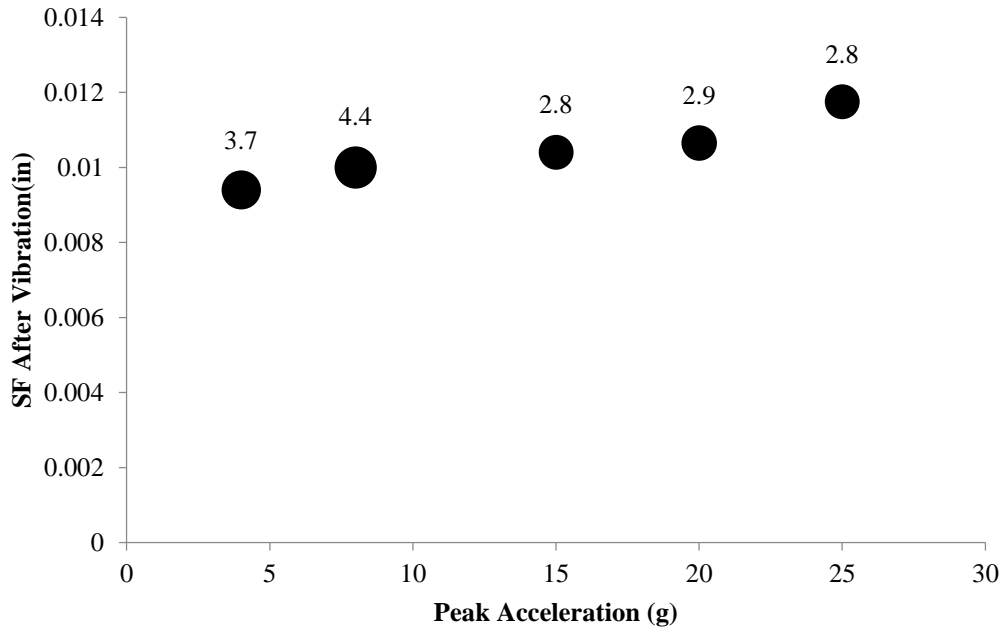


Figure 5.27 Effect of vibration acceleration on the hardened spacing factor of rheological combination 4

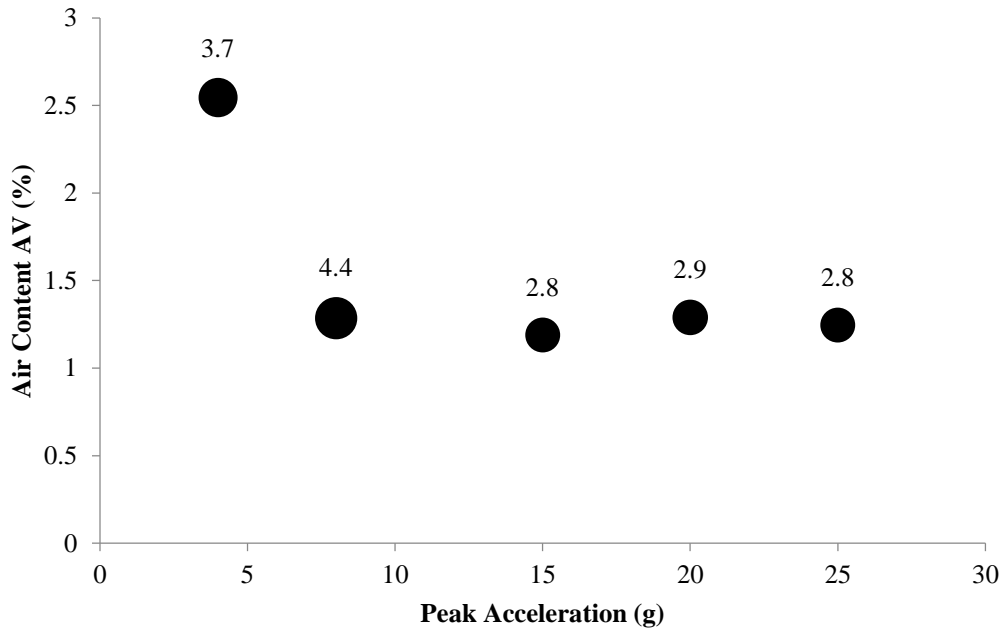


Figure 5.28 Effect of vibration acceleration on the hardened air content of rheological combination 4

Looking at the stiff concrete mixture made using rheological combination 1

(Figure 5.29), it can be observed that all specimens were able to pass the freeze-thaw testing no

matter how high the peak acceleration was. This indicates that mixtures with high yield stress and plastic viscosity have a higher chance of resisting the negative effect of excessive vibration for a given chemical admixture combination. Figure 5.30 and Figure 5.31 show the effect of different vibration acceleration on final spacing factor and air content. While it seems that higher acceleration resulted in more total air loss, the final spacing factor increased slightly with peak vibration acceleration. The total air content decreased with acceleration; however, the total air content after vibration remained higher than seen with rheological combination 4. The higher yield stress and plastic viscosity made the vibrated concrete flow at high viscosities which provided higher resistance to air bubble rising. This in turn preserved more of the air system necessary for freeze-thaw resistance. Although the spacing factors seen after vibration with both rheological combinations were similar, very little freeze-thaw deterioration was seen with rheological combination 1. This highlights the imprecise nature of hardened air void spacing factors.

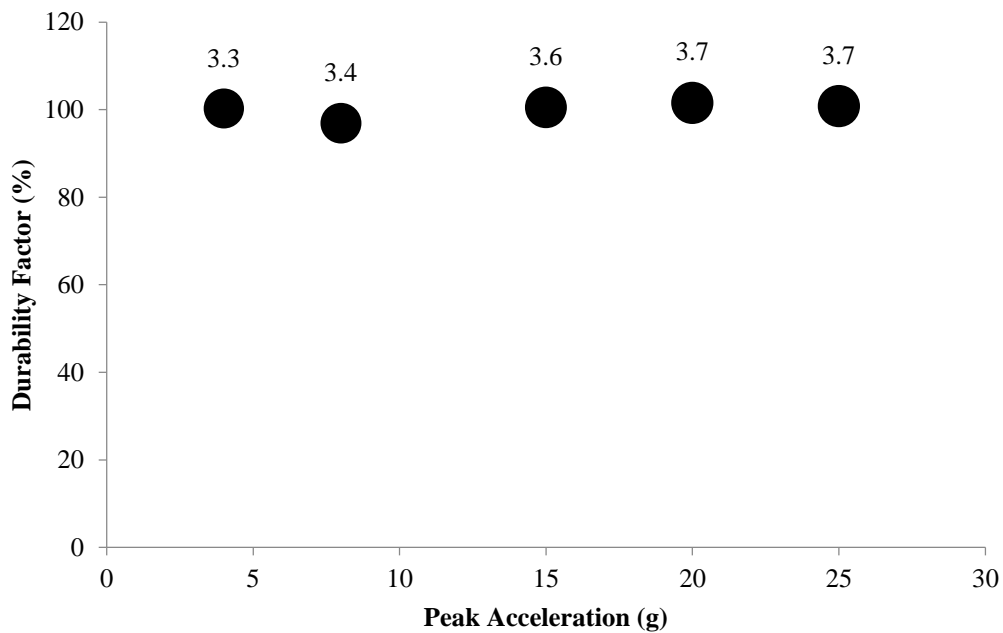


Figure 5.29 Effect of vibration acceleration on the freeze-thaw performance of rheological combination 1

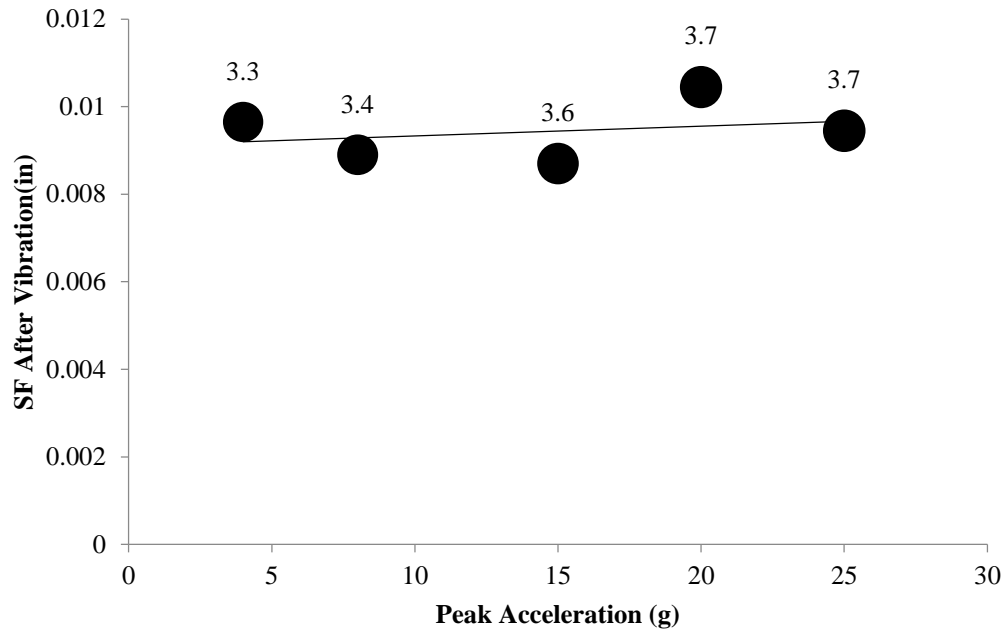


Figure 5.30 Effect of vibration acceleration on the final spacing factor of rheological combination 1

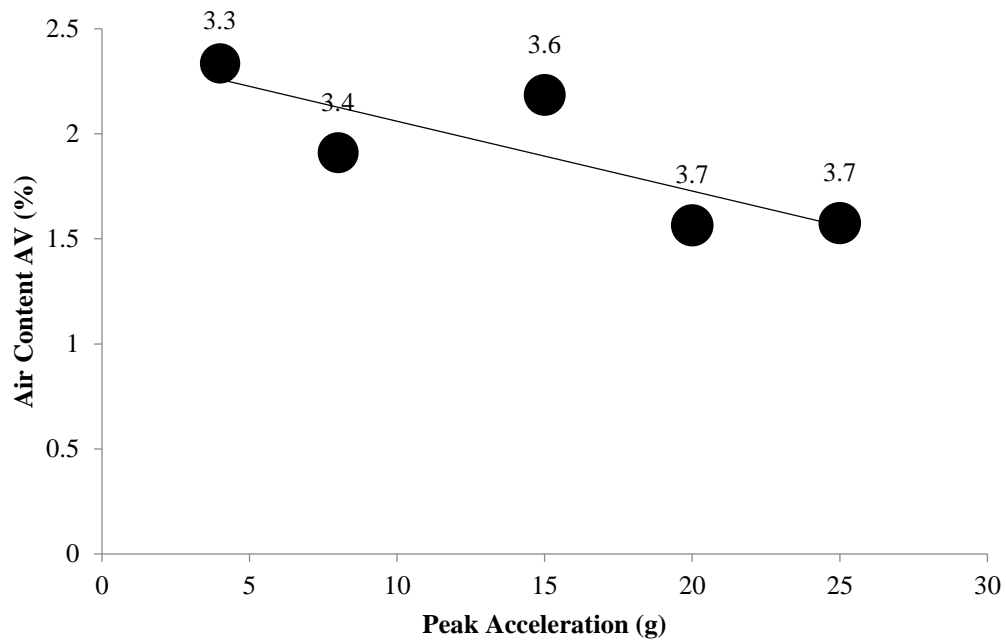


Figure 5.31 Effect of vibration acceleration on the final air content of rheological combination 1

5.2.3. Effect of Vibration Frequency

The effect of vibration frequency during vibration on freeze-thaw durability was studied using rheological combinations 1 and 4 with chemical admixture combination B. The mixtures in this section were subjected to 4 minutes of vibration with a peak vibration acceleration of 8 g. Figure 5.32 shows the rheological properties for both rheological combinations 1 and 4 batches. The size of the markers in this figure corresponds to the amount of vibration frequency applied to the particular mixture. Figure 5.33 illustrates the freeze-thaw results for rheological combination 4 under different vibration frequencies. The size of and the number on the markers in this figure corresponds to the value of the initial air content. Despite the fact that no failure occurred, samples vibrated at 33, 110 and 160 Hz showed more deterioration. Since the air content before vibration for the specimens vibrated at 55 and 75 Hz was higher than the others, it is likely that the improved performance was because of the higher air content. The experiments showed that vibration frequency between 33 and 160 Hz was likely of only minor significance for concrete vibrated at 8g. Supporting the conclusion that vibration frequency has limited effect, Figure 5.34 & Figure 5.35 show that the vibration frequency had minimal to no effect on the final air parameters. It seems from Figure 5.34 that the final spacing factor values for the deteriorated samples were slightly higher than those of the others. This, however, could be attributed to the lower initial air content. Nevertheless, the fact that the spacing factor was somewhat similar for all samples revealed that the spacing factor is not that sensitive of a parameter.

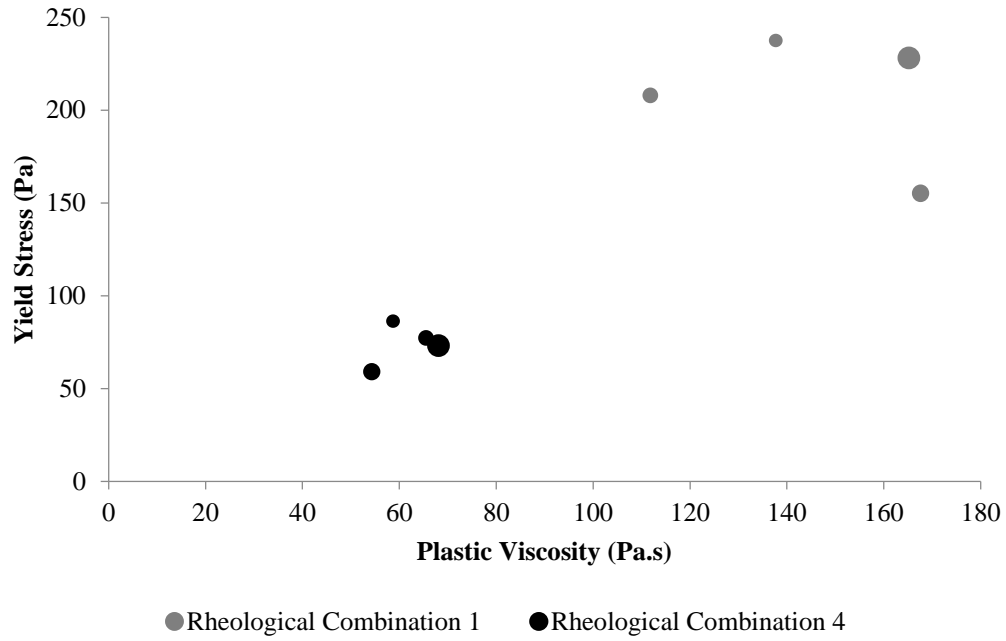


Figure 5.32 Rheological properties for the study of the effect of vibration frequency

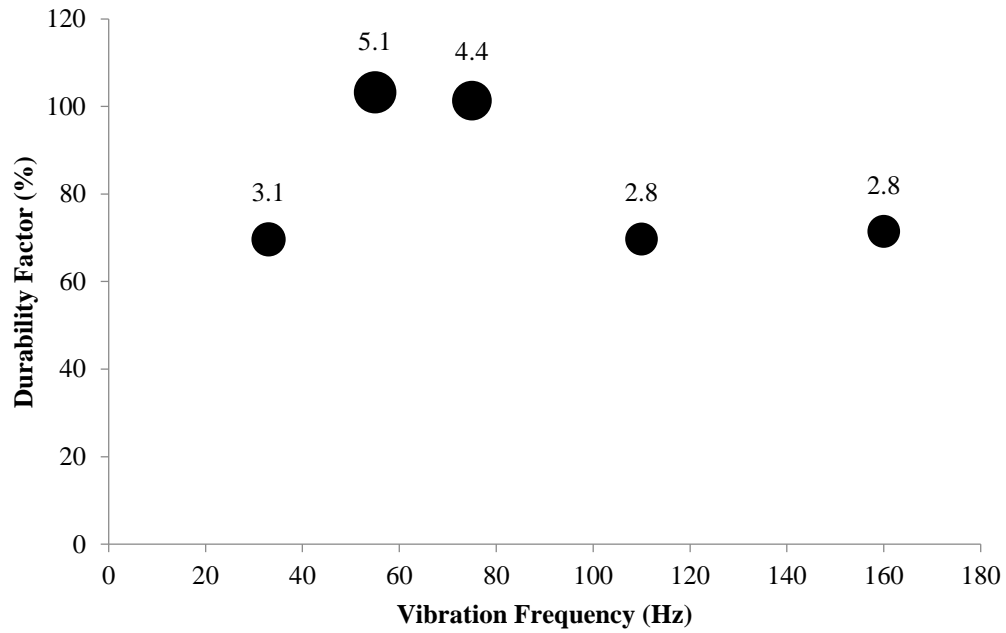


Figure 5.33 Effect of vibration frequency on the freeze-thaw performance of rheological combination 4

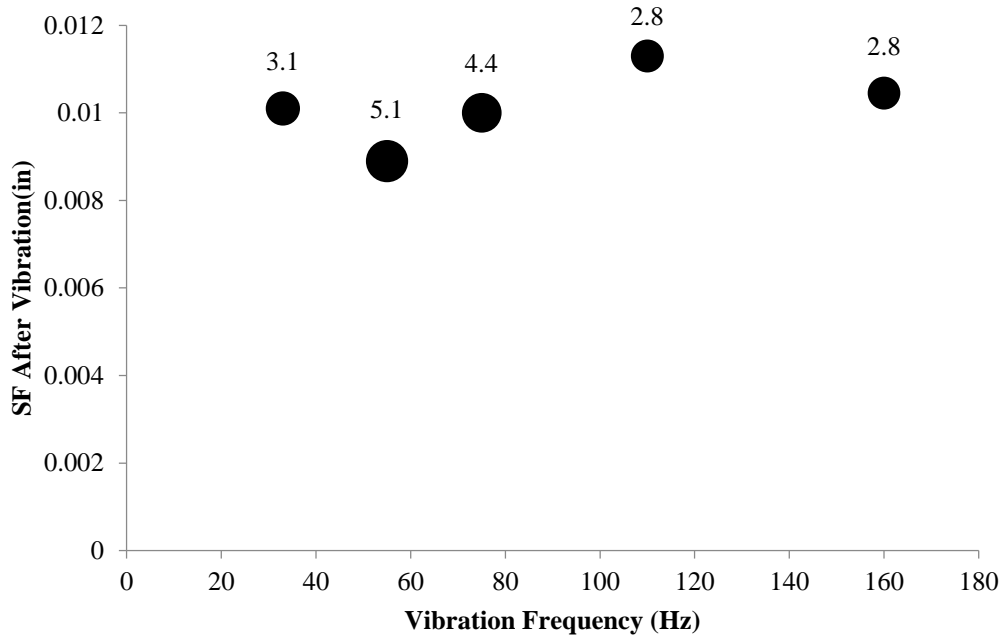


Figure 5.34 Effect of vibration frequency on the final spacing factor of rheological combination 4

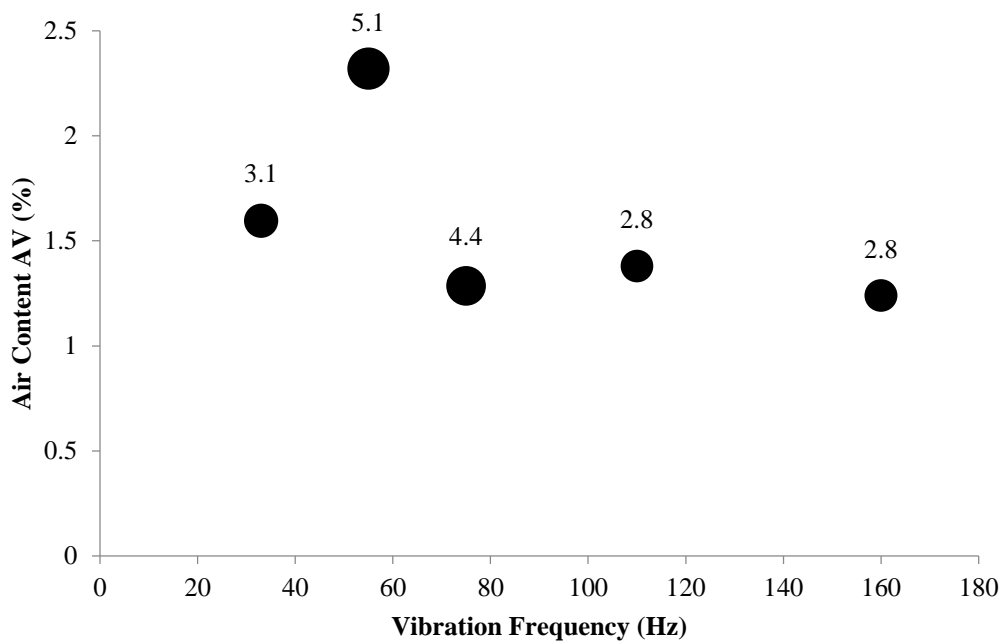


Figure 5.35 Effect of vibration frequency on the final air content of rheological combination 4

For concrete made with rheological combination 1, Figure 5.36 illustrates the freeze-thaw results of chemical admixture combination B. Once again, it was observed that unlike

rheological combination 4, rheological combination 1 did not experience any deterioration regardless of the vibration frequency. This could be attributed to the high yield stress and plastic viscosity that provided more resistance to air loss than seen with rheological combination 4. As shown in Figure 5.37 and Figure 5.38, similar to rheological combination 4, there did not appear to be any significant effect of vibration frequency on the final air parameters.

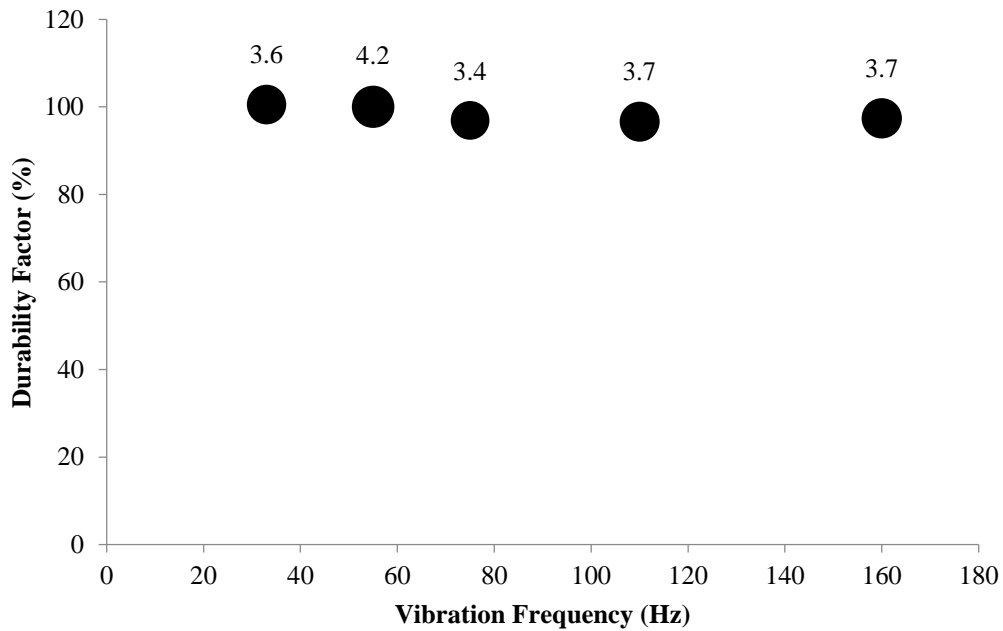


Figure 5.36 Effect of vibration frequency on the freeze-thaw performance of rheological combination 1

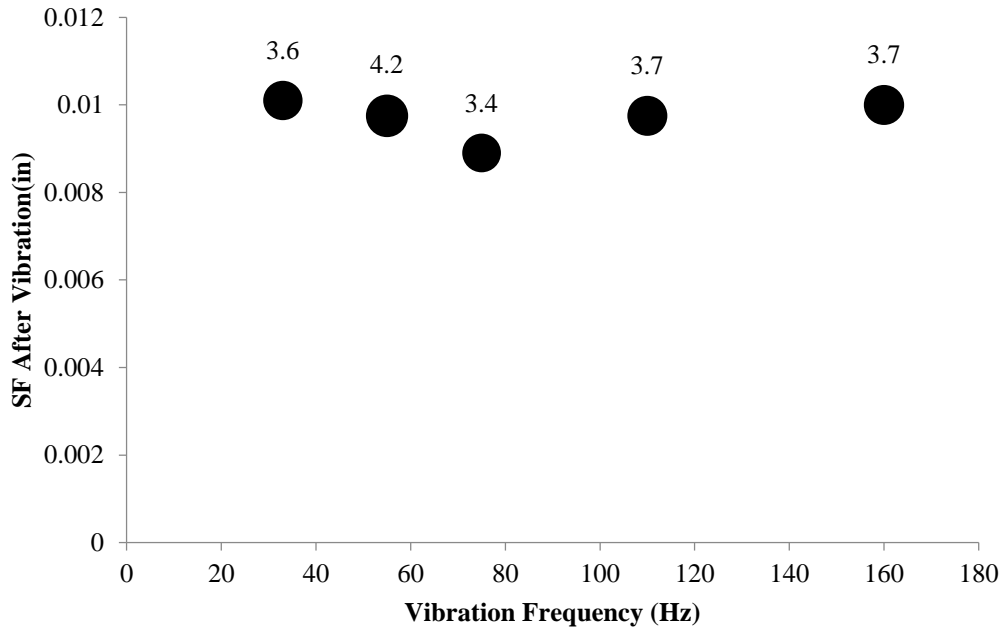


Figure 5.37 Effect of vibration frequency on the final spacing factor of rheological combination 1

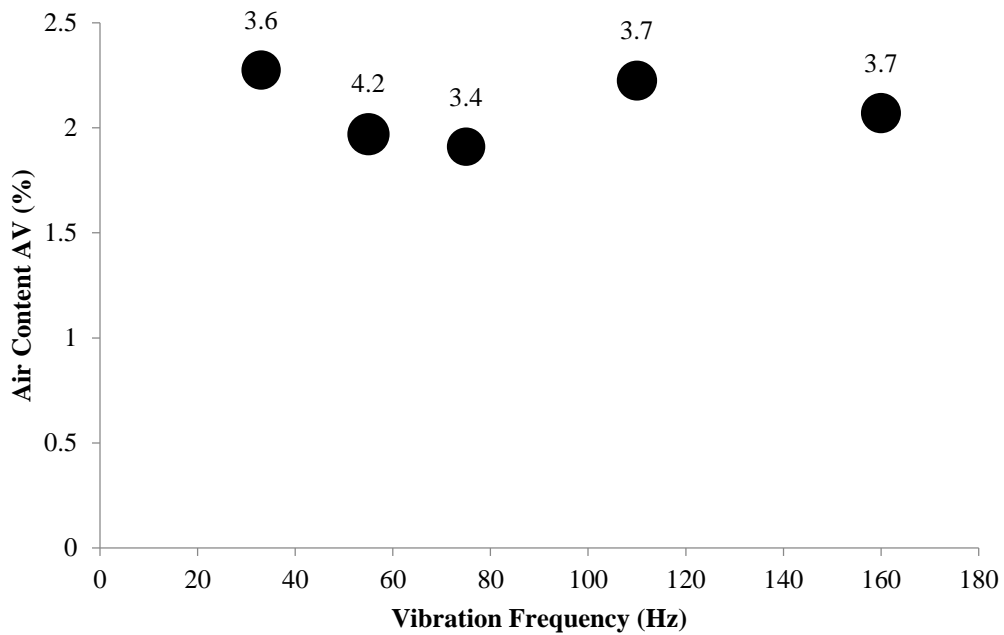


Figure 5.38 Effect of vibration frequency on the final air content of rheological combination 1

5.2.4. Effect of Vibration Velocity

In order to examine the combined effect of variation in vibration frequency and acceleration, the effect of peak vibration velocity on the freeze-thaw performance of rheological combination 1 and 4 of chemical admixture combination B was studied. The peak velocity can be obtained by dividing the peak vibration acceleration by the angular frequency of vibration. The mixtures in this section were subjected to 4 minutes of vibration. Figure 5.39 shows the rheological properties for both rheological combination 1 and 4 batches. The size of the bubbles in this figure corresponds to the amount of peak vibration velocity applied to the particular mixture. Starting with rheological combination 4, one can observe from Figure 5.40 that deterioration occurred at almost all values of peak velocities. The very weak effect of vibration velocity on the final air parameters (Figure 5.41 and Figure 5.42) supported the conclusion that the variation in the vibration velocity did not have a significant effect on the freeze-thaw performance.

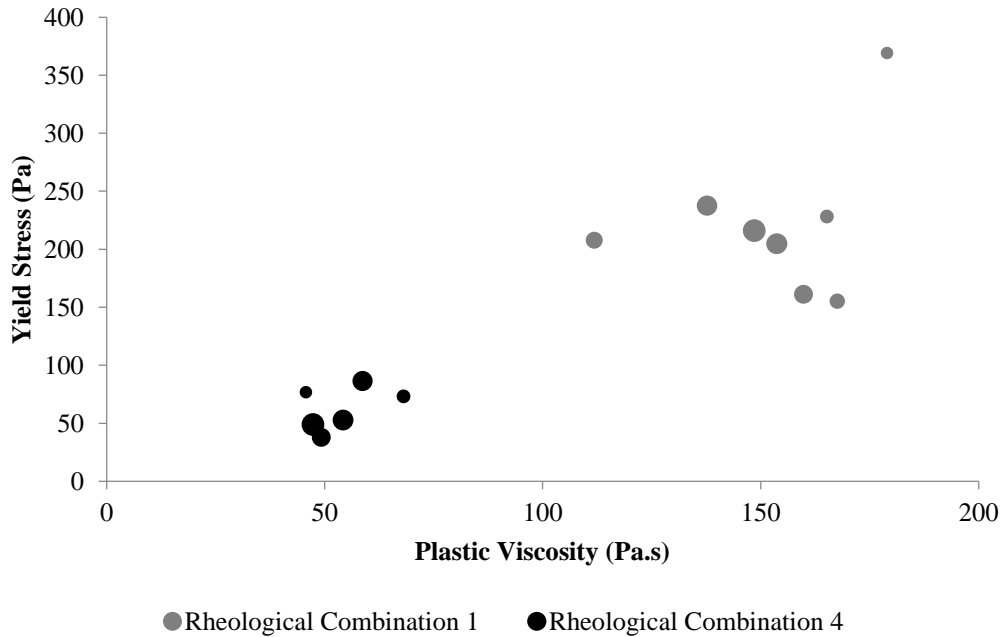


Figure 5.39 Rheological properties for the study of the effect of vibration velocity

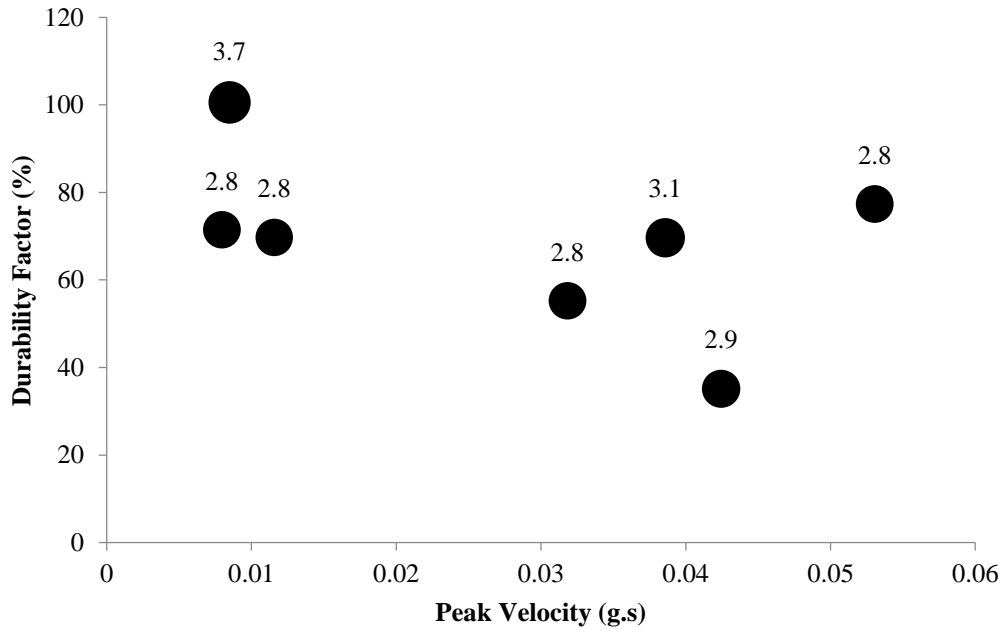


Figure 5.40 Effect of peak vibration velocity on the freeze-thaw performance of rheological combination 4

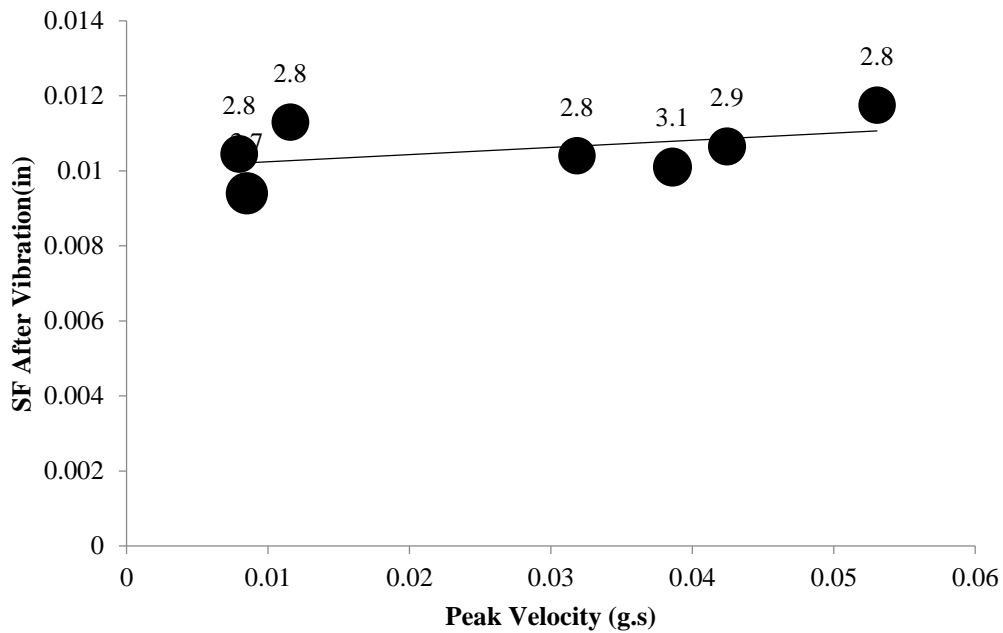


Figure 5.41 Effect of vibration velocity on the final spacing factor of rheological combination 4

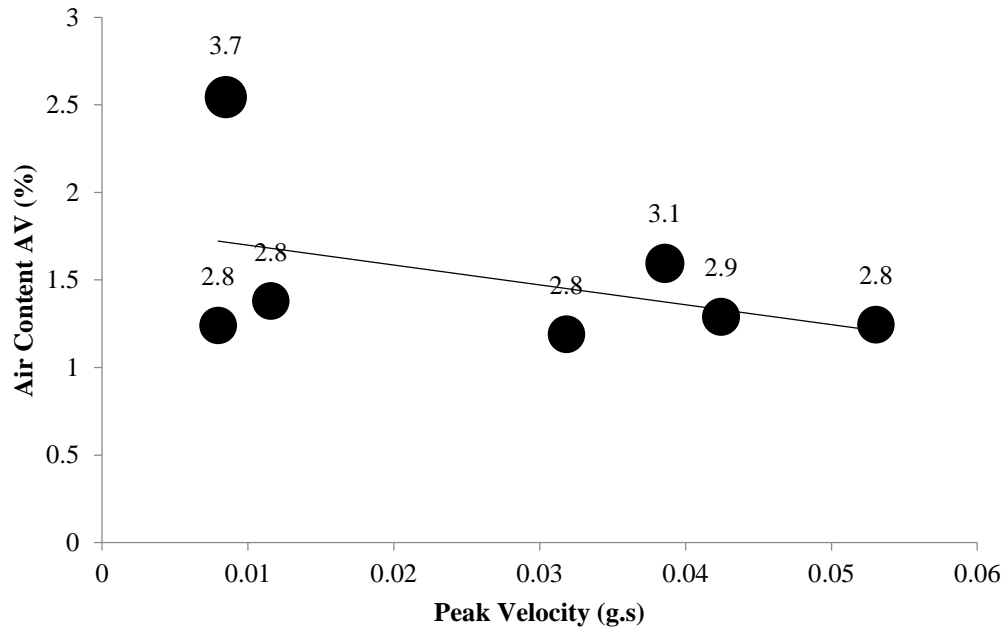


Figure 5.42 Effect of vibration velocity on the final air content of rheological combination 4

Rheological combination 1 results, shown in Figure 5.43, suggest that the stiff mixture performed well in freeze-thaw regardless of the peak vibration velocity due to its high rheological properties. Similarly, there was no apparent relation between the peak vibration velocity and the final air parameters (Figure 5.44 and Figure 5.45). The peak vibration acceleration might be the main vibration factor dictating the freeze-thaw performance of the vibrated concrete.

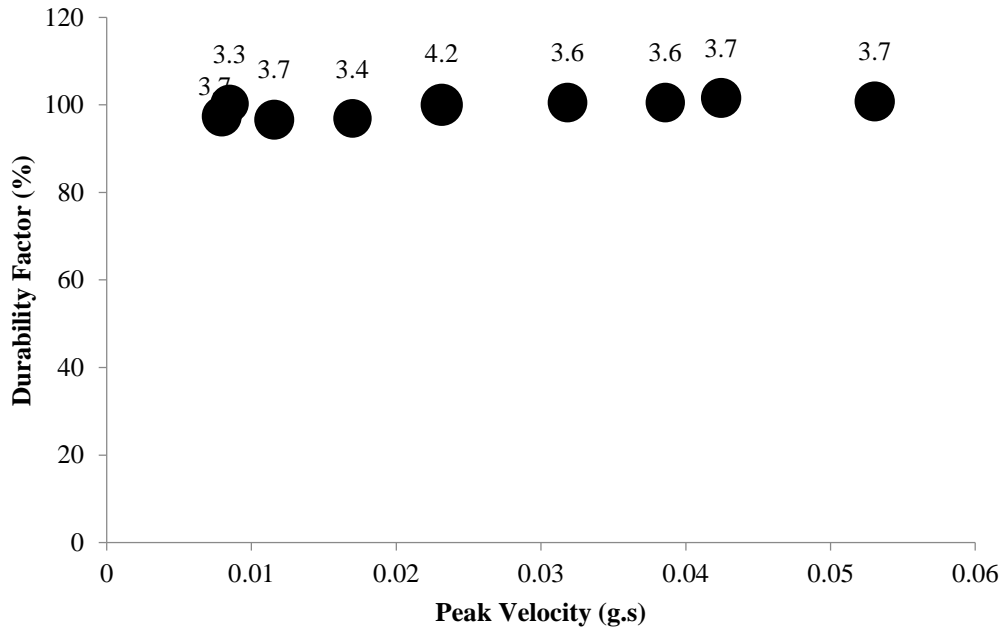


Figure 5.43 Effect of peak vibration velocity on the freeze-thaw performance of rheological combination 1

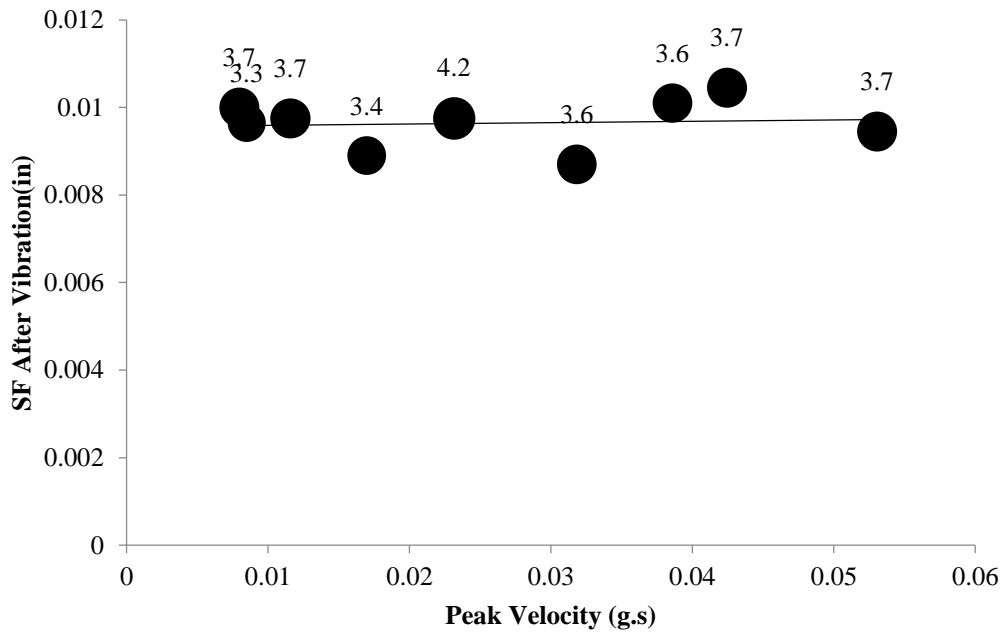


Figure 5.44 Effect of vibration velocity on the final spacing factor of rheological combination 1

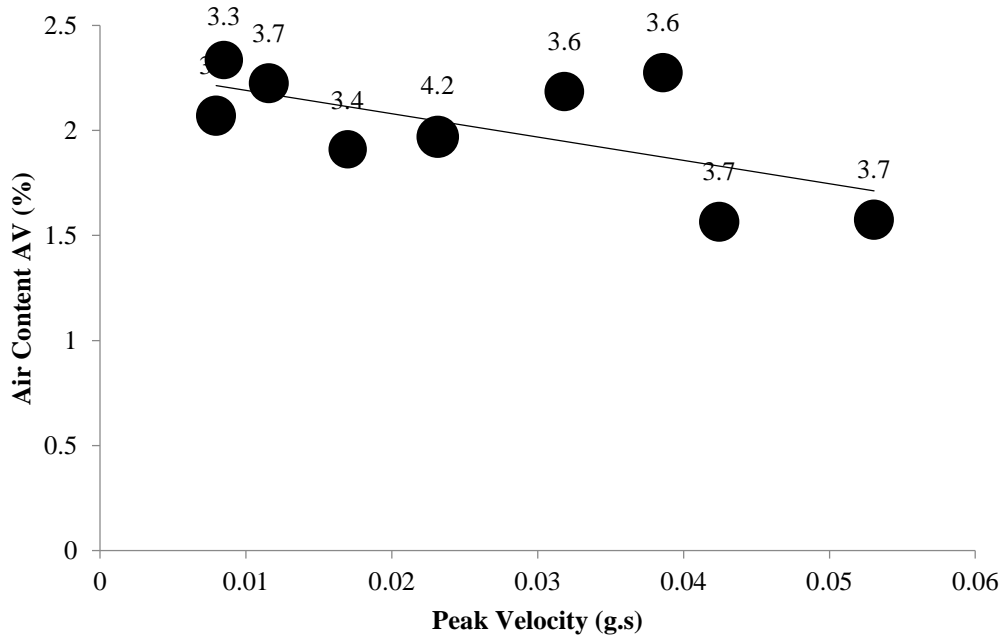


Figure 5.45 Effect of vibration velocity on the final air content of rheological combination 1

5.2.5. Effect of Air Content before Vibration

The relationship between concrete fresh air content before vibration for different chemical admixture combinations and freeze-thaw durability was examined. Fresh air content is the most performed quality control test for concrete freeze-thaw durability. Determination of the concrete fresh air content required to maintain a good air system after vibration is needed to ensure that concrete tie manufacturers can continue to use this quality control test. Both chemical admixture combination B and C were used in order to determine the difference between the minimum initial air contents required to achieve good freeze-thaw resistance for different chemical admixtures combinations. Only rheological combination 4 of chemical admixture combination B was examined in this section since previous sections showed that the stiffest mixture (rheological combination 1) did not experience any deterioration under any vibration condition. Moreover, results also showed that initial air contents as low as 3.5% can safely pass ASTM C666 at a DF of 60% or higher even for the most fluid mixture (rheological combination

4). However, both rheological combinations 1 and 4 of chemical admixture combination C were examined since it was shown that chemical admixture combination C experienced freeze-thaw failure. Starting with chemical admixture combination B, Figure 5.46 shows the rheological properties of batches made with rheological combination 4 vibrated at different frequencies. All of these mixtures were vibrated for 4 minutes at a peak vibration acceleration of 8 g. The size of the markers in this figure corresponds to the initial air content of the particular mixture. The rheological properties of the 110 Hz mixtures do not appear on the figure because they exactly matched with the 160 Hz mixtures. Figure 5.47 shows that the critical value of initial air content is somewhere between 3.1% and 4.2% under which vibrated concrete started to experience some freeze-thaw deterioration for chemical admixture combination B. This conclusion seemed to be the same regardless of the vibration frequency.

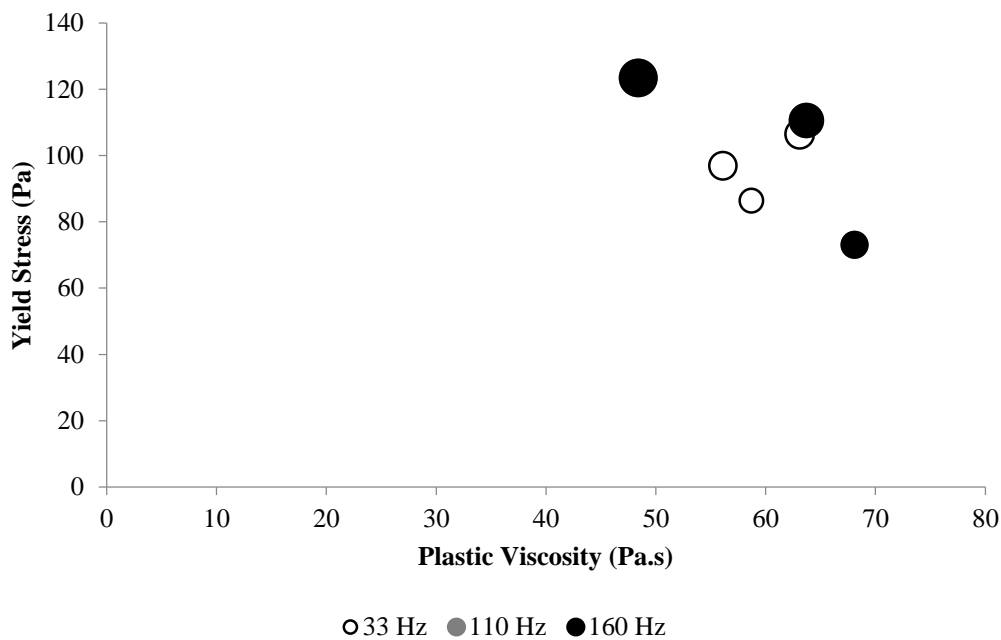


Figure 5.46 Rheological properties of rheological combination 4 of chemical admixture combination A for the study of the effect of air content before vibration

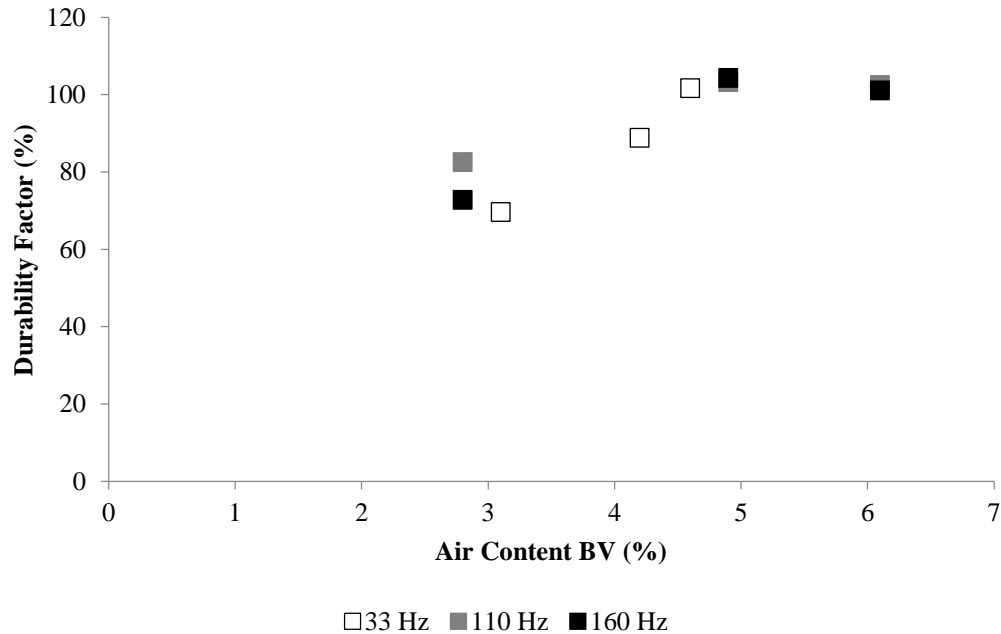


Figure 5.47 Effect of air content before vibration on the freeze-thaw performance of rheological combination 4 of chemical admixture combination A

The results for rheological combination 1 and 4 of chemical admixture combination C are shown in Figure 5.48 and Figure 5.49. The size of the markers in Figure 5.48 corresponds to the amount of initial air content of the particular mixture. All of these mixtures were subjected to 4 minutes of 75 Hz vibration at 8 g peak acceleration. While the rheological properties for one of the rheological combination 1 batches were significantly different (Figure 5.48), Figure 5.49 shows that failure occurred for the 3.6% air batch even though it is the one that had a high yield stress and plastic viscosity. Figure 5.49, also demonstrates that, even with rheological combination 1, an initial air content of 4.1% was not sufficient to provide good freeze-thaw resistance for this chemical admixture combination. The freeze-thaw results also showed that for this admixture combination, it required more air before vibration to provide durability after the air loss associated with vibration. It can be observed that all specimens of rheological combination 4 experienced some deterioration, even those with 6.9% initial air content. This work suggests that concrete railroad ties producers should always test the performance of their

admixture combination and rheological properties in the vibration system planned for their manufacturing process in order to determine the required initial air content sufficient for freeze-thaw resistance.

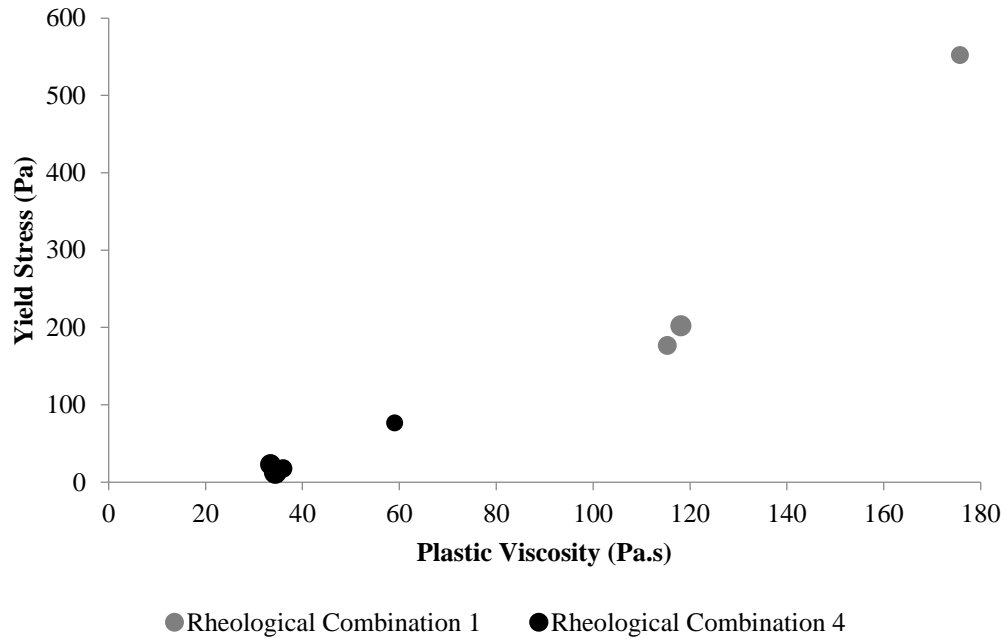


Figure 5.48 Rheological properties of rheological combination 1 and 4 of chemical admixture combination C for the study of the effect of air content before vibration

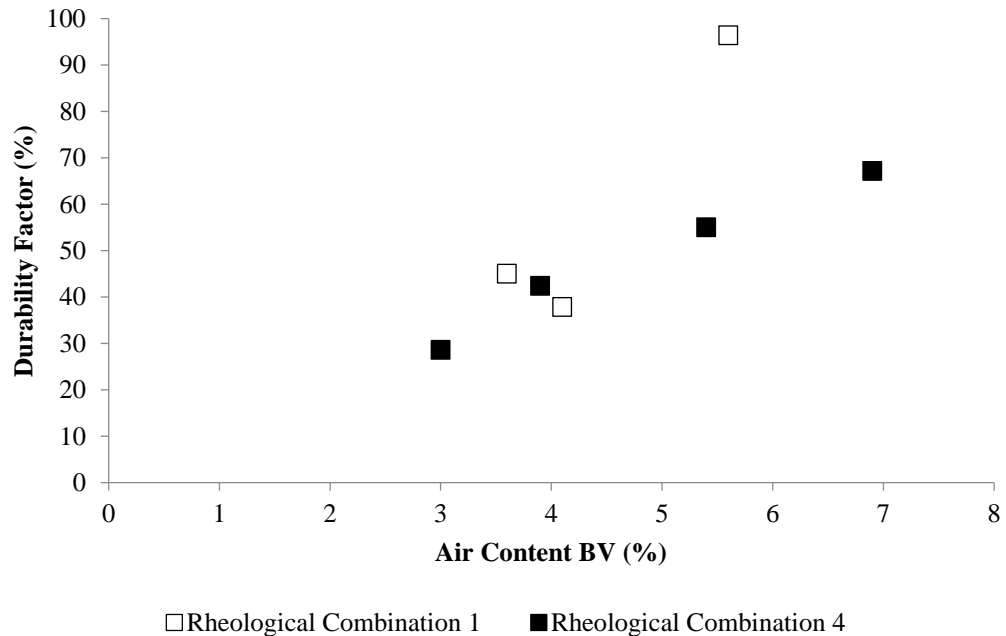


Figure 5.49 Effect of air content before vibration on the freeze-thaw performance of rheological combination 1 and 4 of chemical admixture combination C

5.2.6. Effect of Rheological Properties

The effect of the rheological properties on the concrete freeze-thaw performance considering all mixtures together was examined. The chosen batches for this section all had initial air contents in the range of 3% to 4%. Figure 5.50 and Figure 5.51 illustrate the effect of rheological properties on the freeze-thaw performance. The size of the markers in both of these figures corresponds to the amount of initial air content of the particular mixture. Figure 5.50 shows that the failed specimens for chemical admixture combination B were concentrated in the low yield stress range, specifically less than 200 Pa. This result is rather weak, however, since there are other factors that affect the concrete durability. Figure 5.51 shows no clear correlation between the plastic viscosity and the durability factor. Figure 5.52 and Figure 5.53 present a vague correlation between the yield stress and the final air parameters. While it seems from Figure 5.52 that the overall trend is an increase in the air content as the yield stress increases, the trend does not appear to be statistically significant. Similarly, Figure 5.53 hints at an overall increase of spacing factor with decrease in yield stress.

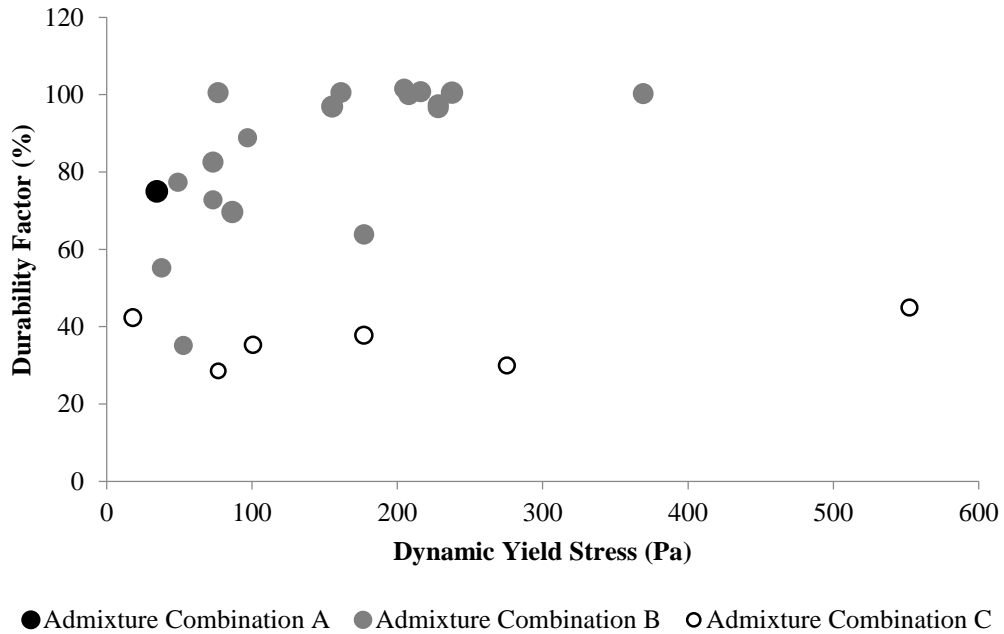


Figure 5.50 Effect of dynamic yield stress on the freeze-thaw durability

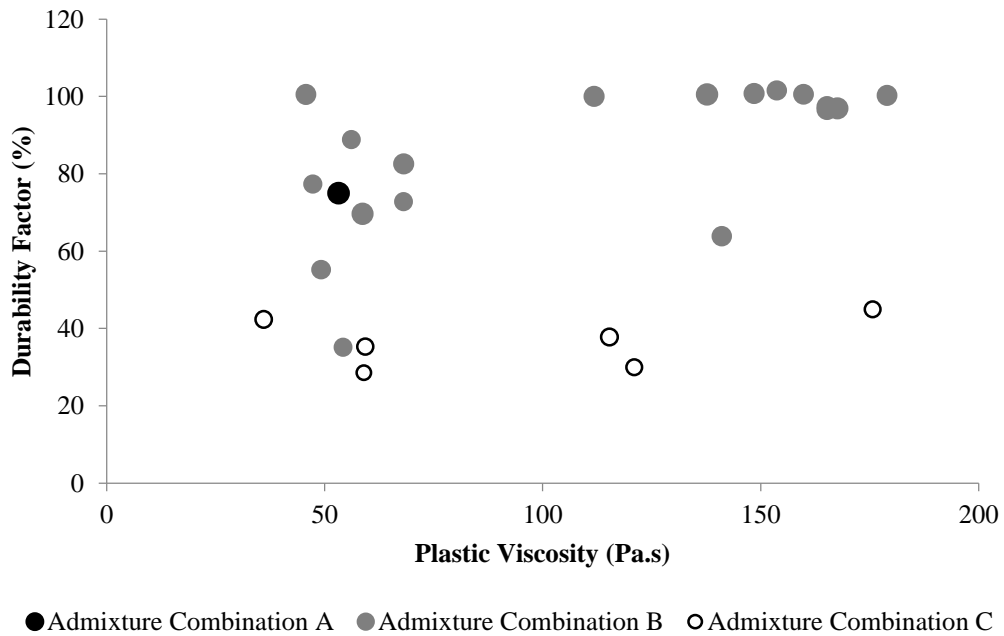


Figure 5.51 Effect of plastic viscosity on the freeze-thaw durability

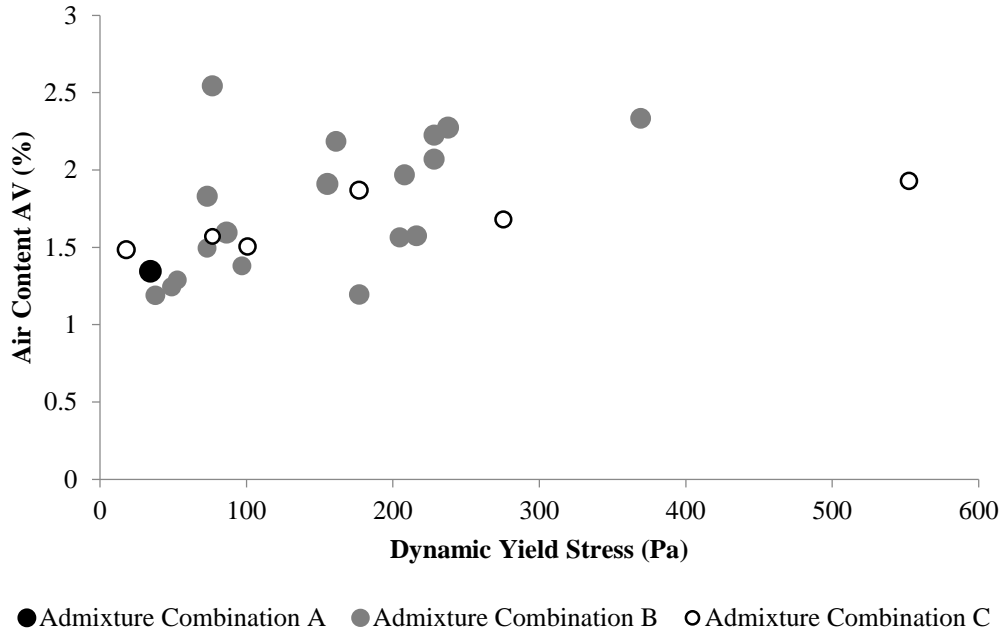


Figure 5.52 Effect of dynamic yield stress on the final air content

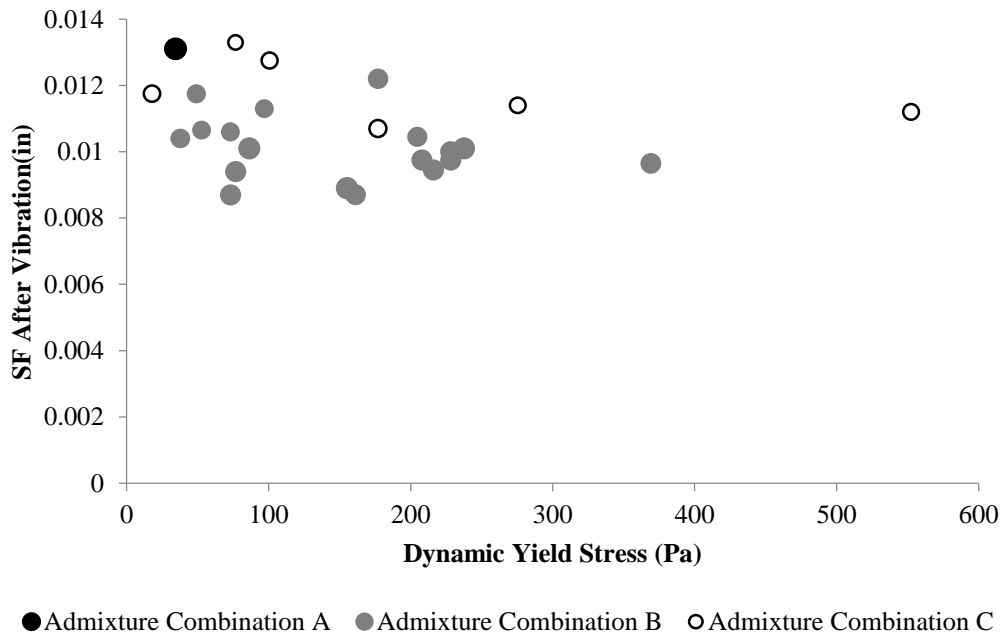


Figure 5.53 Effect of dynamic yield stress on the final spacing factor

5.2.7. Air Entrainment Requirements to Achieve Freeze-Thaw Durability

Figure 5.54 shows the relationship between the durability factor and the initial spacing factor. It can be observed that deterioration occurred even at spacing factor values as low as

0.007 in. Therefore, the spacing factor before vibration is not a reliable parameter to determine the susceptibility to freeze-thaw damage. Figure 5.55 illustrates the correlation between the durability factor and the spacing factor after vibration which showed a better relationship between the spacing factor and freeze-thaw durability. It is evidently apparent from the figure that as the spacing factor increased the samples became more susceptible to freeze-thaw failure. It can be observed that chemical admixture combination C had the highest average spacing factors. The most interesting thing to be observed from Figure 5.55 is the fact that specimens were able to pass the freeze-thaw test as long as they had a spacing factor less than 0.01 in. This maximum limit is, however, 0.002 in larger than the one specified in ACI recommendations. The commonly used 0.008 in spacing factor criteria is known to be a conservative limit and is confirmed by this testing to be very conservative for vibrated concrete. According to the Canadian standards A23.1, the upper limit for the spacing factor is 0.22 mm (0.0087 in) for normal concrete and 0.25 mm (0.0098 in) for high strength concrete. Being high strength concrete, the results presented here seem to match nicely with the 0.0098 in limit. Not all concrete railroad ties are made with high strength concrete. Therefore, it is concluded that 0.0087 in. is the conservative limit that should be adopted for these results. It is also possible to conclude from Figure 5.55 that good freeze-thaw performance can always be achieved regardless of vibration parameters, rheology or chemical admixture combination if the required final spacing factor value is achieved.

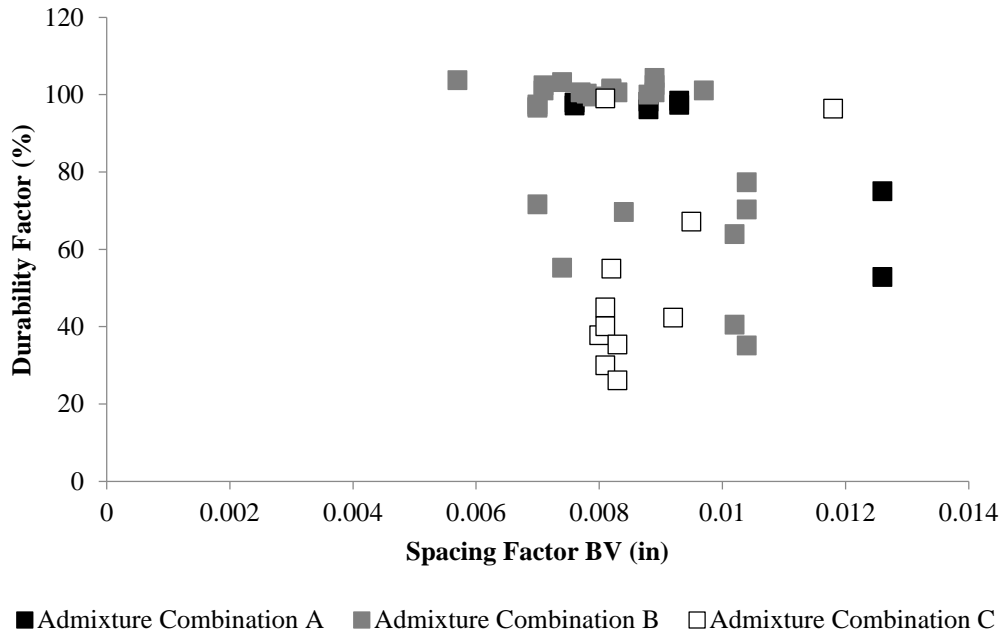


Figure 5.54 Durability factor versus spacing factor before vibration

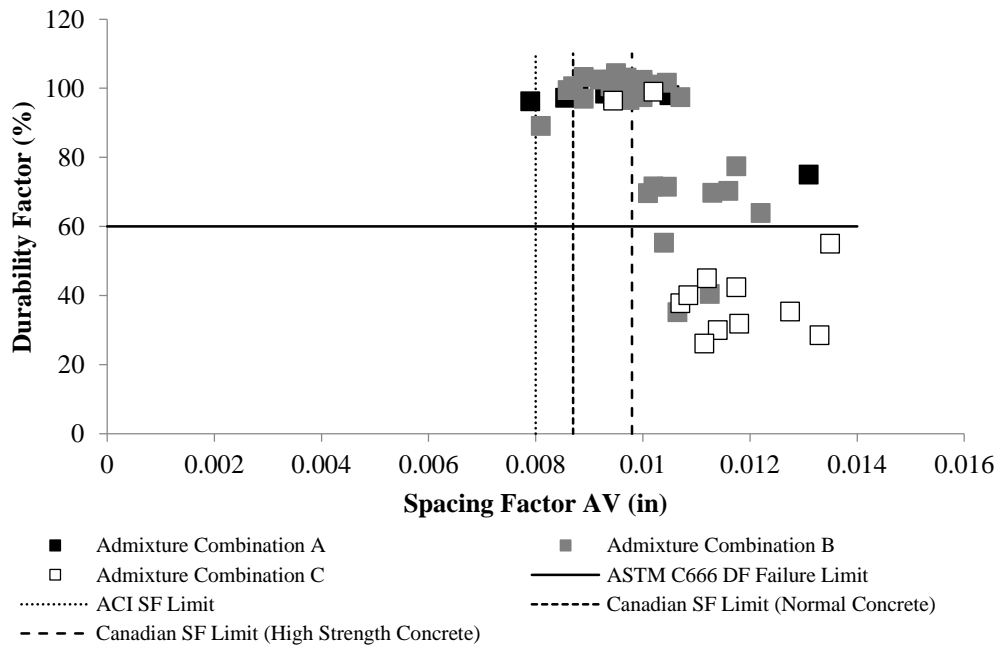


Figure 5.55 Durability factor versus spacing factor after vibration

Figure 5.56 and Figure 5.57 show the relation between the durability factor and fresh and hardened air content before vibration. For the case of chemical admixture combination C, like the spacing factor before vibration, the total air content before vibration was meaningless since

even air contents as high as 6% were not sufficient in some cases. The concrete fresh air content before vibration could be helpful for a given vibration condition if it were correlated to durability after vibration for a given mixture and rheological properties. Figure 5.58 presents the relation between the durability factor and the hardened air content after vibration. The total air content after vibration was not a reliable predictor of durability after vibration.

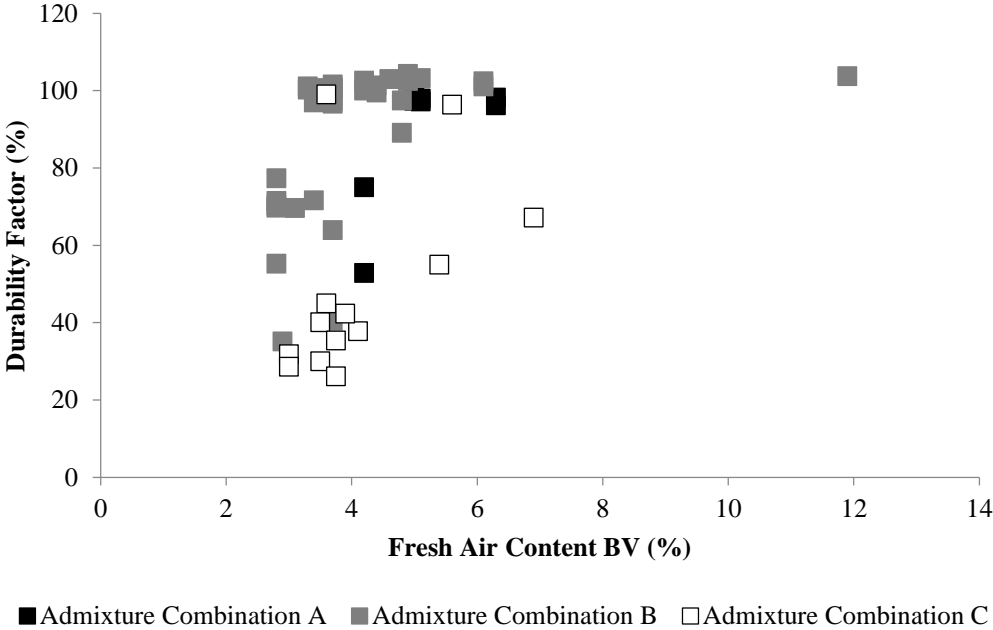


Figure 5.56 Durability factor versus fresh air content before vibration

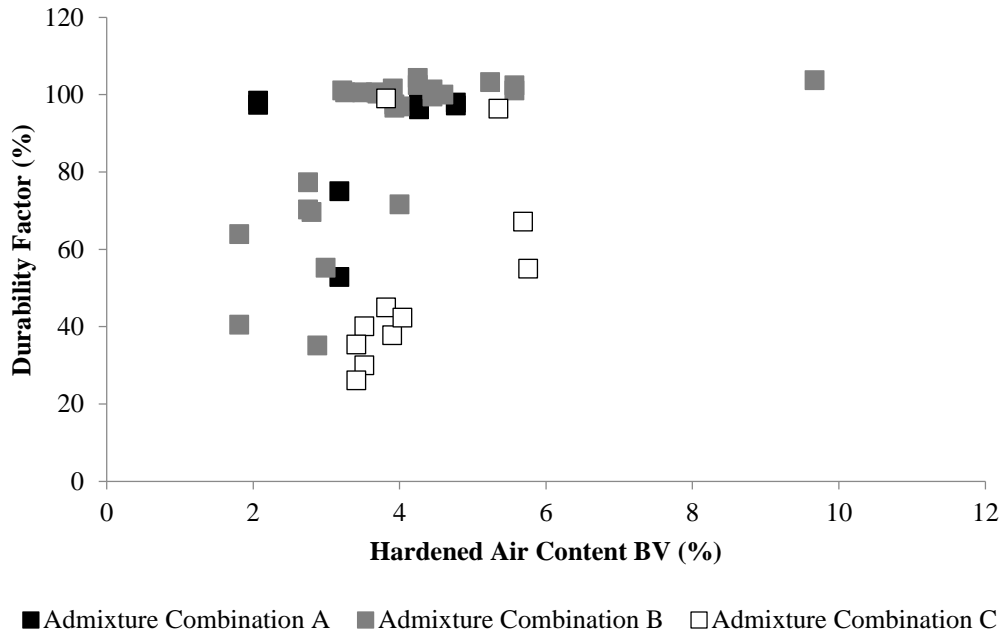


Figure 5.57 Durability factor versus hardened air content before vibration

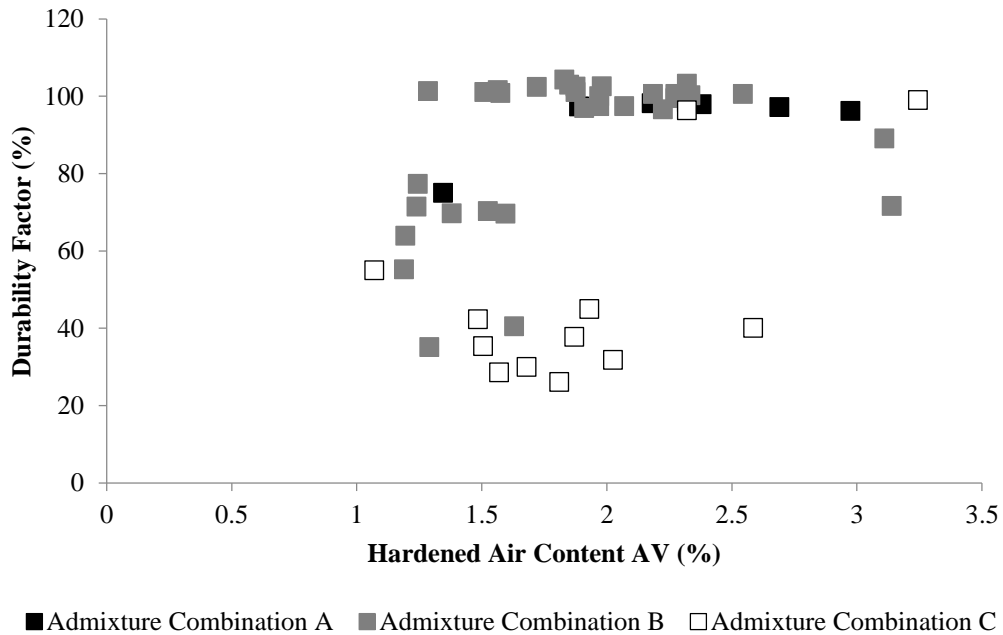


Figure 5.58 Durability factor versus hardened air content after vibration

Figure 5.59 illustrates the correlation between final length change and final spacing factor. According to ASTM, the samples are considered to be failed if the length change exceeds 0.1%. It seems from Figure 5.59 that the 0.0098 in Canadian limit for the spacing factor also

works when considering the length change as a failure criterion. However, it is still not very conservative. The 0.008 spacing factor limit on the other hand, proves to be very conservative even when considering the length change failure criterion. All failed samples had positive or expansive length change values indicating internal cracking. Figure 5.60 shows the relation between the two failure criteria; durability factor and final length change. There is an obvious correlation between the two criteria where the length change increased as the durability factor decreased.

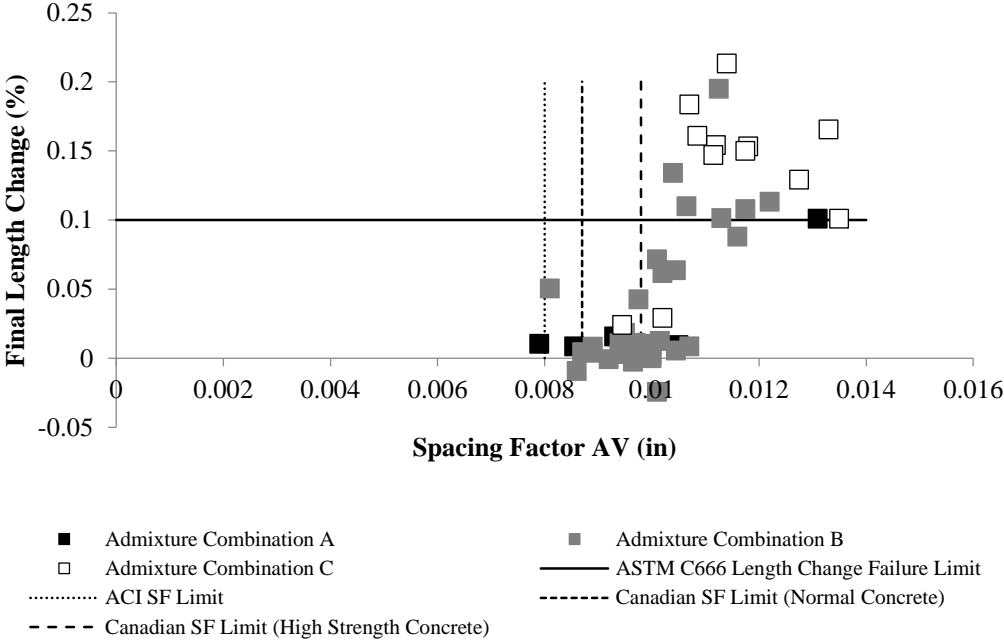


Figure 5.59 Final length change versus spacing factor after vibration

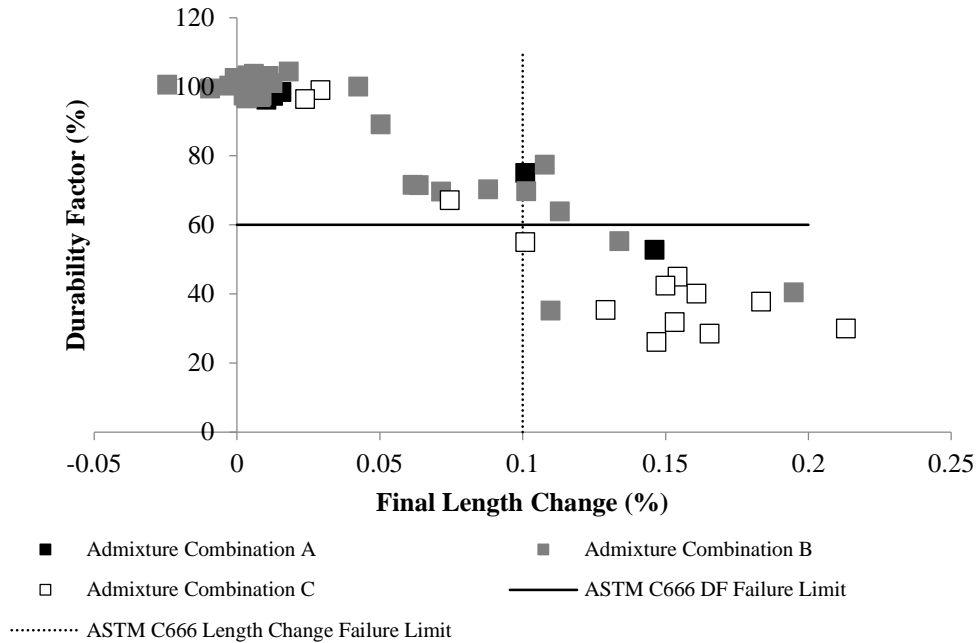


Figure 5.60 Durability factor versus final length change

Figure 5.61 presents the relationship between final weight change and final spacing factor. It shows that samples with high spacing factors tended to have higher weight change. This indicated that there might be a correlation between failure and weight change. Figure 5.62 illustrates the relation between the durability factor and the weight change. While all failed samples had an increase in weight, there are some unaffected samples that also had an increase in weight. The increase in weight in failed samples might be due to some water absorption, but not enough to critically saturate the concrete.

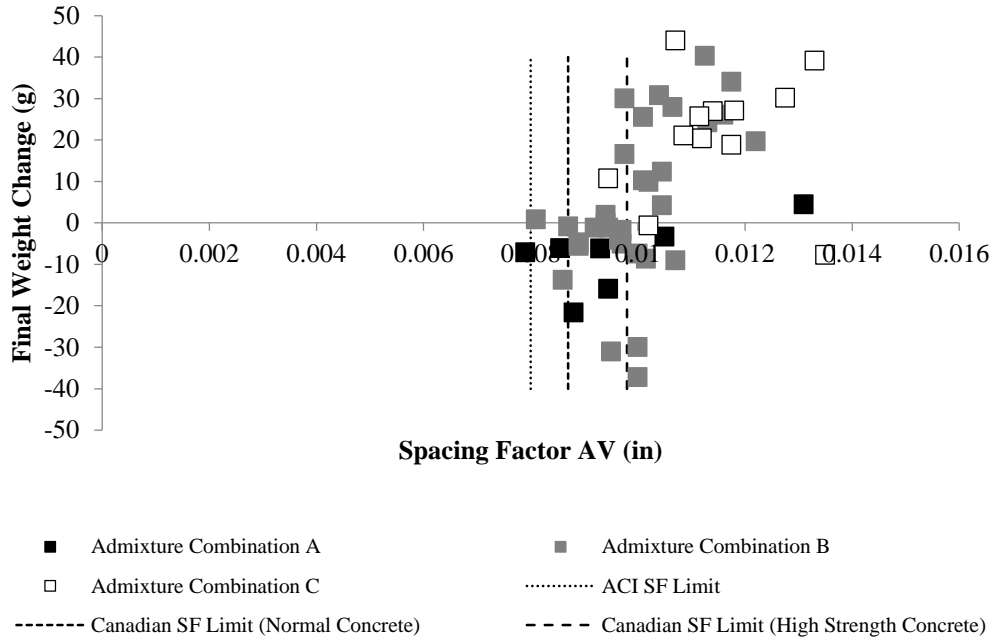


Figure 5.61 Final weight change versus spacing factor after vibration

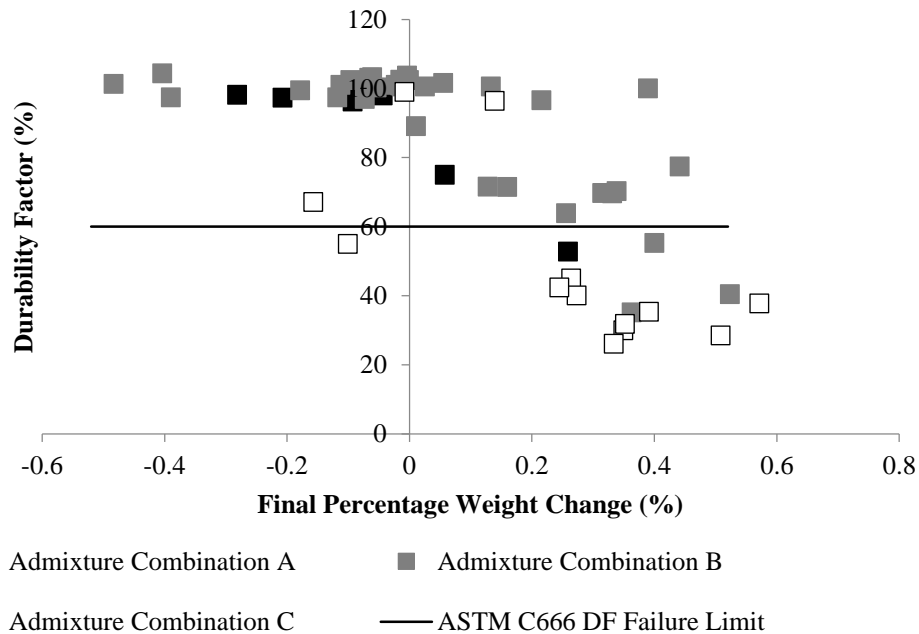


Figure 5.62 Durability factor versus final weight change

5.3. Freeze-Thaw Durability of Internally Vibrated Concrete

Figure 5.63 shows the rheological properties for all four concrete batches used in internally vibrated concrete. The size of the markers in the figure corresponds to the amount of

initial air content of the particular mixture. Concrete rheological combination 4 batches were clearly more fluid than rheological combination 3 batches. Figure 5.64 and Figure 5.65 show the freeze-thaw performance of all mixtures versus the distance from the center of vibration. It seems that as the distance increased the probability of deterioration decreased. Figure 5.64 indicated that if sufficient air content was used, even the point of vibration was able to escape freeze-thaw damage. However, similar to what was found in the table vibration experiments, the more fluid with the lower initial air content mixture at the point of vibration became susceptible to freeze-thaw failure. Figure 5.65, on the other hand, shows that the higher yield stress mixture was able to have good durability even at the low initial air content. All concrete mixtures tested indicated that the influence of immersion vibrator was localized.

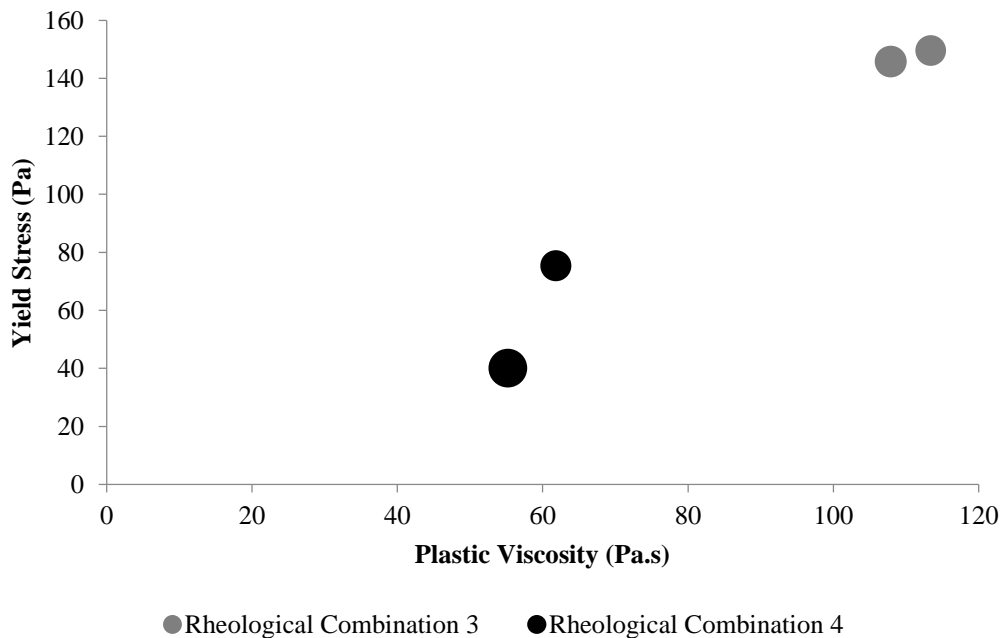


Figure 5.63 Rheological properties for the immersion vibrator experiment

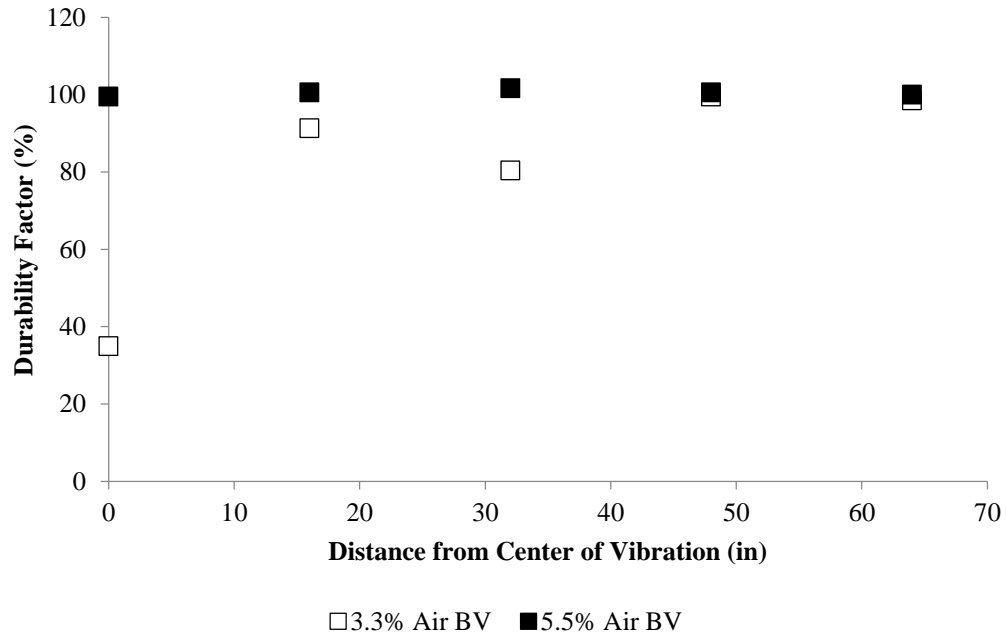


Figure 5.64 Freeze-thaw performance of rheological combination 4 (immersion vibrator experiment)

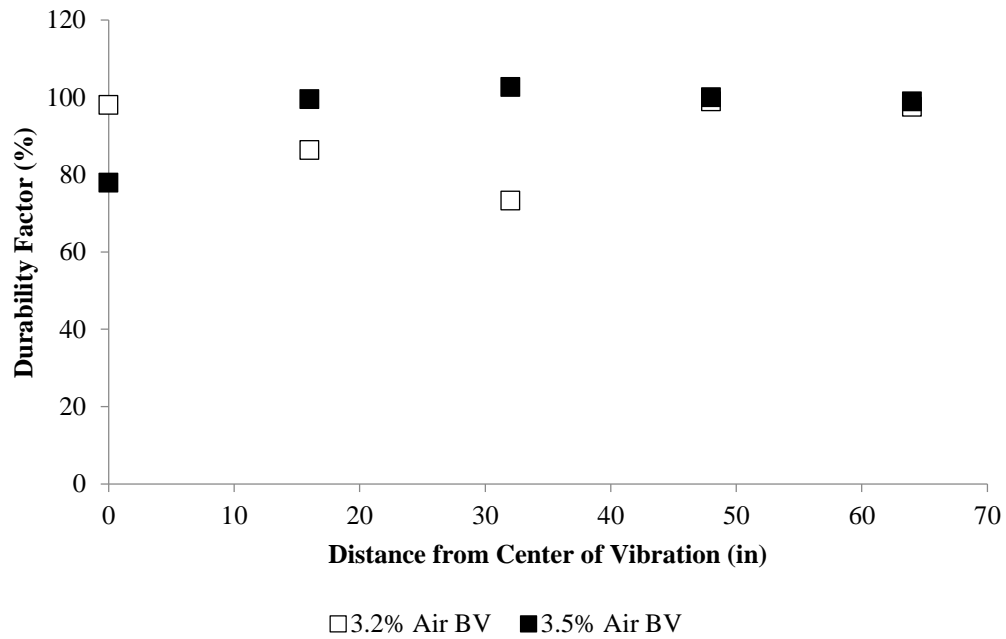


Figure 5.65 Freeze-thaw performance of rheological combination 3 (immersion vibrator experiment)

5.4. Rheology under Vibration

Table 5.1 shows the slump values of all mixtures. The vibration frequencies and peak accelerations measured on the vibrating table and inside mixtures 1, 2, 4 and 5 for all vibration configurations are shown in Table 5.2 and Table 5.3, respectively. It can be observed that the peak acceleration values on the table were much larger compared to inside the concrete away from the bottom of the pot. This was due to the dampening of the waves inside the concrete medium. The peak acceleration values inside the concrete differed from one mixture to another. It seemed that fluid mixtures experienced higher peak accelerations compared to stiff ones. This was believed to be due to the fact that coarse aggregates can move more freely inside fluid mixtures. Consequently, higher acceleration values were measured as a result of coarse aggregates hitting the accelerometer. It could also be due to the different movement of the accelerometer inside concrete mixtures of different fluidities resulting in differences in the transfer of the waves from the concrete to the sensor.

Table 5.1 Slump values of mixtures 1, 2, 3, 4 and 5

Mixture ID	Slump (in)
1	5.25
2	9.5
3	1.25
4	2.5
5	6.25

Table 5.2 Frequency and peak acceleration readings on the vibrating table

Vibration Frequency (Hz)	Weight Offset ID	Average Vibration Acceleration Across All Directions (g)
72.81	1	15.42
73.35	2	18.56
73.9	3	6.52
75	4	2.71

94.93	1	53.55
95.64	2	45.28
116.16	4	15.12

Table 5.3 Frequency and peak acceleration readings inside mixtures 1, 2, 4, and 5

Vibration Frequency (Hz)	Weight Offset ID	Depth (in)	Average Vibration Acceleration Across All Directions (g)			
			Mixture 1	Mixture 2	Mixture 4	Mixture 5
72.81	1	1	4.60	5.85	0.77	2.34
		3	3.00	10.48	2.58	2.27
		6	6.15	9.28	3.29	3.46
		8	6.77	17.72	2.72	5.11
		10	22.99	18.94	9.47	19.86
73.35	2	1	3.01	4.52	0.90	1.60
		3	5.41	5.75	1.96	3.16
		6	6.15	9.12	2.51	4.15
		8	6.75	11.69	2.73	5.97
		10	15.23	32.40	6.76	19.10
73.9	3	1	2.38	2.94	2.02	1.90
		3	3.35	3.66	1.90	2.37
		6	4.44	3.48	2.15	3.21
		8	4.59	5.46	3.68	3.78
		10	8.57	12.76	9.01	9.56
75	4	1	0.65	0.52	0.71	0.39
		3	1.04	0.56	0.60	0.56
		6	0.71	0.86	0.46	0.56
		8	0.77	0.70	0.71	0.76
		10	1.64	1.24	1.37	6.86
94.93	1	1	4.38	18.30	1.44	4.48
		3	8.77	24.14	2.76	7.63
		6	10.83	30.18	5.20	10.27
		8	14.46	40.23	7.91	10.36
		10	41.99	61.10	25.46	25.84

95.64	2	1	10.02	15.84	3.88	12.91
		3	15.32	23.13	4.96	5.80
		6	19.85	23.84	5.67	6.50
		8	18.16	28.24	6.26	7.55
		10	24.28	34.42	21.95	8.73
116.16	4	1	1.63	9.47	3.81	4.25
		3	4.63	9.77	2.96	5.69
		6	4.20	10.74	3.50	4.38
		8	4.61	10.31	3.50	4.65
		10	9.49	15.83	6.85	23.68

From the rheological data without vibration and under vibration, the material and vibration parameters for mixtures 1, 2 and 5 were calculated to be as shown in Table 5.4 and Table 5.5 respectively. This was done by fitting the data using Equation 4.9 and Equation 4.10 as shown in Figure 5.66 through Figure 5.86. It should be noted that for some data sets, the rheological data obtained under vibration intersected with those obtained without vibration as shown in Figure 5.68. A similar phenomenon was observed in the literature for some mixtures [49]. This contradicted the assumption that fresh concrete exhibits shear-thinning properties. This also made it inapplicable for Equation 4.10 to fit the data under vibration without excluding data points at high vane speeds since Equation 4.10 is asymptotic to Bingham Equation 4.9. This could be due to segregation resulting in higher stress readings as the vane might have been shearing a layer of concrete that contained larger fraction of coarse aggregates. This could also possibly be hinting at some kind of shear-thickening behavior that fresh concrete might exhibit at high shear strain rates that are not typically measured by rheometers. This claim can be better understood by considering the apparent viscosity equations for fresh concrete without vibration (Equation 5.1) and under vibration (Equation 5.2):

$$\mu_B(\dot{\gamma}) = \frac{\tau}{\dot{\gamma}} = \frac{\tau_0}{\dot{\gamma}} + \mu_p \quad \text{Equation 5.1}$$

$$\mu_v(\dot{\gamma}) = \frac{\tau}{\dot{\gamma}} = \frac{(\tau_0 + \mu_p \gamma_v) + \mu_p \dot{\gamma}}{\dot{\gamma} + \gamma_v} = \frac{\tau_0 + \mu_p(\dot{\gamma} + \gamma_v)}{\dot{\gamma} + \gamma_v} = \frac{\tau_0}{\dot{\gamma} + \gamma_v} + \mu_p \quad \text{Equation 5.2}$$

Where:

μ_B =Apparent viscosity for the Bingham model

μ_v =Apparent viscosity for the “under vibration” model

It is easy to see that the viscosity obtained from Equation 5.2 at a strain rate $\dot{\gamma}$ is equal to the viscosity obtained from Equation 5.1 at the same strain rate incremented by the shear strain rate imposed by vibration $\dot{\gamma} + \gamma_v$ (Equation 5.3):

$$\mu_v(\dot{\gamma}) = \mu_B(\dot{\gamma} + \gamma_v) \quad \text{Equation 5.3}$$

This happens only if the rheological curve under vibration is always below the rheological curve without vibration. However, the cases where the rheological data obtained under vibration were above those obtained without vibration, such as the one shown in Figure 5.68, indicated that there was a certain shear strain rate above which the viscosity under vibration was more than the viscosity obtained from the Bingham model incremented with γ_v , implying the shear-thickening behavior of fresh concrete above that strain rate.

Table 5.4 Rheological properties of mixtures 1, 2, and 5

Mixture ID	Yield Stress (Pa)	Plastic Viscosity (Pa.s)
1	995.1	19.1
2	150.1	6.0
5	527.4	12.1

Table 5.5 Vibration parameter (γ_v) for mixtures 1, 2, and 5

Vibration Frequency (Hz)	Weight Offset ID	Strain Rate Caused by Vibration γ_v (1/s)		
		Mixture 1	Mixture 2	Mixture 5
72.81	1	0.369	0.357	0.398
73.35	2	0.338	0.178	0.397

73.9	3	0.075	0.073	0.084
75	4	0.034	0.018	0.021
94.93	1	0.834	0.872	1.095
95.64	2	0.715	0.416	0.735
116.16	4	0.101	0.097	0.122

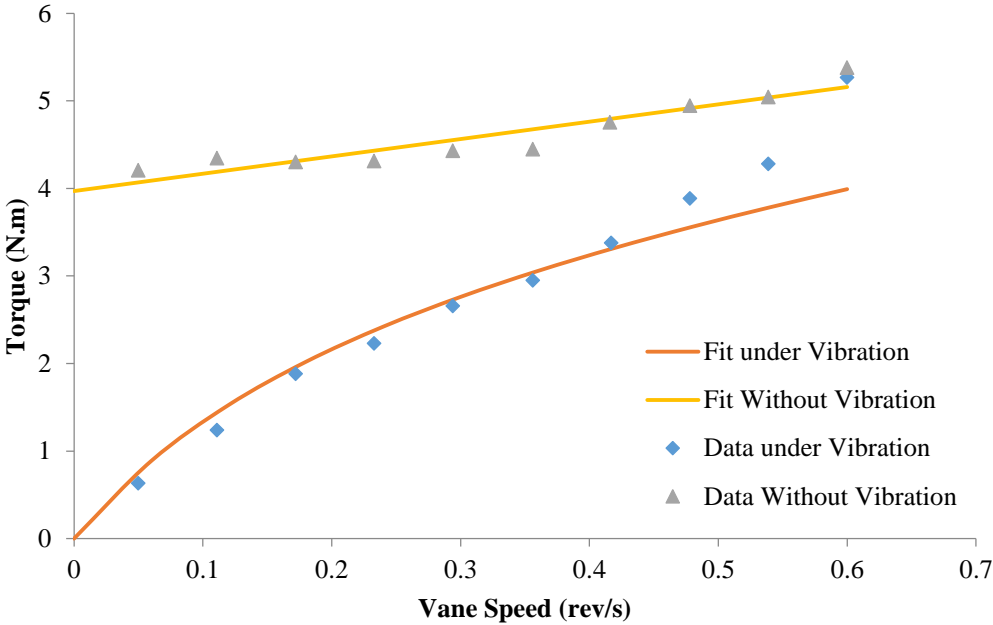


Figure 5.66 Rheological data for mixture 1 at a vibration frequency of 72.81 Hz and weight offset ID # 1

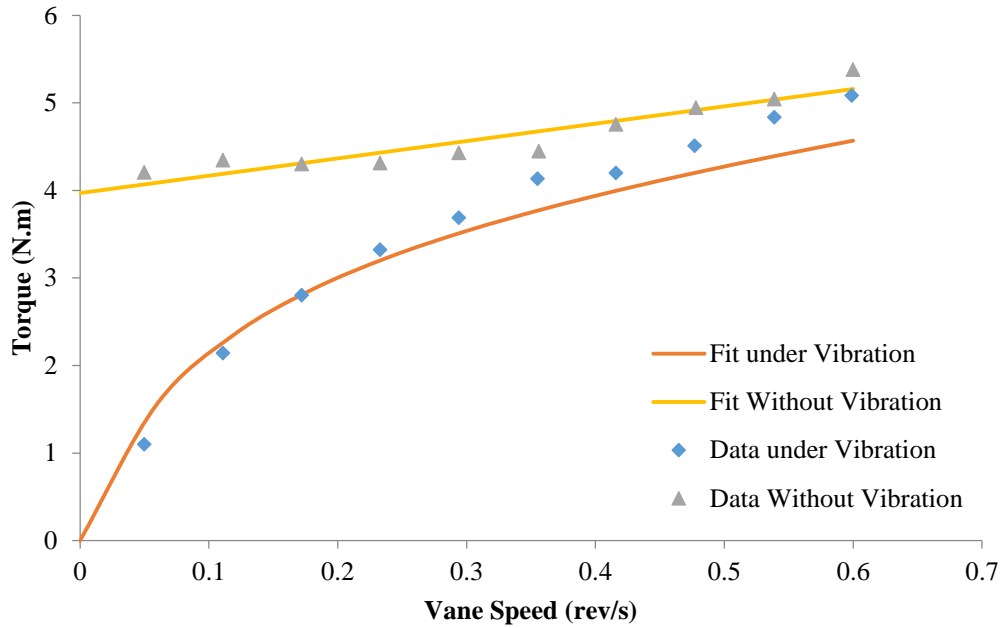


Figure 5.67 Rheological data for mixture 1 at a vibration frequency of 73.35 Hz and weight offset ID # 2

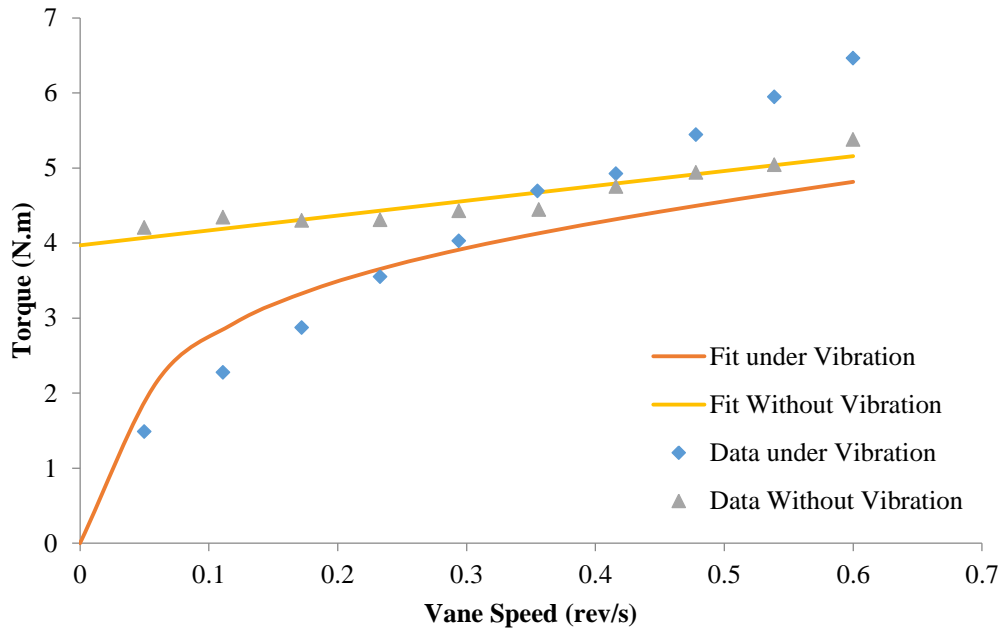


Figure 5.68 Rheological data for mixture 1 at a vibration frequency of 73.9 Hz and weight offset ID # 3

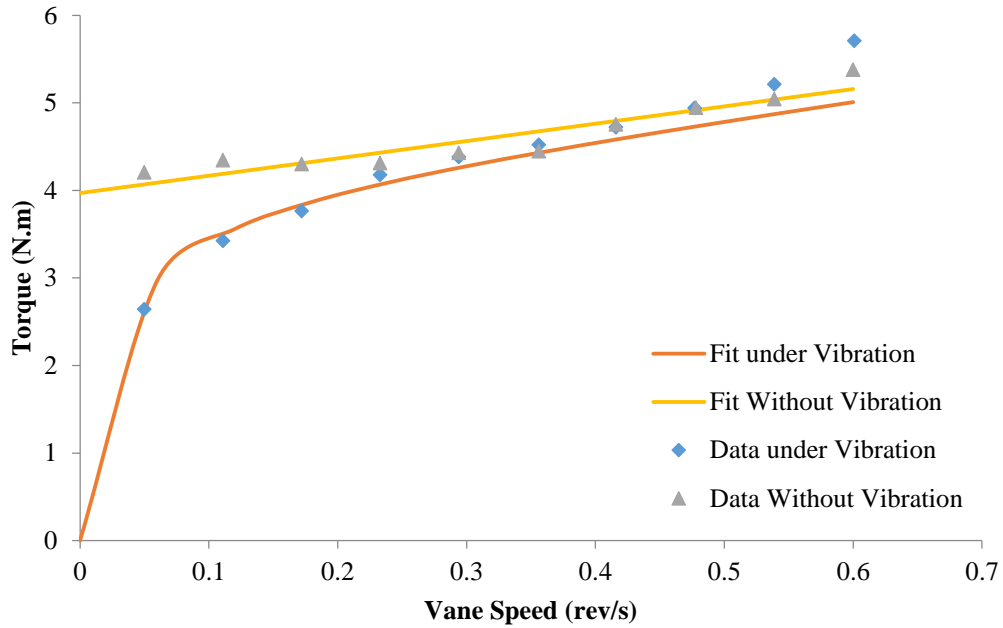


Figure 5.69 Rheological data for mixture 1 at a vibration frequency of 75 Hz and weight offset ID # 4

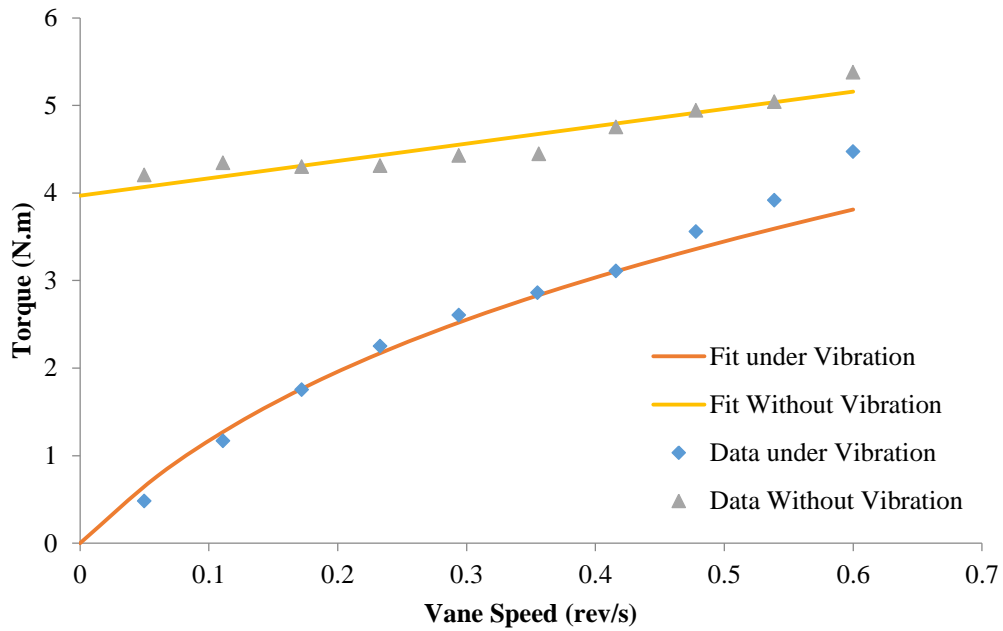


Figure 5.70 Rheological data for mixture 1 at a vibration frequency of 94.93 Hz and weight offset ID # 1

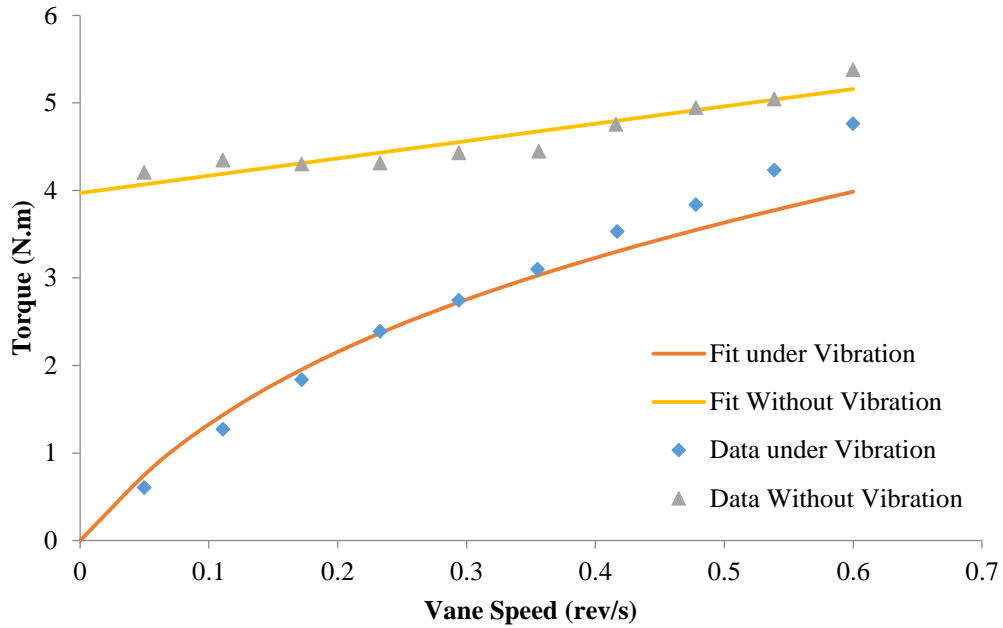


Figure 5.71 Rheological data for mixture 1 at a vibration frequency of 95.64 Hz and weight offset ID # 2

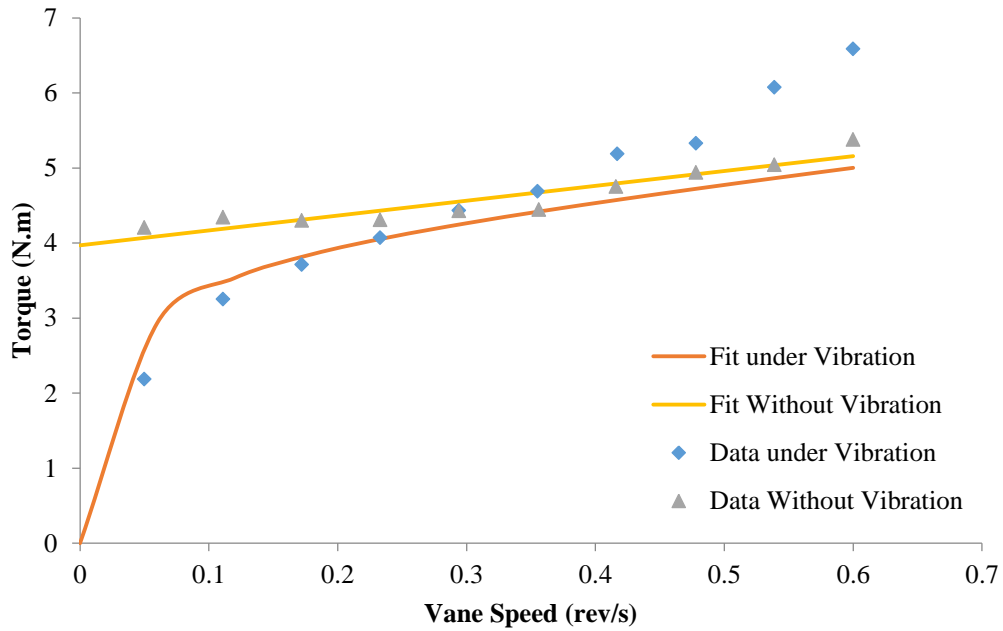


Figure 5.72 Rheological data for mixture 1 at a vibration frequency of 116.16 Hz and weight offset ID # 4

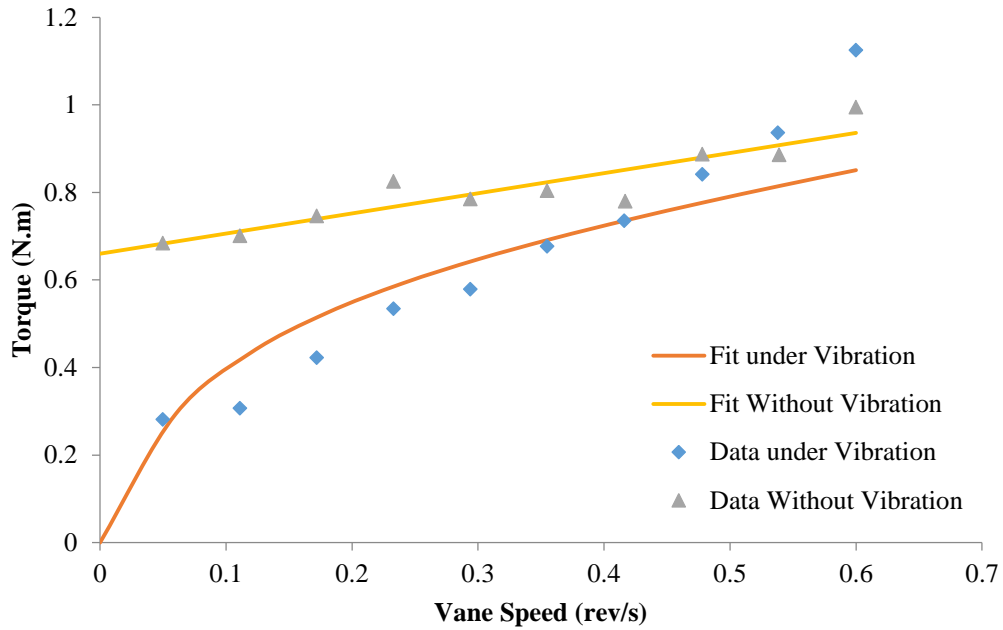


Figure 5.73 Rheological data for mixture 2 at a vibration frequency of 72.81 Hz and weight offset ID # 1

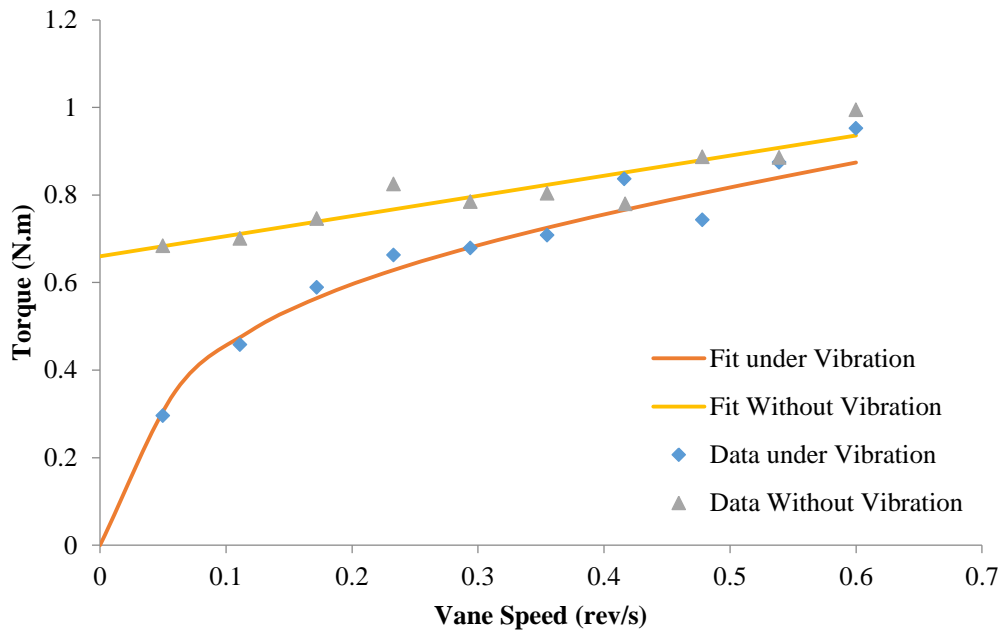


Figure 5.74 Rheological data for mixture 2 at a vibration frequency of 73.35 Hz and weight offset ID # 2

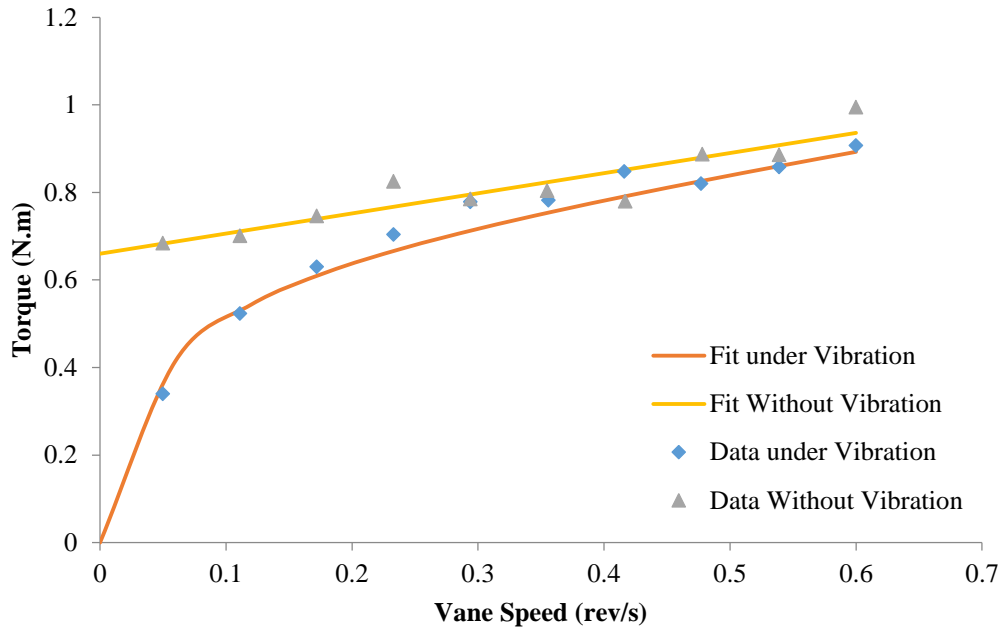


Figure 5.75 Rheological data for mixture 2 at a vibration frequency of 73.9 Hz and weight offset ID # 3

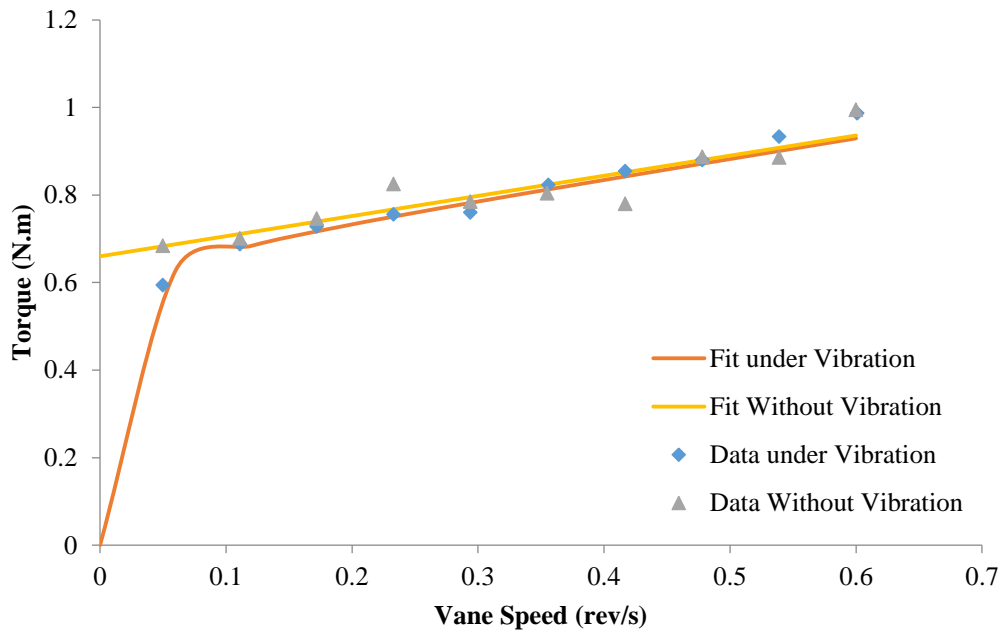


Figure 5.76 Rheological data for mixture 2 at a vibration frequency of 75 Hz and weight offset ID # 4

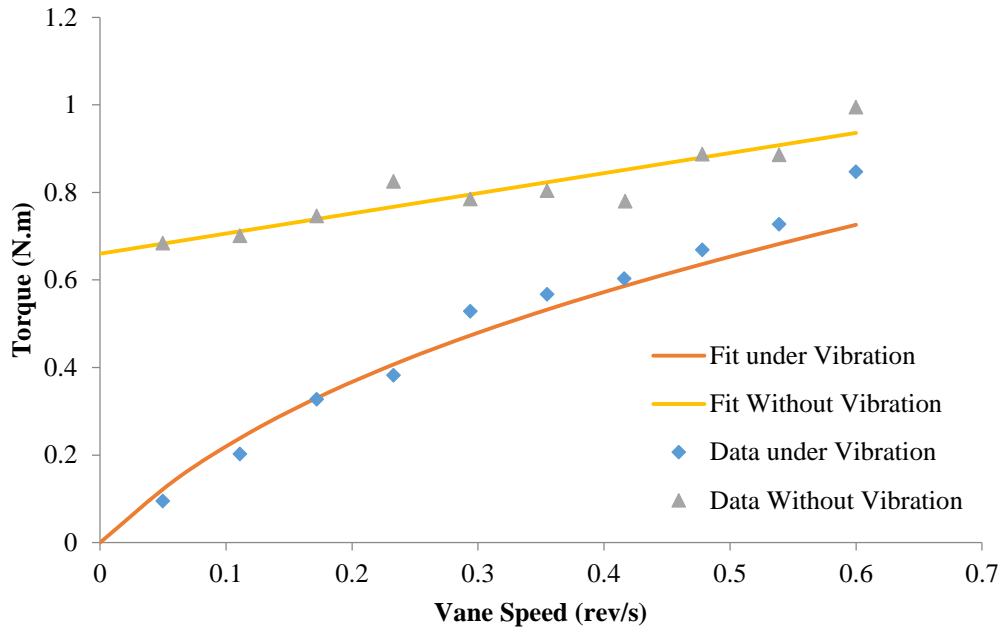


Figure 5.77 Rheological data for mixture 2 at a vibration frequency of 94.93 Hz and weight offset ID # 1

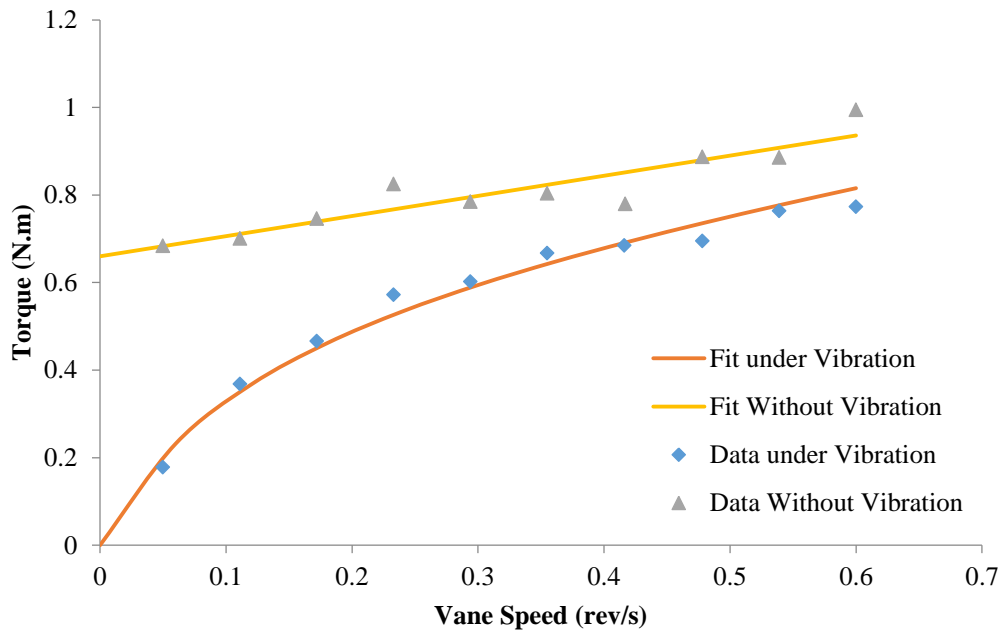


Figure 5.78 Rheological data for mixture 2 at a vibration frequency of 95.64 Hz and weight offset ID # 2

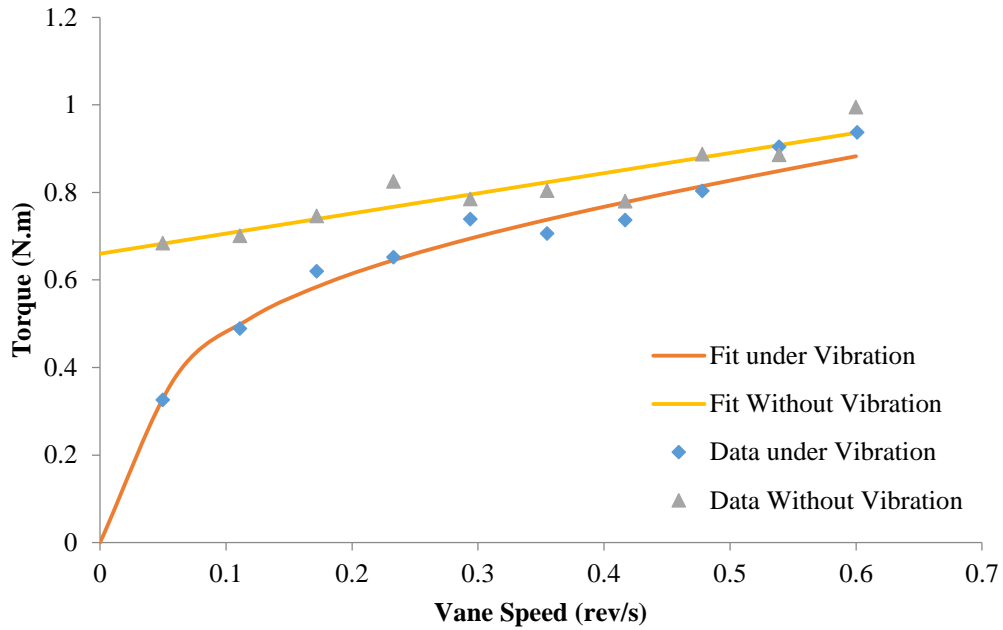


Figure 5.79 Rheological data for mixture 2 at a vibration frequency of 116.16 Hz and weight offset ID # 4

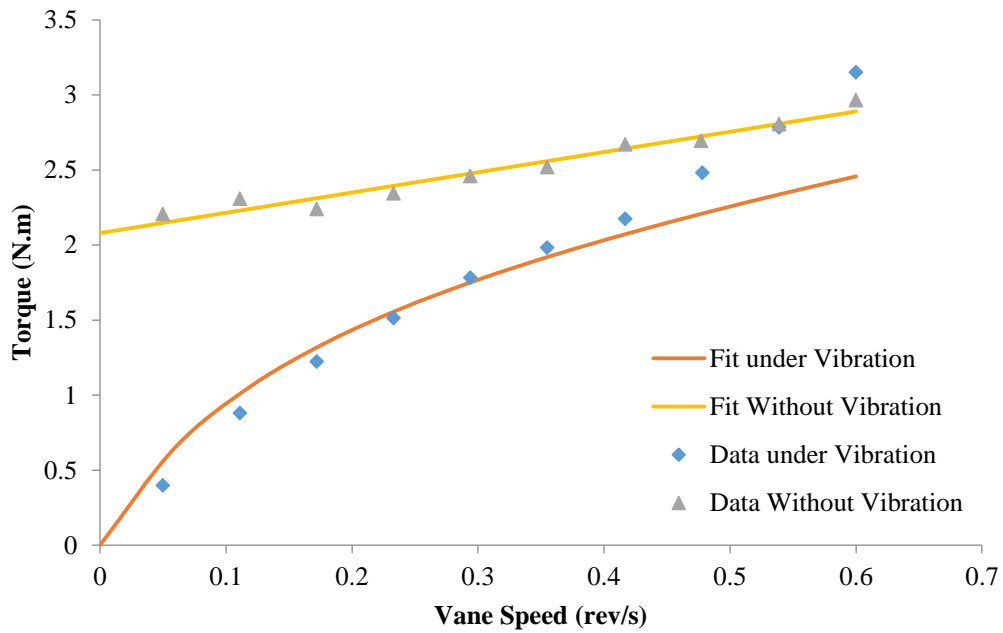


Figure 5.80 Rheological data for mixture 5 at a vibration frequency of 72.81 Hz and weight offset ID # 1

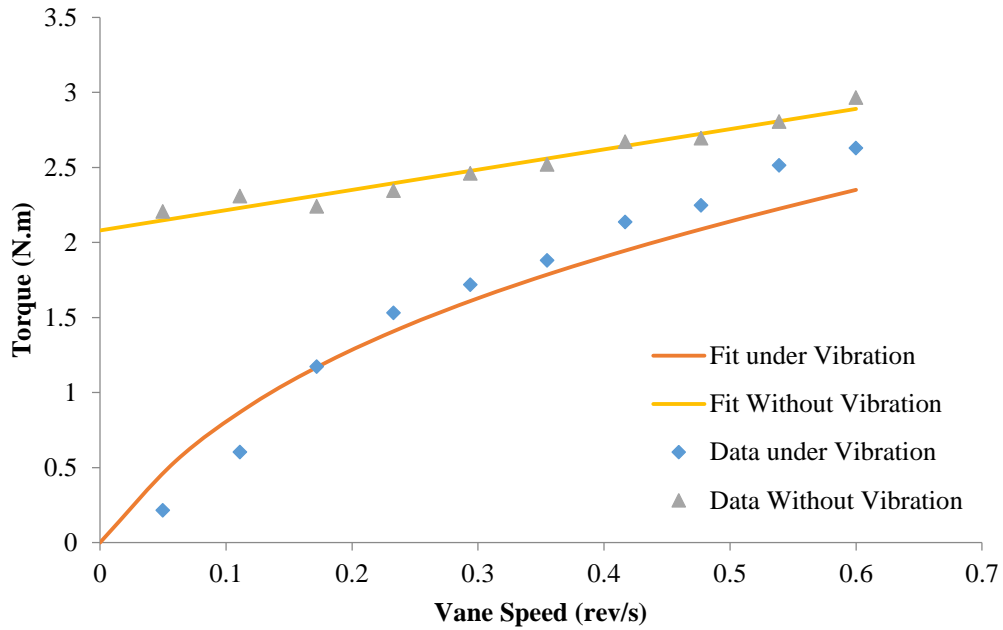


Figure 5.81 Rheological data for mixture 5 at a vibration frequency of 73.35 Hz and weight offset ID # 2

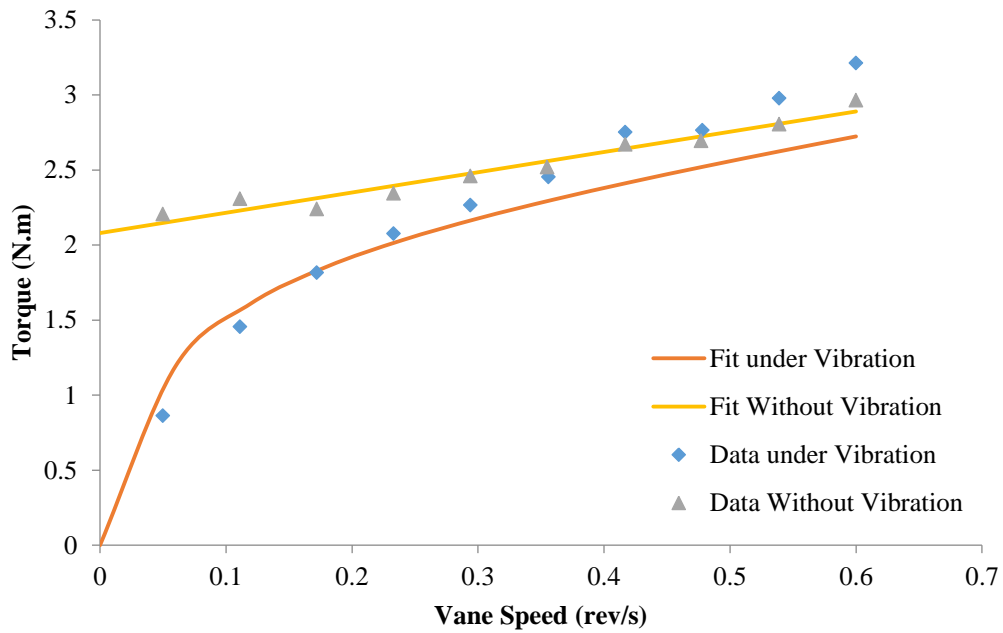


Figure 5.82 Rheological data for mixture 5 at a vibration frequency of 73.9 Hz and weight offset ID # 3

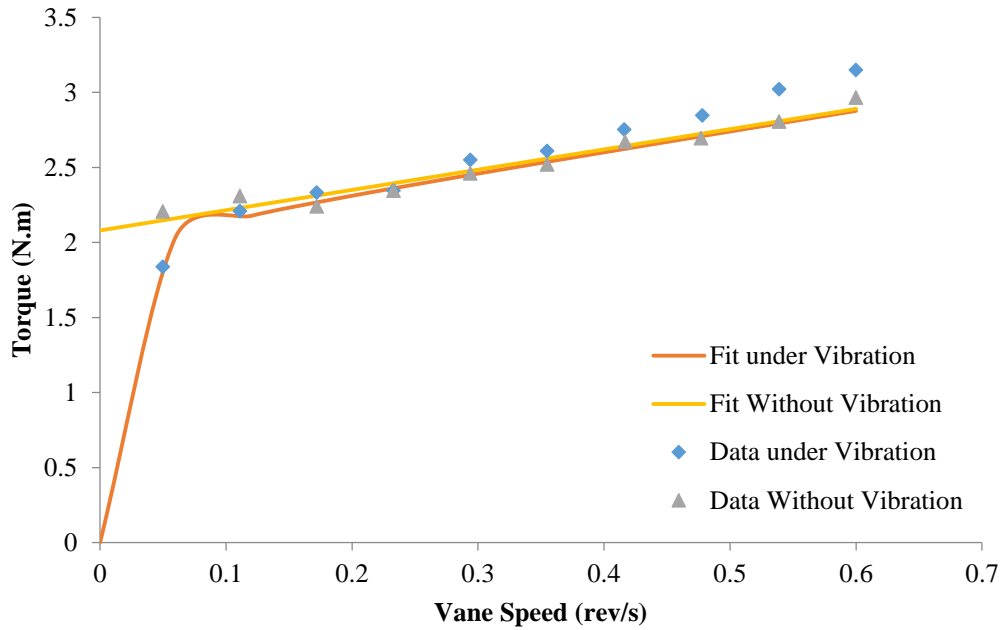


Figure 5.83 Rheological data for mixture 5 at a vibration frequency of 75 Hz and weight offset ID # 4

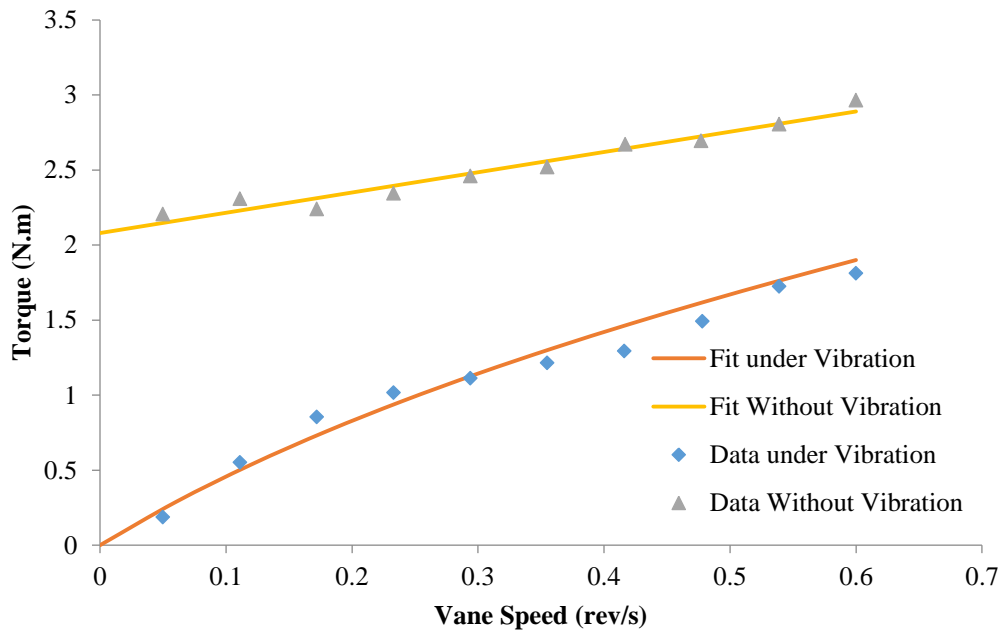


Figure 5.84 Rheological data for mixture 5 at a vibration frequency of 94.93 Hz and weight offset ID # 1

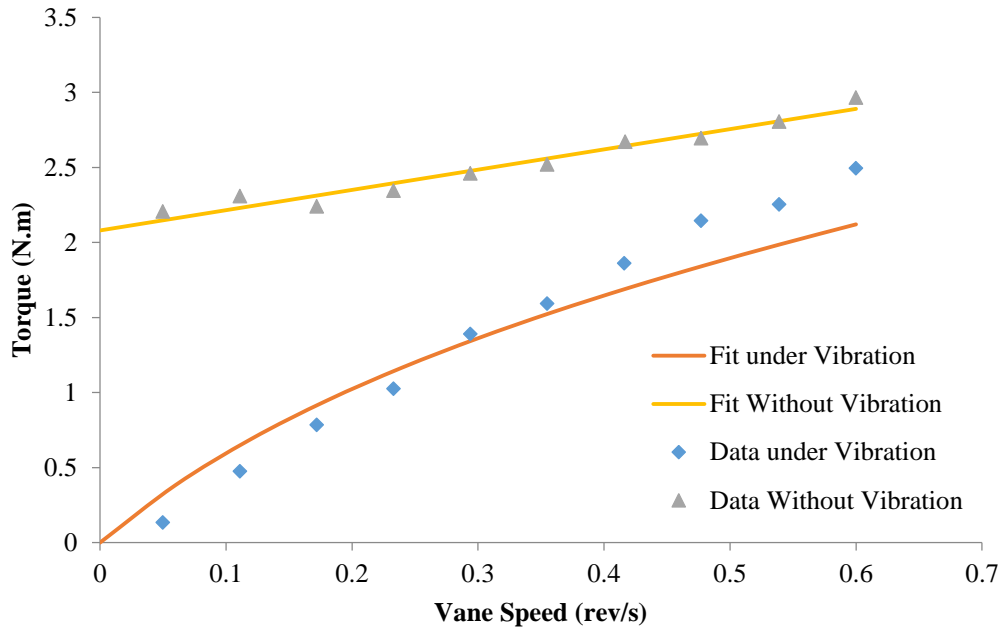


Figure 5.85 Rheological data for mixture 5 at a vibration frequency of 95.64 Hz and weight offset ID # 2

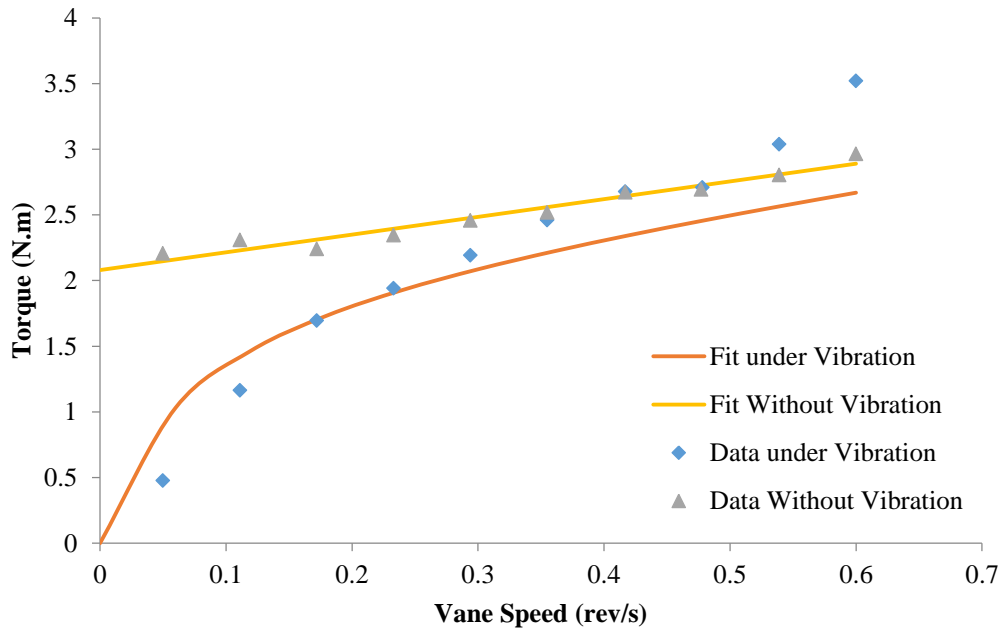


Figure 5.86 Rheological data for mixture 5 at a vibration frequency of 116.16 Hz and weight offset ID # 4

It can be observed from Table 5.5 that the vibration parameters (i.e. shear strain rates caused by vibration) at a specific vibration configuration were not exactly the same for all

mixtures. Therefore, it was believed that this vibration parameter might also be dependent on the fluidity of the mixture.

Since the peak velocity takes both frequency and peak acceleration into account (Equation 5.4) and since the shear strain rate is directly related to the velocity instead of the acceleration (Equation 5.5), it was attempted to correlate the peak velocity values inside concrete with γ_v values as shown in Figure 5.87. It seems from Figure 5.87 that there is no apparent correlation between the peak velocities inside concrete and γ_v values. While Figure 5.87 shows the correlation for a certain depth inside the concrete, the correlations at other depths were as poor as this correlation. However, a good linear correlation can be established between average peak velocity values on the vibrating table and average γ_v values across all three mixtures as shown in Figure 5.88. An even better correlation was established by omitting γ_v values of mixture 2 as shown in Figure 5.89. This was done due to the fact that mixture 2 experienced excessive segregation during testing which was thought to be a potential cause of unreliable data. Therefore, the adopted correlation between peak velocity of the vibrating table and γ_v is as shown in Equation 5.6:

$$v_p = \frac{a_p}{2\pi f} \quad \text{Equation 5.4}$$

$$\dot{\gamma}_{xy} = \frac{\partial v_x}{\partial y} + \frac{\partial v_y}{\partial x} \quad \text{Equation 5.5}$$

$$\gamma_v = 10.056v_p \quad \text{Equation 5.6}$$

Where:

v_p =Peak vibration velocity

a_p =Peak vibration acceleration

f =Vibration frequency

$\dot{\gamma}_{xy}$ =Shear strain rate in the x-y plane

v_x =Velocity in the x-direction

v_y =Velocity in the y-direction

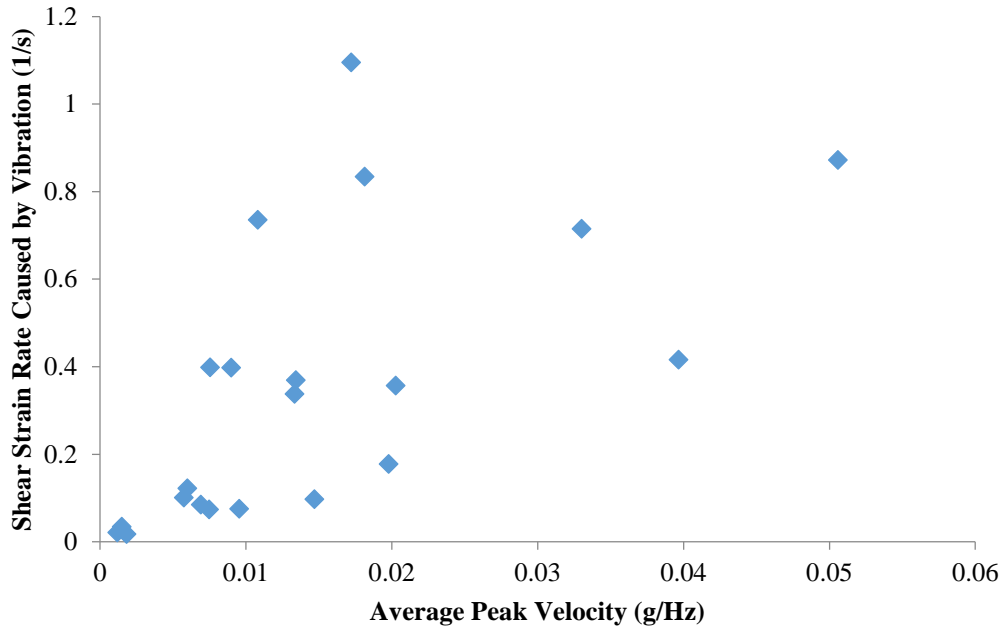


Figure 5.87 Vibration parameter versus average peak velocity at 6 in. deep inside mixtures 1, 2, and 5

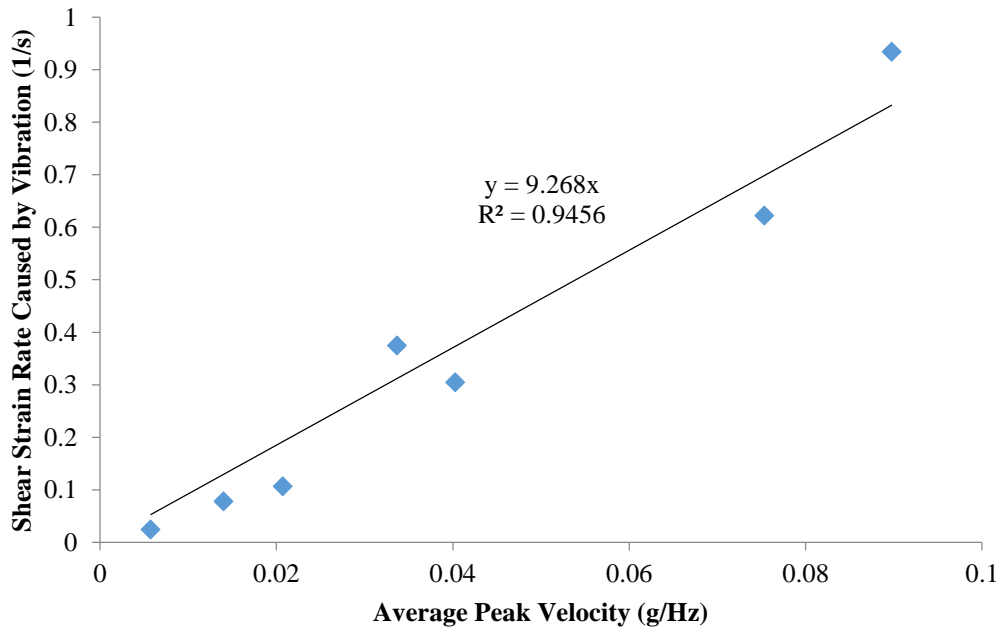


Figure 5.88 Average vibration parameter for mixtures 1, 2, and 5 versus average peak velocity on the vibrating table

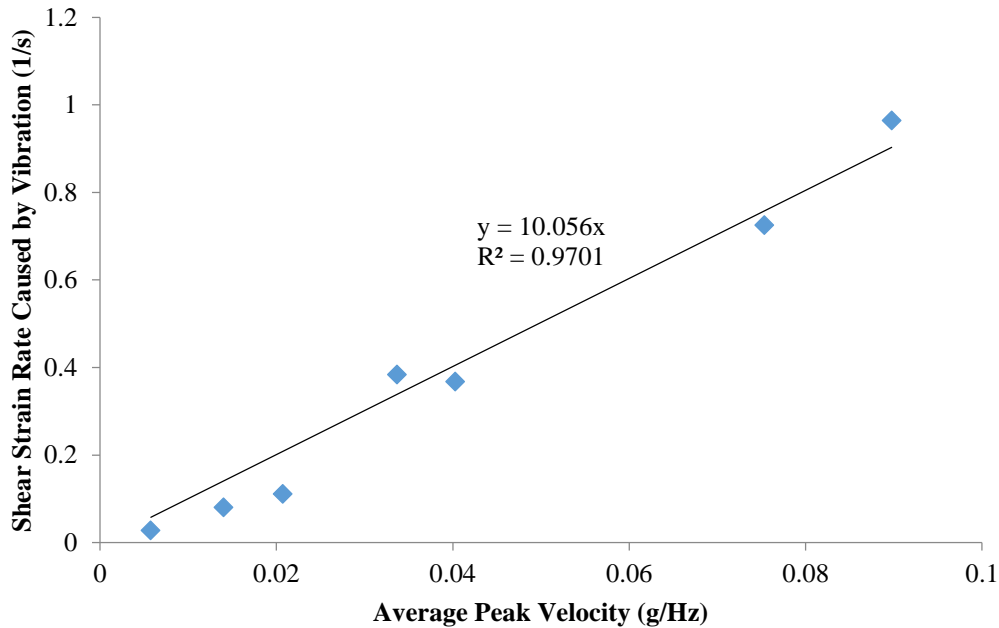


Figure 5.89 Average vibration parameter for mixtures 1 and 5 versus average peak velocity on the vibrating table

The fact that a very good correlation between the peak velocity measured on the vibrating table and the average shear strain rate imposed by vibration inside concrete was established indicated that the shear strain rate imparted by the vibration into the mixture was highly likely to be independent from the fluidity of the mixture. This was true despite the fact that peak velocity values measured inside concrete were very different when comparing one mixture to another. It could be because the readings inside the concrete might have been influenced by other factors such as the contact between coarse aggregates and the accelerometer. Even if the readings inside fresh concrete were indeed representative of the actual peak vibration velocity felt by the concrete, the lack of correlation in Figure 5.87 could still be explained by the fact that the shear strain rate is related to the change of velocity with respect to space not to the magnitude of velocity. Even if different mixtures dampen the waves differently, if the dampening is the same at all points in the medium then the change in velocity with respect to space will remain constant regardless of the dampening effect.

Equation 5.6 was used to obtain the predicated γ_v values for mixture 4 at each vibration configuration. γ_v along with the rheological data during vibration were then used to obtain the yield stress and plastic viscosity values shown in Table 5.6. This was done by fitting the data using Equation 4.10 as shown in Figure 5.90 through Figure 5.96. In some cases such as Figure 5.90, some data points had to be deleted in order to obtain a reasonable fit. The yield stress and plastic viscosity values of mixture 4 were predicted to be the average of the values presented in Table 5.6. These are namely 1234 Pa yield stress and 41.4 Pa.s plastic viscosity.

Table 5.6 Predicted rheological properties of mixture 4

Vibration Frequency (Hz)	Weight Offset ID	Average Vibration Peak Velocity on the Vibrating Table (g)	γ_v Calculated from Equation 5.6	Yield Stress (Pa)	Plastic Viscosity (Pa.s)
72.81	1	0.034	0.339	900.3	29.5
73.35	2	0.040	0.405	1398.1	37.7
73.9	3	0.014	0.141	951.5	67.8
75	4	0.006	0.058	1359.6	17
94.93	1	0.090	0.903	1549.6	27.6
95.64	2	0.075	0.758	1514.8	40.3
116.16	4	0.021	0.208	964.1	70.2

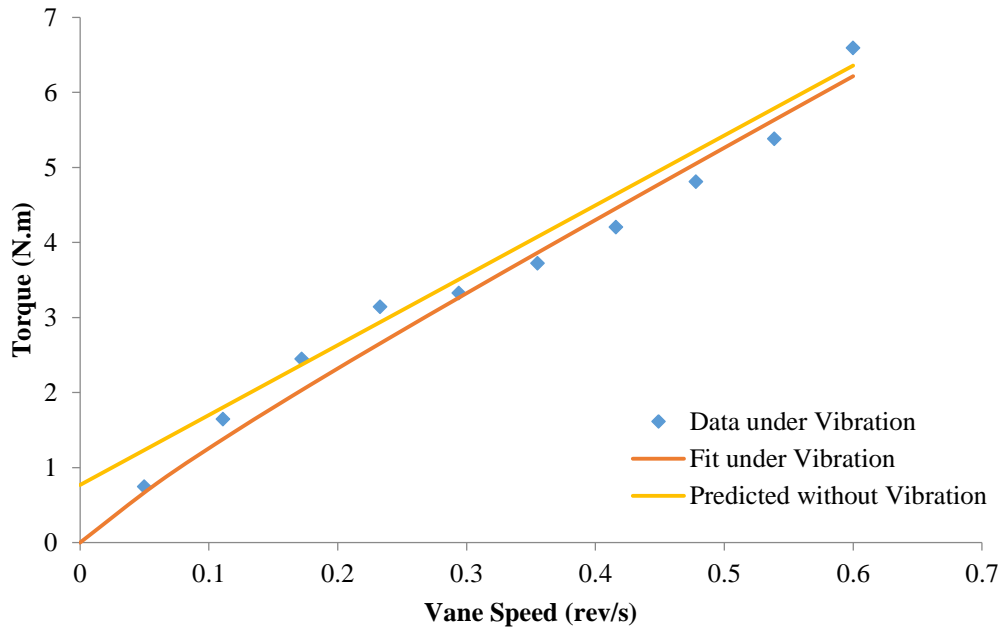


Figure 5.90 Rheological data for mixture 4 at a vibration frequency of 72.81 Hz and weight offset ID # 1

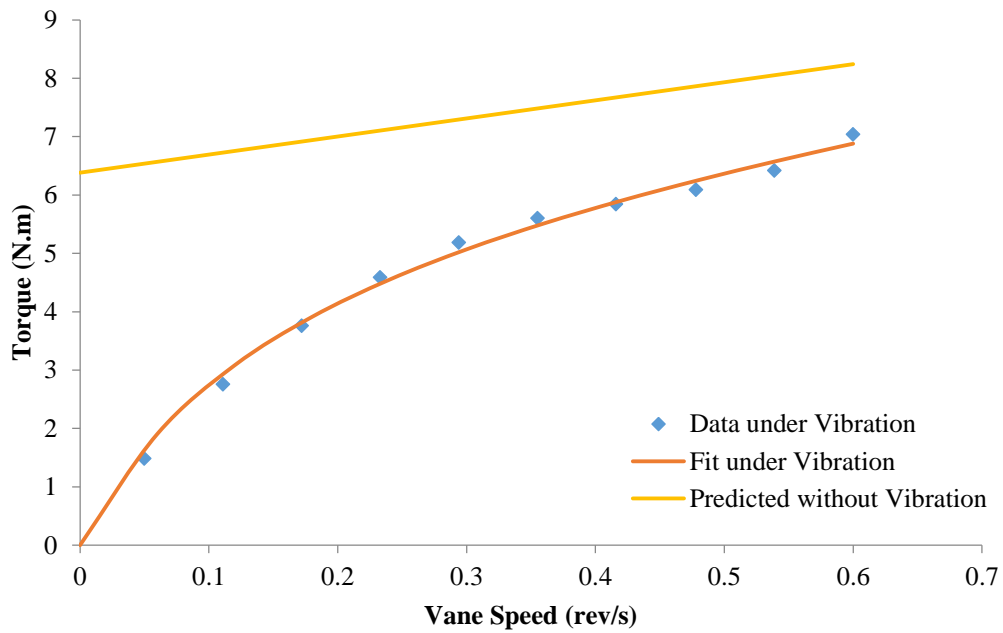


Figure 5.91 Rheological data for mixture 4 at a vibration frequency of 73.35 Hz and weight offset ID # 2

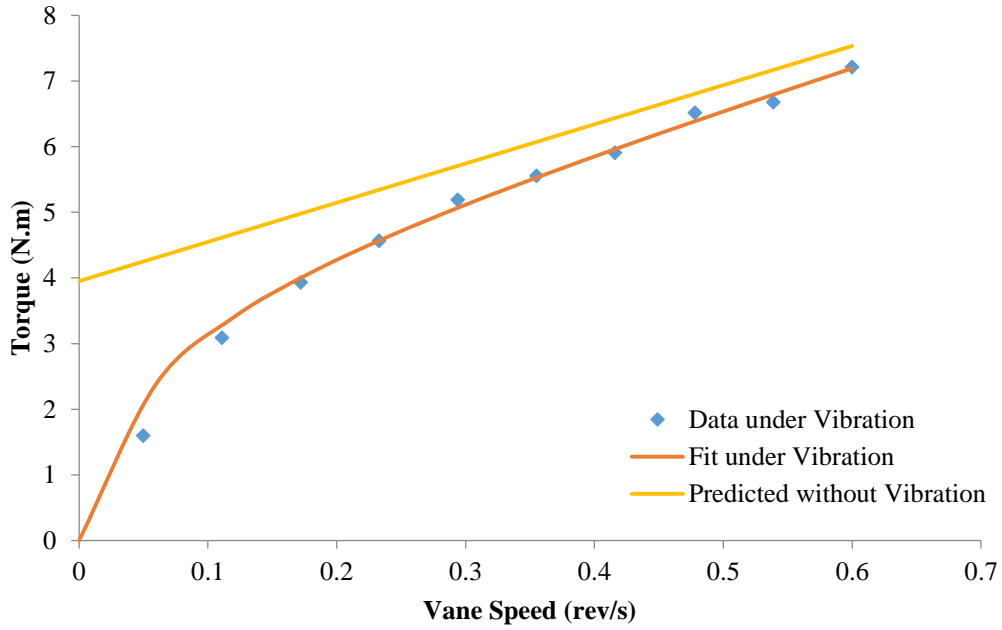


Figure 5.92 Rheological data for mixture 4 at a vibration frequency of 73.9 Hz and weight offset ID # 3

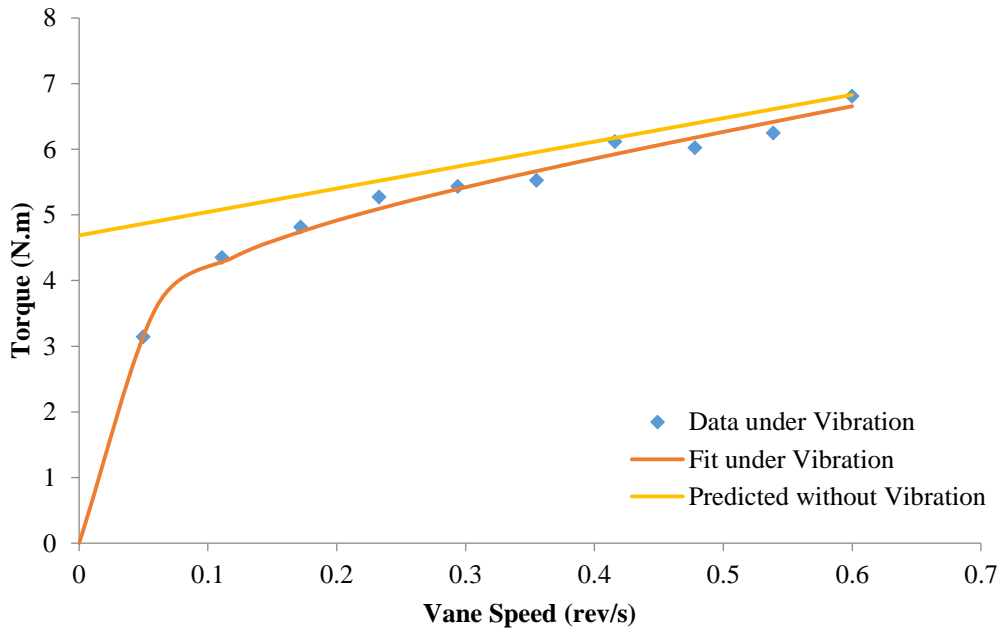


Figure 5.93 Rheological data for mixture 4 at a vibration frequency of 75 Hz and weight offset ID # 4

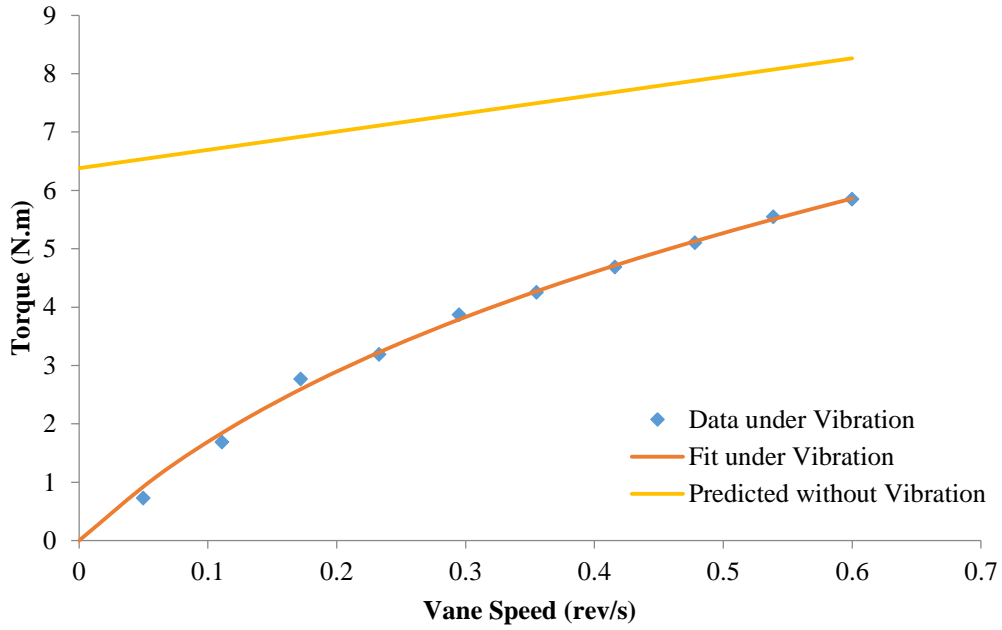


Figure 5.94 Rheological data for mixture 4 at a vibration frequency of 94.93 Hz and weight offset ID # 1

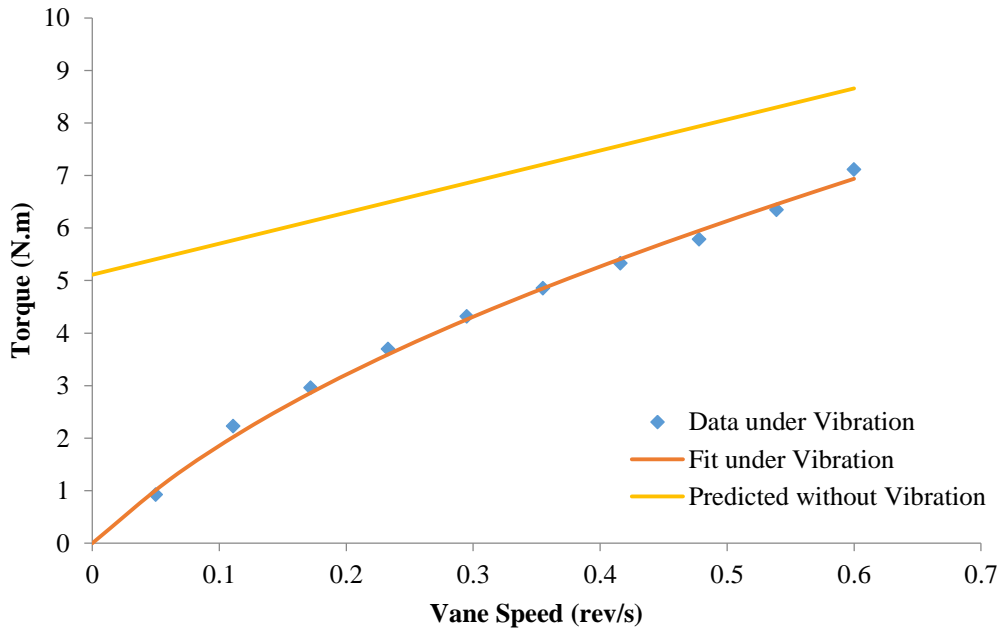


Figure 5.95 Rheological data for mixture 4 at a vibration frequency of 95.64 Hz and weight offset ID # 2

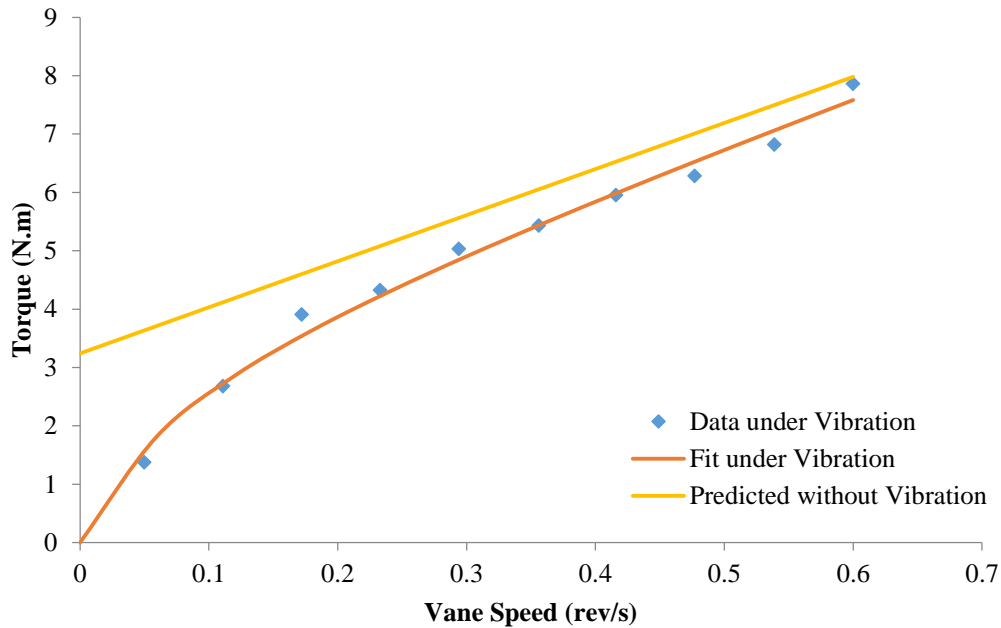


Figure 5.96 Rheological data for mixture 4 at a vibration frequency of 116.16 Hz and weight offset ID # 4

In order to test the reliability of this method to estimate the rheological properties of concrete mixtures, the same procedures were performed on mixture 2 in which the actual yield stress and plastic viscosity are known. Table 5.7 shows the predicted yield stress and plastic viscosity values for mixture 2. The averages of these values were found to be 200.2 Pa for yield stress and 4.6 Pa.s for plastic viscosity. These are relatively close to the actual measured values shown in Table 5.4. It is believed that better estimations can be achieved if a more reliable rheometer is used.

Table 5.7 Predicted rheological properties of mixture 2

Vibration Frequency (Hz)	Weight Offset ID	Average Vibration Peak Velocity on the Vibrating Table (g)	γ_v Calculated from Equation 5.6	Yield Stress (Pa)	Plastic Viscosity (Pa.s)
72.81	1	0.034	0.339	112.1	11.5
73.35	2	0.040	0.405	268.3	1.2
73.9	3	0.014	0.141	206.2	2.0
75	4	0.006	0.058	173.2	4.6

94.93	1	0.090	0.903	152.7	6.8
95.64	2	0.075	0.758	313.0	1.8
116.16	4	0.021	0.208	176.3	4.5

Unfortunately, this method of back-calculating the rheological properties using data obtained during vibration was not applicable for extremely stiff concrete mixtures. For instance, it was not possible to obtain rheological data, even during vibration, for mixture 3 which had the lowest slump value of 1.25 in. It was observed visually for mixture 3 that the concrete was almost moving as a single block with the rheometer pot instead of being sheared by the pot's wall. This phenomenon is called rigid body motion of fluids where each fluid particle assumes the same acceleration resulting in the absence of shear stresses within the fluid body [27]. This was believed to have happened in mixture 3 due to the high friction between the fresh concrete particles.

Chapter 6 - Conclusions and Recommendations

6.1. Summary

The main goal of this research was to study the effect of vibration on the freeze-thaw durability of concrete having low w/cm and containing HRWRs and AEAs. To that end, an experimental program was conducted. This program included:

1. Studying the effect of delaying vibration on the air loss from fresh concrete.
2. Looking at the effect of chemical admixtures on the freeze-thaw durability of concrete.
3. Exploring the effect of vibration parameters and rheological properties on the freeze-thaw deterioration of concrete.
4. Investigating the air requirements to achieve freeze-thaw resistance.
5. Examining the possibility of measuring rheological properties of stiff concrete mixtures.

The effect of vibration delay was looked at mainly by measuring the fresh air content of concrete before vibration and after 2 minutes of vibration that was initiated at different times from the start of mixing. Both 3 g and 10 g peak vibration accelerations were examined. Also, several admixture combinations were used in the studied concrete mixtures. Freeze-thaw testing of some specimens was also carried out.

In order to investigate the effect of chemical admixtures, vibration parameters, rheological properties and air parameters on the freeze-thaw performance of concrete, a lot of specimens from several concrete mixtures were tested for freeze-thaw durability. Air content and spacing factor values were also measured for these specimens. Three different admixture combinations using two different HRWRs and two different AEAs were examined in this study.

Some specimens were vibrated for 30 seconds while others were vibrated for 4 minutes. Vibration frequencies ranging from 30 Hz to 160 Hz and peak vibration accelerations ranging from 4 g to 25 g were explored. The effect of rheological properties was incorporated in the study by looking at four different categories of rheology. The effect of different initial air contents was also tested. Fresh and hardened air contents and spacing factors were related to the durability factor, weight change and length change.

Efforts to measure the rheological properties of stiff concrete mixtures were made by performing the rheology test during vibration. Three mixtures of known different rheological properties were tested under vibration with different peak vibration velocities. The shear strain rates imposed by vibration were estimated by fitting the data with a model used for granular suspensions. A correlation between peak vibration velocity and strain rate imposed by vibration was then established and used to estimate the rheological properties of a stiffer concrete mixture that could not be tested without vibration.

6.2. Conclusions

It was found that the amount of air loss from fresh concrete increased as the initiation of vibration was delayed. The relationship between percentage air lost and the initiation time of vibration was shown to be linear with time and eventually occurred even in the mixtures without HRWRs. The rate of the air loss after vibration with time can be used to determine the stability of the air system inside the concrete. For a given chemical admixture combination, the stability of the air system remained the same regardless of the initial fluidity of the mixture. However, fluid mixtures generally lose more air compared to stiff mixtures. No significant differences between AEAs on the air void stability were seen. While higher peak vibration acceleration generally results in higher air loss, the air void stability was found to be the same regardless of

the peak vibration acceleration. The air stability study arrived at the main conclusion that vibrating concrete in precast concrete railroad tie plants at room temperature within 30 minutes after mixing should not produce any significant issues with regard to the air stability with time inside the concrete.

Air can be lost from concrete naturally even without vibration. Longer durations of vibration up to 4 minutes using a table vibrator could cause higher air loss but would only cause marginal increase in spacing factor compared to shorter durations of vibration. Most of the air loss affecting freeze-thaw durability appeared to occur during the initial period of vibration. Some combinations of chemical admixtures that normally produce suitable air void systems for freeze-thaw durability could produce air void systems with larger air voids that could be removed during vibration, especially in mixtures with low yield stress. Higher peak vibration acceleration generally resulted in higher spacing factor and slightly higher susceptibility to freeze-thaw damage. Vibration frequency and velocity seemed to have minimal effect on the air system and the freeze-thaw durability. No apparent correlation between durability and plastic viscosity was observed. Immersion vibrators were shown to have a local negative influence on the concrete air void system.

Concrete mixtures with a spacing factor after vibration below 0.0087 in. (0.22 mm) were shown to have good freeze-thaw durability. The spacing factor was, however, not able to predict the durability of concrete above 0.0087 in. (0.22 mm). Several concrete mixtures with a spacing factor after vibration higher than 0.0087 in. (0.22 mm) had excellent freeze-thaw durability. Concrete freeze-thaw durability tests are needed to distinguish the freeze-thaw durability of concrete with a spacing factor above 0.0087 in. (0.22 mm).

A rheology model under vibration for granular suspensions was found to be applicable for fresh concrete in most cases. A strong correlation between the vibrating table peak vibration velocity and the average shear strain rate imposed by vibration on the concrete mixture was obtained. This correlation was found to be independent of the fluidity of the concrete mixture. While it is possible to predict the rheological properties of stiff concrete mixtures (i.e. mixtures having a slump value less than 3 in.) by performing rheological tests during vibration, it was found to be relatively difficult to do the same with extremely stiff mixtures (i.e. mixtures having a slump value around 1 in.). This may be because these mixtures behave more like granular materials than liquids, even under the large vibration used in this study.

6.3. Recommendations

While significant conclusions were obtained from this research, there is a lot of room for future research that can be conducted to acquire additional knowledge about the subject. The following recommendations are to be taken into account for any related future research:

1. For the stability of the air system with time from mixing until vibration, mixtures with lower initial air contents (i.e. air contents closer to the values at which freeze-thaw damage would be expected to happen) should be tested.
2. A chemistry-oriented study can greatly help in pinpointing the cause of poor performance of some admixture combinations when it comes to freeze-thaw resistance.
3. Relating the air loss to the apparent viscosity (if possible to compute) of the mixture instead of the yield stress and plastic viscosity might yield better correlations.

4. In order to obtain more statistically reliable results and conclusions, a more extensive study for estimating rheological properties of stiff concrete mixtures should be carried out. Using a different more reliable rheometer is also encouraged.

References

- [1] M. Pigeon and R. Pleau, *Durability of Concrete in Cold Climates*, Abingdon: Taylor & Francis, 1995.
- [2] ACI Committee 201, "Guide to Durable Concrete," American Concrete Institute, Farmington Hills, MI, 2008.
- [3] C. H. Scholer, "Report on Significance of Tests of Concrete and Concrete Aggregates: Durability of Concrete," ASTM, Philadelphia, 1943.
- [4] C. H. Scholer, "Significance of Tests and Properties of Concrete and Concrete Aggregates: Resistance to Weathering - General Aspects," ASTM, 1956.
- [5] T. C. Powers, "Significance of Tests and Properties of Concrete and Concrete Aggregates: Hardened Concrete, Resistance to Weathering - Freezing and Thawing," ASTM, Philadelphia, 1956.
- [6] T. C. Powers, "A Working Hypothesis for Further Studies of Frost Resistance of Concrete," *Journal of the American Concrete Institute*, vol. 16, no. 4, 1945.
- [7] ASTM, "ASTM C457: Standard Test Method for Microscopical Determination of Parameters of the Air-Void System in Hardened Concrete," ASTM International, West Conshohocken, PA, 2008.
- [8] ASTM, "ASTM C666: Standard Test Method for Resistance of Concrete to Rapid Freezing and Thawing," ASTM International, West Conshohocken, PA, 2008.
- [9] ASTM, "ASTM C672: Standard Test Method for Scaling Resistance of Concrete Surfaces Exposed to Deicing Chemicals," ASTM International, West Conshohocken, PA, 2008.
- [10] L. Du and K. J. Folliard, "Mechanisms of air entrainment in concrete," *Cement and Concrete Research*, vol. 35, pp. 1463-1471, 2005.
- [11] M. T. Hasholt, "Air Void Structure and Frost Resistance: A Challenge to Powers' Spacing Factor," *Materials and Structures*, vol. 47, no. 5, pp. 911-923, 2013.
- [12] H. Newlon and T. M. Mitchell, "Significance of Tests and Properties of Concrete and Concrete-Making Materials: Freezing and Thawing," ASTM, Philadelphia, 1994.
- [13] M. O. Withey, "Progress Report, Committee on Durability of Concrete," *Highway Research*

Board Proceedings, vol. 24, pp. 174-202, 1944.

- [14] ASTM, "ASTM C260: Standard Specification for Air-Entraining Admixtures for Concrete," ASTM International, West Conshohocken, PA, 2008.
- [15] K. H. Khayat and J. Assaad, "Air-Void Stability in Self-Consolidating Concrete," *ACI Materials Journal*, vol. 99, no. 4, pp. 408-416, 2002.
- [16] M. Lachemi, K. L. V. Hossain, P.-C. Nkinamubanzi and N. Bouzoubaa, "Self-consolidating concrete incorporating new viscosity modifying admixtures," *Cement and Concrete Research*, vol. 34, no. 6, p. 917-926, 2004.
- [17] K. H. Khayat, "Optimization and Performance of Air-Entrained, Self-Consolidating Concrete," *ACI Materials Journal*, vol. 97, no. 5, pp. 526-535, 2000.
- [18] B. L. Piekarczyk, "Effect of viscosity type modifying admixture on porosity, compressive strength and water penetration of high performance self-compacting concrete," *Construction and Building Materials*, vol. 48, pp. 1035-1044, 2013.
- [19] B. L. Piekarczyk, "The frost resistance versus air voids parameters of high performance self compacting concrete modified by non-air-entrained admixtures," *Construction and Building Materials*, vol. 48, pp. 1209-1220, 2013.
- [20] ASTM, "ASTM C231: Standard Test Method for Air Content of Freshly Mixed Concrete by the Pressure Method," ASTM International, West Conshohocken, PA, 2008.
- [21] ASTM, "ASTM C173: Standard Test Method for Air Content of Freshly Mixed Concrete by the Volumetric Method," ASTM International, West Conshohocken, PA, 2008.
- [22] ASTM, "ASTM C138: Standard Test Method for Density (Unit Weight), Yield, and Air Content (Gravimetric) of Concrete," ASTM International, West Conshohocken, PA, 2008.
- [23] R. E. D. Bishop, *Vibration*, New York, NY: Cambridge University Press, 1979.
- [24] K. U. Ingard, *Fundamentals of Waves and Oscillations*, Cambridge, UK: Cambridge University Press, 1988.
- [25] Z. Tian, J. Guo and C. Gu, "Study on Permeability Coefficient and Volumetric Deformation Modulus of Fresh Concrete for Different Mix Designs," in *Earth and Space*, 2010.
- [26] R. D. Corsaro and L. H. Sperling, *Sound and Vibration Damping with Polymers*, Washington, DC: American Chemical Society, 1990.

- [27] Y. A. Cengel and J. M. Cimbala, *Fluid Mechanics: Fundamentals and Applications*, New York, NY: McGraw-Hill, 2006.
- [28] W. J. Bottega, *Engineering Vibrations*, Boca Raton, FL: Taylor & Francis Group, 2006.
- [29] R. A. Anderson, *Fundamentals of Vibrations*, New York: The Macmillan Company, 1967.
- [30] S. Braun, D. Ewins and S. Rao, *Encyclopedia of Vibration*, London, UK: Academic Press, 2002.
- [31] F. Fahy, *Sound and Structural Vibration: Radiation, Transmission and Response*, London, UK: Academic Press, 1985.
- [32] A. G. Fredrickson, *Principles and Applications of Rheology*, Englewood Cliffs: Prentice-Hall, 1964.
- [33] F. A. Morrison, *Understanding Rheology*, Oxford: Oxford University Press, 2001.
- [34] A. Y. Malkin, *Rheology Fundamentals*, Toronto, ON: ChemTec Publishing, 1994.
- [35] Z. Sobotka, *Rheology of Materials and Engineering Structures*, New York: Elsevier Science Publishing Co, 1984.
- [36] O. H. Wallevik, *Introduction to Rheology of Fresh Concrete*, Iceland: ICI, 2009.
- [37] T. K. Erdem, K. H. Khayat and A. Yahia, "Correlating Rheology of Self-Consolidating Concrete to Corresponding Concrete-Equivalent Mortar," *ACI Materials Journal*, vol. 106, no. 2, pp. 154-160, 2009.
- [38] L. Shen, H. B. Jovein, S. Shen and M. Li, "Effects of Aggregate Properties and Concrete Rheology on Stability Robustness of Self-Consolidating Concrete," *Journal of Materials in Civil Engineering*, vol. 27, no. 5, 2015.
- [39] P. Ghoddousi, A. A. S. Javid and J. Sobhani, "Effects of particle packing density on the stability and rheology of self-consolidating concrete containing mineral admixtures," *Construction and Building Materials*, vol. 53, pp. 102-109, 2014.
- [40] S. E. Chidiac, O. Maadani, A. G. Razaqpur and N. P. Mailvaganam, "Correlation of rheological properties to durability and strength of hardened concrete," *Journal of Materials in Civil Engineering*, vol. 15, pp. 391-399, 2003.
- [41] Z. Toutou and N. Roussel, "Multi scale experimental study of concrete rheology: From water scale to gravel scale," *Materials and Structures*, vol. 39, pp. 189-199, 2006.

- [42] K. K. Teranishi, Y. Tanigawa, H. Mori and K.-i. Terada, "Study on sinking behavior of coarse aggregate in fresh concrete subjected to vibration," *Transactions of The Japan Concrete Institute*, vol. 17, pp. 1-8, 1995.
- [43] H. Kitaoji, Y. Tanigawa, H. Mori and Y. Kurokawa, "Analytical study on vibration transmission properties of fresh concrete," *Transactions of The Japan Concrete Institute*, vol. 20, pp. 1-8, 1998.
- [44] P. F. G. Banfill, M. A. O. M. Teixeira and R. J. M. Craik, "Rheology and vibration of fresh concrete: Predicting the radius of action of poker vibrators from wave propagation," *Cement and Concrete Research*, vol. 41, pp. 932-941, 2011.
- [45] K. C. Hover, "Vibration Tune-Up," *Concrete International*, vol. 23, no. 9, pp. 30-35, 2001.
- [46] M. Pigeon and V. M. Malhotra, "Frost Resistance of Roller-Compacted High-Volume Fly Ash Concrete," *Journal of Materials in Civil Engineering*, vol. 7, no. 4, pp. 208-211, 1995.
- [47] Y. C. Zhang and L. L. Gao, "Effect of High Frequency Vibration on Pore Parameters and Frost Resistance of Air Entrained Concrete," *Advanced Materials Research*, Vols. 671-674, pp. 1680-1683, 2013.
- [48] X. H. Zheng, Y. Ge and J. Yuan, "Influence of Air Content and Vibration Time on Frost Resistance of Air Entrained Concrete," *Advanced Materials Research*, vol. 857, pp. 110-115, 2014.
- [49] G. H. Tattersall and P. H. Baker, "The effect of vibration on the rheological properties of fresh concrete," *Magazine of Concrete Research*, vol. 40, no. 143, pp. 79-89, 1988.
- [50] S. Juradin, "Determination of rheological properties of fresh concrete and similar materials in a vibration rheometer," *Materials Research*, vol. 15, no. 1, pp. 103-113, 2012.
- [51] P. Krstulovic and S. Juradin, "Modelling of fresh concrete behaviour under vibration," *Engineering Modelling*, vol. 12, no. 1-4, pp. 43-51, 1999.
- [52] C. F. Ferraris, "Measurement of the rheological properties of high performance concrete: State of the art report," *Journal of Research of the National Institute of Standards and Technology*, vol. 104, no. 5, 1999.
- [53] ASTM, "ASTM C143: Standard Test Method for Slump of Hydraulic-Cement Concrete," ASTM International, West Conshohocken, PA, 2015.
- [54] ASTM, "ASTM C1611: Standard Test Method for Slump Flow of Self-Consolidating Concrete," ASTM International, West Conshohocken, PA, 2014.

- [55] ASTM, "ASTM C1437: Standard Test Method for Flow of Hydraulic Cement Mortar," ASTM International, West Conshohocken, PA, 2015.
- [56] ASTM, "ASTM C403: West Conshohocken, PA," ASTM International, West Conshohocken, PA, 2008.
- [57] S. Popovics, *Fundamentals of Portland Cement Concrete: A Quantitative Approach*, Hoboken, NJ: John Wiley & Sons, 1982.
- [58] N. Miura, N. Takeda, R. Chikamatsu and S. Sogo, "Application of Super Workable Concrete to Reinforced Concrete Structures with Difficult Construction Conditions," *ACI SP-140: High Performance Concrete in Severe Environments*, vol. 140, pp. 163-186, 1993.
- [59] P. Bartos, *Fresh Concrete: Properties and Tests*, Elsevier, 1992.
- [60] C. J. Hopkins and J. G. Cabrera, "The Turning-Tube Viscometer: An Instrument to Measure the Flow Behavior of Cement-pfa Pastes," *Magazine of Concrete Research*, vol. 37, pp. 101-109, 1985.
- [61] G. H. Tattersall, *The Workability of Concrete*, PCA, 1976.
- [62] F. De Larrard, C. Hu, T. Sedran, J. C. Sziitkar, M. Joly, F. Claux and F. Derkx, "A New Rheometer for Soft-to-Fluid Fresh Concrete," *Materials Journal*, vol. 94, no. 3, pp. 234-243, 1997.
- [63] S. H. Lamb, *Hydrodynamics*, 6th ed., London: Cambridge University Press, 1993.
- [64] G. K. Batchelor, *An Introduction to Fluid Dynamics*, New York, NY: Cambridge University Press, 2000.
- [65] S. Amziane, C. F. Ferraris and E. P. Koehler, "Measurement of Workability of Fresh Concrete Using a Mixing Truck," *Journal of Research of the National Institute of Standards and Technology*, pp. 55-66, 2005.
- [66] K. Peterson, "Air void analysis of hardened concrete via flatbed scanner," Unpublished Master's Thesis, Michigan Technological University, Houghton, MI, 2001.
- [67] C. Hanotin, S. K. De Richter, L. J. Michot and P. Marchal, "Viscoelasticity of Vibrated Granular Suspensions," *Journal of Rheology*, vol. 59, no. 1, pp. 253-273, 2015.
- [68] K. H. Khayat and J. Assaad, "Air-Void Stability of Self-Consolidating Concrete," *ACI Materials Journal*, vol. 99, no. 4, pp. 408-416, 2002.

- [69] M. T. Ley, R. Chancey, M. C. Juenger and K. J. Folliard, "The physical and chemical characteristics of the shell of air-entrained bubbles in cement paste," *Cement and Concrete Research*, vol. 39, no. 5, pp. 409-416, 2009.